Final Report for NASA Grant No. NAG-1-709

Title: Asymptotic Modal Analysis and Statistical Energy Analysis

Principal Investigator: Dr. Earl H. Dowell
Dept. of Mechanical Engineering
School of Engineering
Duke University
Durham, NC 27706

Other Personnel Covered Under this Grant:
Heather D. Dionne
Linda F. Peretti

Period Covered by Grant:
October 15, 1986 - February 15, 1992

NASA Contract Monitor:
Dr. Kevin P. Shepherd
ACOD M/S 463
NASA Langley Research Center
Hampton, VA 23665

July 1992

Publications and Presentations During Award Period

Papers Published Under Grant:

Dionne, H. D., "Asymptotic Modal Analysis and Statistical Energy Analysis of an Acoustic Cavity," Duke University Master's Thesis, April 15, 1987.

Kubota, Y., H. D. Dionne and E. H. Dowell, "Asymptotic Modal Analysis and Statistical Energy Analysis of an Acoustic Cavity," Journal of Vibration, Acoustics, Stress and Reliability in Design, **110**, 371 - 376, 1988.

Peretti, L., "Asymptotic Modal Analysis of a Rectangular Acoustic Cavity," Duke University Master's Thesis, 1988.

Peretti, L. and Earl H. Dowell, "Asymptotic Modal Analysis of a Rectangular Acoustic Cavity Excited by Wall Vibration," AIAA Journal, **30**, 1191-1198, 1992.

Peretti, L. and Earl H. Dowell, "A Study of Intensification Zones in a Rectangular Acoustic Cavity," AIAA Journal, **30**, 1199-1206, 1992.

Peretti, L. and Earl H. Dowell, "Experimental Verification of the Asymptotic Modal Analysis Method as Applied to a Rectangular Acoustic Cavity Excited by Structural Vibration." accepted for publication in ASME Journal of Vibration and Acoustics.

Presentations Made Under Grant:

Dowell, E. H., "Asymptotic Modal Analysis and Statistical Energy Analysis of an Acoustic Cavity," ASME Winter Annual Meeting, Boston, MA, Dec. 13-18, 1987.

Peretti, L. and Earl H. Dowell, "Asymptotic Modal Analysis of Structural Wall - Acoustic Cavity Systems," SAE-NASA 3rd Interior Noise Workshop, Norfolk, VA, April 1988.

Peretti, L. and Earl H. Dowell, "Asymptotic Modal Analysis of a Rectangular Acoustic Cavity and Characterization of Its Intensification Zones." Paper presented at the AIAA Aeroacoustics Conference. San Antonio, TX April 1989.

Peretti, L. and Earl H. Dowell, "Bandwidth and Absorption Effects on Intensification in a Structural-Acoustic Enclosure." Presented at the 118th Meeting of the Acoustical Society of America, St. Louis, MO November 27 - December 1, 1989.

Peretti, L. and Earl H. Dowell, "Experimental Verification of the Asymptotic Modal Analysis Method as Applied to a Rectangular Acoustic Cavity Excited by Structural Vibration." Presented at the ASME Winter Annual Meeting, Dallas, TX November 1990.

Introduction

Asymptotic Modal Analysis (AMA) is a method which has been used successfully to model and understand linear dynamical systems with many participating modes. The AMA method was originally developed by Dowell [1] to show the relationship between statistical energy analysis (SEA) and classical modal analysis (CMA). In the limit of a large number of modes of a vibrating system, the classical modal analysis result can be shown to be equivalent to the statistical energy analysis result. As the CMA result evolves into the SEA result, a number of systematic assumptions are made. Most of these assumptions are based upon the supposition that the number of modes approaches infinity. It is for this reason that the term "asymptotic" is used. AMA is the asymptotic result of taking the limit of CMA as the number of modes approaches infinity. AMA refers to any of the intermediate results between CMA and SEA, as well as the SEA result which is derived from CMA.

The main advantage of the AMA method is that individual modal characteristics are not required in the model or computations. By contrast, CMA requires that each modal parameter be evaluated at each frequency. In the latter, contributions from each mode are computed and the final answer is obtained by summing over all the modes in the particular band of interest. AMA evaluates modal parameters only at their center frequency, and does not sum the individual contributions from each mode in order to obtain a final result. The method is similar to SEA in this respect. However, SEA is only capable of obtaining spatial averages or means, as it is a statistical method. Since AMA is systematically derived from CMA, it can obtain local spatial information as well.

Summary of Research Conducted Under the Grant

AMA is considered in this work within the framework of those linear dynamical systems called structural-acoustics. Some general analytical results were obtained for the case where part of an otherwise rigid enclosure is vibrating with a large number of structural modes, which excite either a finite or an infinite number of acoustic modes in the interior. In Reference 2, it was shown that Statistical Energy Analysis is an asymptotic limit of classical modal analysis. The basic asymptotic theory for structural wall-acoustic cavity interaction was described, and several numerical examples were presented for the acoustic cavity response.

In Reference 3, the AMA results for an infinite number of structural modes were applied to the specific case of a rectangular acoustic cavity. The rectangular acoustic cavity had rigid walls except for a flexible portion on one of its walls. The flexible portion vibrated with an infinite number of structural modes which were temporally uncorrelated ("white noise"). The interior sound field was studied using asymptotic modal analysis. Both local mean-square pressures and spatially averaged mean-square pressures in a bandwidth were computed. The AMA results were compared to CMA results. In addition, the effect of varying the size and the location of the flexible vibrating portion was studied.

It was found that the interior sound pressure levels are nearly uniform, with exceptions occurring at the boundaries. The boundaries exhibited elevated levels which were 8, 4, and 2 times greater than the interior level, for corners, edges and walls respectively. These areas of elevated sound pressure level were termed "intensification zones."

In the numerical study, the size and location of the flexible portion of the wall was varied, and the resulting effects on the interior sound field were studied. An interesting phenomenon was discovered. When a small source (smaller than an acoustic wavelength) was placed on a point of symmetry of the cavity, elevated sound pressure levels occurred along the planes of symmetry, creating new effective boundaries of the sub-divided cavity.

These effective boundaries retained the same ratios of 8, 4, and 2 for differences between corner, edge, and wall intensification, relative to the interior (of each sub-cavity). Another result of the numerical study was that sound sources placed in the corner, rather than elsewhere on the wall away from a boundary, raise the sound pressure levels by a factor of four. It was further deduced that sound sources placed on an edge would raise sound pressure levels by a factor of two.

In Reference 4, the intensification zones were studied using AMA and other traditional methods. The system parameters which define the structure of an intensification zone were determined. Using AMA and non-dimensionalizing the spatial variable by the center frequency wavenumber, the intensification zone description was found to be independent of the cavity dimensions. In fact, the non-dimensional spatial variation of sound pressure level was only dependent upon the ratio of bandwidth to center frequency (f_b/f_c). Upon further study, it was shown that the bandwidth effect is second order in f_b/f_c.

The independence of cavity dimensions suggested that intensification could be modelled as a local system. This led to modelling using oblique incidence sound waves. This alternative method gave identical results. Reflections from an absorptive surface were also studied and an analytical expression for the sound pressure levels near an absorptive wall was developed. This result can be expressed as the sum of a rigid wall term plus a term containing the impedance information for the absorptive surface.

Experiments were performed in order to validate the AMA method for the structural-acoustic application. The results of the experiments are presented in Reference 5. The experiments tested for uniformity of the interior, intensification near corners, edges and walls of the cavity, and accuracy of the method for predicting sound pressure levels in the interior. In all cases, the agreement between experiment and analysis was very good.

Qualitatively, it was shown from the experimental results that AMA works best for moderate bandwidths. If the bandwidth is too narrow, there may not be enough modes for

the AMA assumptions to apply. However, if the bandwidth is too wide, there will be enough modes, but there may be too much variation in the modal variables which are assumed constant throughout the band in the AMA methodology.

The AMA method was used to predict the spatially averaged sound pressure levels in the cavity interior from the measured acceleration of the vibrating wall. The predicted levels were compared to the experimentally measured levels and good agreement was obtained.

Further theoretical work was done to develop an AMA result which is valid for the case where the number of structural modes is finite and the number of acoustic modes is infinite. These results are reported in Reference 6. The previous AMA work considered the case where the number of structural modes was very large or, formally, infinite. It was found that different AMA results are obtained if the limits of an infinite number of structural modes or an infinite number of acoustic modes are taken in a different order. Therefore, when there are both a large number of acoustic modes and a large number of structural modes, it is important to use the appropriate limiting sequence. This decision should be based on which set of modes is approaching infinity most rapidly.

References 2 through 6 are presented in Appendices A through E of this document.

Recommendations for Future Work

One outstanding issue is worthy of mention. In the usual linear dynamical systems theory, be it CMA, SEA or AMA, the assumption of small damping is often made. From the experimental work done under the present grant, there is clear evidence that all of these theoretical models need to be extended to describe accurately the physical phenomena for large damping. The high damping case, it may be noted, is of considerable practical importance.

References

1. Dowell, E. H., "Vibration Induced Noise in Aircraft: Asymptotic Modal Analysis and Statistical Energy Analysis of Dynamical Systems," R82-112447, United Technologies Research Center, 1983.

2. Kubota, Y., H. D. Dionne and E. H. Dowell, "Asymptotic Modal Analysis and Statistical Energy Analysis of an Acoustic Cavity," Journal of Vibration, Acoustics, Stress and Reliability in Design, **110**, 371 - 376, 1988.

3. Peretti, L. F. and E. H. Dowell, "Asymptotic Modal Analysis Of A Rectangular Acoustic Cavity Excited by Wall Vibration," AIAA Journal, **30**, 1191-1198, 1992.

4. Peretti, L.F. and E.H. Dowell, "A Study of Intensification Zones in a Rectangular Acoustic Cavity," AIAA Journal, **30**, 1199-1206, 1992.

5. Peretti, L. F. and E. H. Dowell, "Experimental Verification of the Asymptotic Modal Analysis Method As Applied To A Rectangular Acoustic Cavity Excited By Structural Vibration," presented at the ASME Winter Annual Meeting, November 1990 in Dallas, TX, to appear in ASME Journal of Vibrations and Acoustics , 1992.

6. Peretti, L. F., "Chapter 4: Asymptotic Modal Analysis for Structural-Acoustic Systems with Finite Structural and Infinite Acoustic Modes," Asymptotic Modal Analysis for Structural-Acoustic Systems, Ph.D. Thesis, Duke University, 1991.

Appendix A:

Kubota, Y., H. D. Dionne and E. H. Dowell, "Asymptotic Modal Analysis and Statistical Energy Analysis of an Acoustic Cavity," Journal of Vibration, Acoustics, Stress and Reliability in Design, **110**, 371 - 376, 1988.

Y. Kubota[2]
Visiting Scholar.

H. D. Dionne
Research Assistant.

E. H. Dowell
Dean.

rtment of Mechanical Engineering
and Materials Science,
School of Engineering,
Duke University,
Durham, North Carolina 27706

Asymptotic Modal Analysis and Statistical Energy Analysis of an Acoustic Cavity[1]

One of the outstanding theoretical questions in interior noise is the connection between modal analysis and statistical energy analysis. Recently substantial progress has been made in understanding this connection for structural vibrations including both fundamental theoretical work and experimental verification. It has been shown that many of the results of Statistical Energy Analysis can be derived as an asymptotic limit of classical modal analysis and thus this approach is called Asymptotic Modal Analysis. The basic asymptotic theory for structural wall-acoustic cavity interaction is described in this paper. Several numerical examples are presented for acoustic cavity response with a prescribed wall motion to illustrate the key results of the theory.

luction

well [1] showed that the results commonly referred to as ical Energy Analysis (SEA) [2] as developed by Lyon thers can be obtained by studying the asymptotic or of classical modal analysis (CMA) for a general, structural system; those asymptotic results are called totic Modal Analysis (AMA). In [1], moreover, specific lizations were made for structural-acoustic systems and cting subsystems. Since AMA results can be derived atically from CMA, AMA allows an assessment of the ptions and consequent simplifications which are made ain such results and a combination of CMA and AMA EA) may prove useful in applications.

[3], a comparison of AMA (or SEA) and CMA was made e response of a single general linear structure and the ptotic characteristics of AMA were discussed. It was that the asymptotic behavior of AMA (or SEA) ds upon the number of modes in a frequency interval of st and the location of the point forces. Moreover, ptotically, all points on the structure except for some l ones have the same response; the exceptional points are the points of excitation and near the structural system ndary. Some numerical examples for a beam were ted in [3].

[4] the response of a rectangular plate under a point ran- force was investigated experimentally and theoretically. re were two objectives in this study. The first one was to nstrate experimentally the manner in which the asymp- limit is approached. The second one was to show ex- entally that the response of almost all points of the plate mes the same in the asymptotic limit.

perimental measurements were carried out for several frequency bandwidths in which the maximum one corresponds to 47.1 modes of plate vibration, for several band center frequencies, and for two locations of the point force which were the center of the plate and near the plate edge, respectively. All experimental results verified the asymptotic behavior of the plate response which is predicted by AMA and were in good quantitative agreement with the theory as the number of modes became sufficiently large.

The important work of Crandall and his colleagues should also be cited [5–8]. Their work has been directed primarily toward those aspects of structural response under wide-band random excitation where SEA-type results of the usual sort do not hold. Both analytical and experimental work has been carried out.

Modal sum and image sum analytical methods have been used by Crandall. The modal sum methods are similar to those employed here. Image sum methods involve repeatedly using traveling waves on an infinite structure to form an appropriate cancellation of image sources to model finite plate response. Both methods have led to the identification of "intensification zones" where the local response is higher than the nearly uniform response of the rest of the structure. Special attention has been given to square and circular plates where such zones are most pronounced.

Here the emphasis is on extending the earlier work in the area of structural-acoustic systems. A theoretical discussion of this subject is given next, followed by a section with numerical examples. A complementary discussion of this subject for acoustic sources internal to the acoustic cavity is contained in [9].

Theoretical Discussion: Noise Transmission Through a Structural Wall into an Interior Acoustic Cavity in the Asymptotic Modal Analysis (AMA) Limit

The structural wall modal equation of motion is (see [1], [3], and [4] for technical background and nomenclature).

work was supported, in part, by NASA Research Grant NAG-1-709 Structural Acoustics Branch of the Langley Research Center. Dr. Kevin is the Technical Officer.

leave from Toshiba Corporation, Tokyo, Japan.

tributed by the Noise Control and Acoustics Division for publication in JOURNAL OF VIBRATION, ACOUSTICS, STRESS, AND RELIABILITY IN DESIGN. cript received at ASME Headquarters, September 15, 1987

$$M_m[\ddot{q}_m + 2\zeta_m\omega_m\dot{q}_m + \omega_m^2 q_m] = Q_m^L \tag{1}$$

where the modal expansion for the wall deflection is

$$w = \sum_m q_m(t)\psi_m(x,y) \tag{2}$$

and the structural generalized mass is

$$M_m \equiv \iint_{A_F} m_p \psi_m^2 dxdy$$

and the generalized force due to a given external pressure is

$$Q_m^E \equiv \iint_{A_F} p^E \psi_m dxdy \tag{3}$$

The acoustic cavity modal equation is

$$\ddot{P}_r + 2\zeta_r^A\omega_r^A\dot{P}_r + \omega_r^{A^2}P_r = Q_r^w \tag{4}$$

where the modal expansion for the acoustic cavity pressure is

$$p = \rho_0 c_0^2 \sum_r \frac{P_r(t)F_r(x,y,z)}{M_r^A} \tag{5}$$

and the acoustic generalized mass is

$$M_r^A \equiv \frac{1}{V}\iiint_v F_r^2 dxdydz \tag{6}$$

and the generalized acceleration due to the structural wall is

$$Q_r^w \equiv -\frac{1}{V}\iint_{A_F} \ddot{w}\, F_r dxdy$$

Define f, a nondimensional cavity pressure,

$$f(t,x,y,z) \equiv \frac{p}{\rho_0 c_0^2}$$

From (5) the auto-power spectrum of f may be determined as

$$\Phi_f(\omega,x,y,z) = \sum_r \sum_s \frac{F_r(x,y,z)}{M_r^A}\frac{F_s(x,y,z)}{M_s^A}\Phi_{P_rP_s} \tag{7}$$

where the cross-spectra are defined as

$$\Phi_{P_rP_s} \equiv \frac{1}{\pi}\int_{-\infty}^{\infty} R_{P_rP_s}(\tau)e^{i\omega\tau}d\tau$$

and the cross-correlations of the modal generalized pressure coordinates are

$$R_{P_rP_s} \equiv \lim_{T\to\infty}\frac{1}{2T}\int_{-T}^{T} P_r(t)P_s(t+\tau)dt$$

Similarly from (6) the cross-power spectra of Q_r^w and Q_s^w are

$$\Phi_{Q_r^wQ_s^w}(\omega) = \frac{1}{V^2}\iint_{A_F}\iint_{A_F} F_r(x,y,z)F_s(x^*,y^*,z^*)\phi_{\ddot{w}}(\omega;x,y,x^*,y^*)dxdydx^*dy^* \tag{8}$$

From (4) and standard random response theory, the relationship between $\phi_{P_rP_s}$ and $\Phi_{Q_r^wQ_s^w}$ is

$$\Phi_{P_rP_s}(\omega) = H_r^A(\omega)H_s^A(-\omega)\Phi_{Q_r^wQ_s^w}(\omega) \tag{9}$$

where the modal transfer function is defined as

$$H_r^A(\omega) \equiv \frac{1}{[-\omega^2 + \omega_r^{A^2} + 2i\zeta_r^A\omega_r^A\omega]} \tag{10}$$

From (7), (8), and (9)

$$\Phi_f(\omega;x,y,z) = \frac{1}{V^2}\sum_r\sum_s \frac{F_r(x,y,z)}{M_r^A}\cdot\frac{F_s(x,y,z)}{M_s^A}\cdot H_r^A(\omega)\cdot H_s^A(-\omega)\cdot\iint_{A_F}\iint_{A_F} F_r(x,y,z_0)F_s(x^*,y^*,z_0^*)\phi_{\ddot{w}}(\omega;x,y,x^*,y^*)dxdydx^*dy^* \tag{11}$$

This is the basic expression for the power spectra of the cavity pressure in terms of the power spectra of the wall acceleration.

I. When the number of excited structural modes is large, $\Delta M \to \infty$, it can be shown that

$$\Phi_{\ddot{w}}(\omega;x,y,x^*,y^*) \equiv A_F\Phi_{\ddot{w}}(\omega)\delta(x-x^*)\delta(y-y^*) \tag{12}$$

This means that the power spectra of the wall response is uncorrelated in space. This assumption is reasonable for large ΔM, because

$$\frac{1}{\Delta M}\phi_{\ddot{w}}(\omega;x,y,x^*,y^*) \to \begin{cases} 0 & (x\neq x^*,\ y\neq y^*) \\ \text{constant} & (x=x^*,\ y=y^*) \end{cases} \quad \text{as } \Delta M\to\infty \tag{13}$$

Recall [1, 3]

$$\Phi_{\ddot{w}}(\omega;x,y,x^*,y^*) \equiv \sum_m\sum_n \psi_m(x,y)\psi_n(x^*,y^*)\omega^2H_m(\omega)\omega^2H_n(-\omega)\cdot\sum_i\sum_j \psi_m(x_i,y_i)\psi_n(x^*_j,y^*_j)\Phi_{F_{ij}}(\omega)$$

(13) is readily derived from the above relationship and involving the basic methods of AMA. $\Phi_{F_{ij}}$ is the cross spectra for point forces, F_i, F_j, on the structural wall. Also for a smoothly varying power spectrum, it is assumed that

$$\Phi_{\ddot{w}}(\omega) \equiv \Phi_{\ddot{w}}(\omega_c) \tag{14}$$

This is just the usual white noise assumption. Thus, equation (11) becomes

$$\Phi_f(\omega;x,y,z) = \frac{A_F}{V^2}\cdot\Phi_{\ddot{w}}(\omega_c)\sum_r\sum_s \frac{F_r(x,y,z)}{M_r^A}\cdot\frac{F_s(x,y,z)}{M_s^A}\cdot H_r^A(\omega)\cdot H_s^A(-\omega)\cdot\iint_{A_F} F_r(x,y,z_0)F_s(x,y,z_0)dxdy \tag{15}$$

The mean square response of the nondimensional cavity pressure is

$$\overline{f^2} \equiv \frac{\overline{p^2}(x,y,z)}{(\rho_0c_0^2)^2} = \int_0^\infty \Phi_f(\omega;x,y,z)d\omega \cong \frac{\pi}{4}\frac{A_F}{V^2}\phi_{\ddot{w}}(\omega_c)\sum_r \frac{F_r^2(x,y,z)}{M_r^{A^2}\omega_r^{A^3}\zeta_r^A}\iint_{A_F} F_r^2(x,y,z_0)dxdy \tag{16}$$

Note that (16) is the result for a large number of structural modes, $\Delta M \to \infty$, and a moderate number of acoustic cavity modes, ΔN_A.

Taking a spatial average of (16), and noting that $M_r^{A^2}$, $\omega_r^{A^3}$, ζ_r^A, $\langle F_r^2\rangle$ do not vary rapidly with respect to modal number r, for large ΔN_A, equation (16) becomes

$$\frac{\langle\overline{p^2}\rangle}{(\rho_0c_0^2)} \cong \frac{\pi}{4}\frac{A_F}{V^2}\phi_{\ddot{w}}(\omega_c)\frac{\langle F_c^2\rangle}{M_c^{A^2}\omega_c^{A^3}\zeta_c}\sum_r\iint_{A_F} F_r^2(x,y,z_0)dxdy$$

where $\langle\ \rangle$ denotes spatial average.

Now consider a cavity acoustic modal function

$$F_r(x,y,z) = X_r(x)Y_r(y)Z_r(z)$$

Take the plane at $z = z_0$ as the boundary of the acoustic cavity where the structural wall is vibrating. $Z_r(z_0)$ is usually independent of mode number r or it can be so normalized. Then for large ΔN^A,

$$F_r^2(x,y,z_0)dxdy \equiv \sum_r A_F < X_r^2 >_{A_F} < Y_r^2 >_{A_F} Z_r^2(z_0)$$

$$\rightarrow A_F \cdot \Delta N^A \frac{< F_c^2 >}{< Z_c^2 >} \tag{19}$$

$$< Z_c^2 > \equiv \frac{< F_c^2 >}{< F_c^2 >_{A_F}}$$

$$M_c^A \equiv < F_c^2 >$$

$$< \ddot{\bar{w}}^2 >_{\Delta\omega} \equiv \Delta\omega \, \Phi_{\ddot{w}}(\omega_c)$$

•> denotes a spatial average. $< F_c^2 >$ is a volume of F_c^2 and $< F_c^2 >_{A_F}$ is an area average over the structural wall. Hence, equation (17) becomes as $\rightarrow \infty$,

$$\frac{< \bar{p}^2 >}{(\rho_0 c_0^2)^2} \equiv \frac{\pi}{4} \frac{\Delta N^A}{\Delta\omega^A} \left(\frac{A_F}{V}\right)^2 \frac{< \ddot{\bar{w}}^2 >_{\Delta\omega}}{\omega_c^{A^3} \zeta_c^A < Z_c^2 >} \tag{20}$$

$$< \ddot{\bar{w}}^2 >_{\Delta\omega} \equiv \omega_c^4 < \bar{w}^2 >_{\Delta\omega} \tag{21}$$

From the AMA results for structural wall motion,

$$< \bar{w}^2 >_{\Delta\omega} \equiv \frac{\pi}{4} \frac{\Delta M}{\Delta\omega} \frac{< \bar{F}^2 >_{\Delta\omega}}{M_p^2 \omega_c^3 \zeta_c} \tag{22}$$

Then, equation (20) becomes

$$\frac{< \bar{p}^2 >}{(\rho_0 c_0^2)^2} \equiv \left(\frac{\pi}{4}\right)^2 \frac{\Delta M}{\Delta\omega} \frac{\Delta N^A}{\Delta\omega^A} \left(\frac{A_F}{V}\right)^2 \frac{\Delta\omega^A}{\Delta\omega}$$

$$\cdot \frac{\omega_c < \bar{F}^2 > \Delta\omega}{\omega_c^{A^3} \zeta_c^A \zeta_c M_p^2 < Z_c^2 >} \tag{23}$$

is the result for $\Delta M \rightarrow \infty$ and $\Delta N_A \rightarrow \infty$. (16) is the result $\Delta M \rightarrow \infty$ and finite ΔN_A.

e above derivation is not the only one which leads to (23). lso instructive to consider an alternative derivation which en below.

When equation (12) can not be assumed, then

$$x,y,z) = \frac{1}{V^2} \sum_r \sum_s \frac{F_r(x,y,z)}{M_r^A} \cdot \frac{F_s(x,y,z)}{M_s^A} \cdot H_r^A(\omega)$$

$$(-\omega) \cdot \iint_{A_F} \iint_{A_F} F_r(x,y,z_0) F_s(x^*,y^*,z_0^*) \phi_{\ddot{w}} \tag{24}$$

$$(\omega;x,y,x^*,y^*)dxdydx^*dy^* \tag{11}$$

$$\omega;x,y,x^*,y^*) \equiv \sum_m \sum_n \psi_m(x,y)\psi_n(x^*,y^*)\omega^2 H_m(\omega)$$

$$^2 H_n(-\omega) \cdot \sum_i \sum_j \psi_m(x_i,y_i)\psi_n(x_j^*,y_j^*) \cdot \Phi_{F_{ij}}(\omega)$$

stitute equation (24) into equation (11), then

$$x,y,z) = \frac{1}{V^2} \sum_r \sum_s \sum_m \sum_n \frac{F_r(x,y,z)}{M_r^A} \cdot \frac{F_s(x,y,z)}{M_s^A}$$

$$\cdot H_r^A(\omega) H_s^A(-\omega) \cdot \omega^2 H_m(\omega) \omega^2 H_n(-\omega)$$

$$\cdot \sum_i \sum_j \psi_m(x_i,y_i)\psi_n(x_j^*,y_j^*) \cdot \Phi_{F_{ij}}(\omega)$$

$$_{A_f} \iint_{A_f} F_r(x,y,z_0) F_s(x^*,y^*,z^*{}_0) \psi_m(x,y)\psi_n$$

$$(x^*,y^*)dxdydx^*dy^* \tag{25}$$

Equation (25) will be dominated by the terms for which $r = s$, $m = n$, $i = j$. Thus, equation (25) becomes

$$\Phi_f(\omega;x,y,z) \equiv \frac{1}{V^2} \sum_r \sum_m \sum_i \frac{F_r^2(x,y,z)}{M_r^{A^2}} |H_r^A(\omega)|^2$$

$$\cdot \omega^4 |H_m(\omega)|^2 \cdot \Phi_{F_{ii}}(\omega)$$

$$\cdot \psi_m^2(x_i,y_i) \cdot I_{rm}^2 \tag{26}$$

where

$$I_{rm} \equiv \iint_{A_f} F_r(x,y,z_0)\psi_m(x,y)dx\,dy$$

The mean square response for the nondimensional cavity acoustic pressure is

$$\bar{f}^2 \equiv \frac{\bar{p}^2(x,y,z)}{(\rho_0 c_0^2)^2} \equiv \int_0^\infty \Phi_f(\omega;x,y,z)d\omega$$

Using (26),

$$\bar{f}^2 \equiv \frac{\pi}{4} \frac{1}{V^2} \sum_r \sum_m \sum_i \frac{\alpha_{rm}}{\beta_{rm}} \frac{\omega_m^4 F_r^2(x,y,z)}{M_m^2 M_r^{A^2} \omega_m^3 \omega_r^{A^3} \zeta_m \zeta_r^A}$$

$$\cdot \Phi_{F_{ii}}(\omega_m)\psi_m^2(x_i,y_i) \cdot I_{rm}^2 \tag{27}$$

where

$$\alpha_{rm} \equiv \zeta_m \omega_m^3 + \zeta_r^A \omega_r^{A^3} + 4\zeta_m \zeta_r^A \omega_m \omega_r^A (\zeta_m \omega_m + \zeta_r^A \omega_r^A)$$

$$\beta_{rm} \equiv (\omega_m^2 - \omega_r^{A^2})^2 + 4\omega_m \omega_r^A (\zeta_m \omega_m + \zeta_r^A \omega_r^A)(\zeta_m \omega_r^A + \zeta_r^A \omega_m)$$

This result assumes that the acoustic and structural resonances are well separated.

See Crandall and Mark [10], p. 72, for the evaluation of

$$\int_0^\infty |H_r^A(\omega)|^2 |H_m(\omega)|^2 d\omega$$

When ζ_m, ζ_r^A are small, then

$$\alpha_{rm} \equiv \zeta_m \omega_m^3 + \zeta_r^A \omega_r^{A^3} \tag{28}$$

When $\Delta\omega/\omega_c$, $\Delta\omega^A/\omega_c^A \ll 1$, then

$$\beta_{rm} \equiv (\omega_m^2 - \omega_r^{A^2})^2 + 4\omega_m^2 \omega_r^{A^2} (\zeta_m + \zeta_r^A)^2 \tag{29}$$

All (29) really assumes is that $\omega_m - \omega_r^A$ is small. Hence in summing, ω_m and ω_r^A, one need not distinguish between them.

Taking a spatial average, and noting that

$$\alpha_{rm}, \omega_m^4, < F_r^2 >, M_m^2, M_r^{A^2}, \omega_m^3, \omega_r^{A^3}, \zeta_m, \zeta_r^A, \Phi_{F_{ii}}(\omega_m)$$

do not vary rapidly with modal number for large ΔM and ΔN_A and letting

$$\omega_c = \omega_c^A, \Delta\omega = \Delta\omega^A,$$

then equation (27) becomes

$$< \bar{f}^2 > \equiv \frac{< \bar{p}^2 >}{(\rho_0 c_0^2)^2} \equiv \frac{\pi}{4} \frac{1}{V^2} \frac{\alpha_c < F_c^2 >}{M_c^2 M_c^{A^2} \omega_c^2 \zeta_c \zeta_c^A} \sum_i \Phi_{F_{ii}}$$

$$(\omega_c) \sum_r \sum_m \frac{1}{\beta_{rm}} \psi_m^2(x_i,y_i) I_{rm}^2 \tag{30}$$

where

$$\alpha_c \equiv \omega_c^3 (\zeta_c + \zeta_c^A)$$

For large ΔM, ΔN^A. we can write

$$\sum_r \sum_m \frac{1}{\beta_{rm}} \psi_m^2(x_i,y_i) I_{rm}^2 \equiv \frac{1}{\beta_c} \sum_r \sum_m \psi_m^2(x_i,y_i) I_{rm}^2 \tag{31}$$

where $1/\beta_c$ is the average of $\sum_r \sum_m (1/\beta_{rm})$

$1/\beta_c$ can be approximated by an integral expression

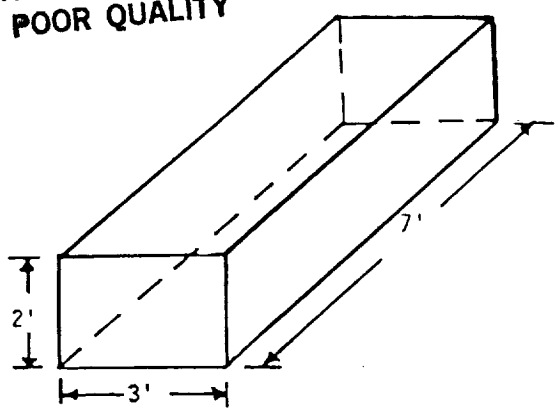

2' x 3' x 7' Cavity

2' x 3' Flexible Vibrating Wall

Fig. 1 Cavity geometry

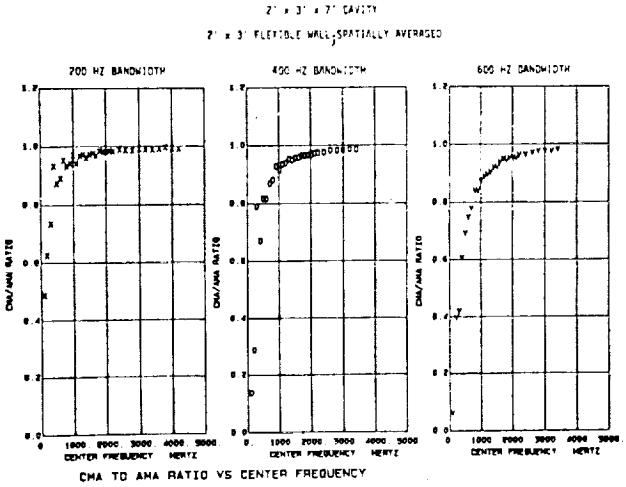

Fig. 2

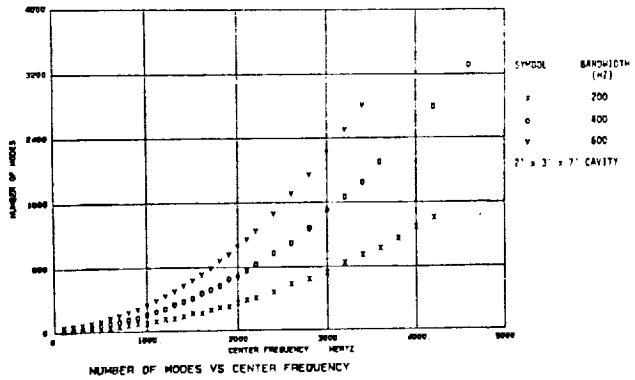

Fig. 3 Number of modes versus center frequency

$$\frac{1}{\beta_c} \cong \frac{1}{\Delta\omega}\int_0^{\infty} \frac{1}{\beta_{rm}}\, d\omega_r^A$$

or

$$\frac{1}{\beta_c} \cong \frac{1}{\Delta\omega}\int_0^{\infty} \frac{1}{\beta_{rm}}\, d\omega_m \tag{32}$$

$$\cong \frac{\pi}{4}\,\frac{1}{\Delta\omega}\,\frac{1}{\omega_c^3(\zeta_c+\zeta_c^A)}$$

Thus, equation (30) becomes

$$\frac{<p^2>}{(\rho_0 c_0^2)^2} \cong \left(\frac{\pi}{4}\right)^2 \frac{1}{\Delta\omega}\,\frac{1}{V^2}\cdot\frac{<F_c^2>}{M_c^2 M_c^{A^2}\omega_c^2\zeta_c\zeta_c^A}\sum_i \Phi_{F_{ii}}(\omega_c)$$

$$\cdot \sum_r \sum_m \psi_m^2(x_i,y_i) f_{rm}^2 \tag{33}$$

Now, the summation $\sum_r \sum_m \psi_m^2 f_{rm}^2$, can be written as

$$S_{rm} \equiv \sum_r \sum_m \psi_m^2(x_i,y_i) f_{rm}^2$$

$$= \sum_r \sum_m \psi_m^2(x_i,y_i)\left[\iint_{A_F} F_r(x,y,z_0)\psi_m(x,y)dxdy\right]$$

$$\cdot\left[\iint_{A_F} F_r(x^*,y^*,z_0^*)\psi_m(x^*,y^*)dx^*dy^*\right]$$

$$= \sum_r \iint_{A_F}\iint_{A_F} F_r(x,y,z_0)F_r(x^*,y^*,z_0^*)$$

$$\cdot\left[\sum_m \psi_m^2(x_i,y_i)\psi_m(x,y)\psi_m(x^*,y^*)\right]dxdydx^*dy^* \tag{34}$$

For large ΔM, the summation, $\sum_m \psi_m^2(x_i,y_i)\,\psi_m(x,y)\,\psi_m(x^*,y^*)$, will be dominated by $x = x^*$, $y = y^*$ and

$$\sum_m \psi_m^2(x_i,y_i)\psi_m^2(x,y) - \Delta M[<\psi_c^2>]^2 \tag{35}$$

as $\Delta M \to \infty$

Thus, S_{rm} can be written

$$S_{rm} \cong \Delta M[<\psi_c^2>]^2 \cdot \sum_r \iint_{A_F}\iint_{A_F} F_r^2(x,y,z_0)dxdydx^*dy^*$$

$$= \Delta M[<\psi_c^2>]^2 \cdot A_F \sum_r \iint_{A_F} F_r^2(x,y,z_0)dxdy \tag{36}$$

For large ΔN^A, S_{rm} becomes

$$S_{rm} \equiv \Delta M \cdot \Delta N^A A_F^2[<\psi_c^2>]^2 \cdot \frac{<F_c^2>}{<Z_c^2>} \tag{37}$$

Substitute equation (37) into equation (33) and note that

$$M_c \equiv M_p <\psi_c^2>$$

$$M_c^A \equiv <F_c^2>$$

$$\sum_i \Phi_{F_{ii}}(\omega_c)\cdot\Delta\omega \equiv <\overline{F^2}>_{\Delta\omega}$$

Then equation (33) becomes

$$\frac{<\overline{p^2}>}{(\rho_0 c_0^2)^2} \cong \left(\frac{\pi}{4}\right)^2 \cdot \frac{\Delta M}{\Delta\omega}\cdot\frac{\Delta N^A}{\Delta\omega}\left(\frac{A_F}{V}\right)^2$$

$$\cdot\frac{<\overline{F^2}>_{\Delta\omega}}{M_p^2\omega_c^2\zeta_c\zeta_c^A}\cdot\frac{1}{<Z_c^2>}$$

Equation (38) is the same as equation (23) for $\omega_c = \omega_c^A$, $\Delta\omega = \Delta\omega^A$.

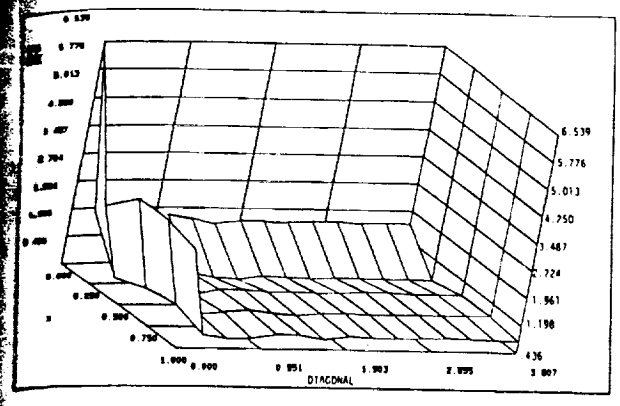

Fig. 4

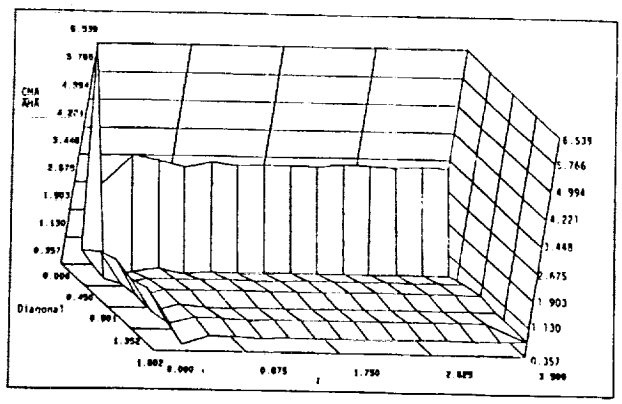

Fig. 6

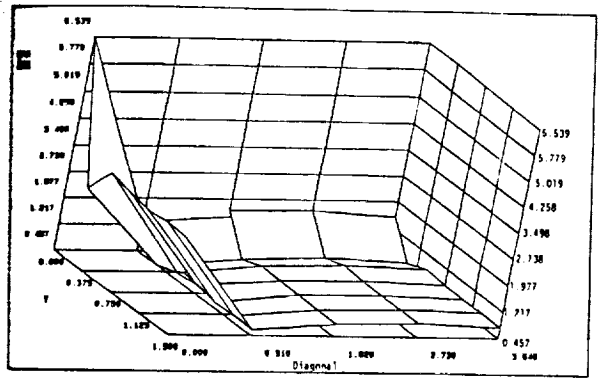

Fig. 5

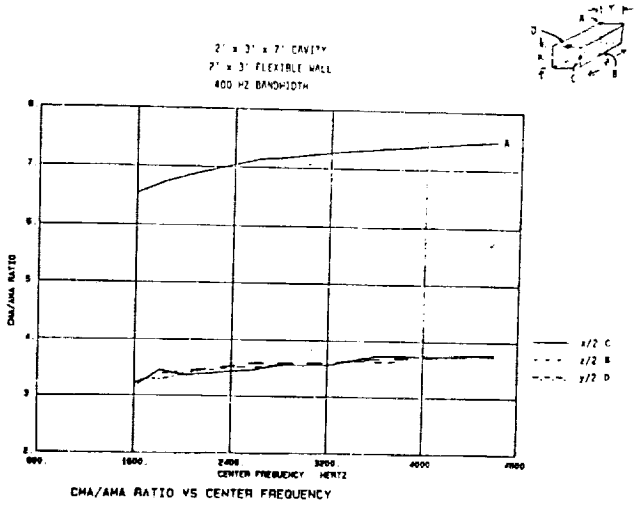

Fig. 7 CMA/AMA ratio versus center frequency

Illustrative Numerical Examples

Consider a rectangular cavity of dimensions $2' \times 3' \times 7'$. See Fig. 1. The $2' \times 3'$ wall is taken to vibrate in a large number of structural modes, $\Delta M \to \infty$. We wish to compare the results of Asymptotic Modal Analysis for the acoustic cavity response, equation (20), to that of Classical Modal Analysis, equation (16). For simplicity and to focus the discussion on acoustic response, the wall motion is assumed to be given.

The ratio of the spatial average of equation (16), CMA, to equation (20), AMA, is shown in Fig. 2. This ratio is shown for three different frequency bandwidths and as a function of the center frequency. The bandwidth, $\Delta\omega$, is defined as

$$\Delta\omega \equiv \omega_{max} - \omega_{min}$$

and the center frequency, ω_c, as

$$\omega_c \equiv (\omega_{max}\omega_{min})^{1/2}$$

where ω_{max}, ω_{min} are the maximum and minimum frequencies of the frequency interval. All acoustic modes are assumed to have the same modal critical damping ratio, ζ_r^A, for simplicity. As can be seen from Fig. 2, all results approach unity as the center frequency becomes large. The approach is modestly more rapid for the *smaller* bandwidths. To better understand the results of Fig. 2, consider Fig. 3. Here is shown the number of modes, ΔM, in a given bandwidth as a function of center frequency. It is expected that CMA/AMA $\to$ 1 as $\Delta M \to \infty$. This clearly explains why CMA/AMA $\to$ 1 as the center frequency becomes large. However considering Fig. 3 it is perhaps initially surprising that in Fig. 2 the asymptotic approach is modestly more rapid for the *smaller* bandwidths. This is explained by recalling that in AMA we neglect the variation of natural frequencies from one mode to another within a given bandwidth. Thus while increasing the bandwidth increases the number of modes (which improves the accuracy of AMA), it also increases the variation among the natural frequencies (thus decreasing the accuracy of AMA). The net effect of these two competing factors is to decrease modestly the accuracy of AMA as the bandwidth is increased.

The above results are all for the spatially averaged pressure inside the cavity. Now consider the ratio, CMA/AMA, for local response at various positions within the acoustic cavity. In Figs. 4, 5, 6 the ratio is shown versus position in three different diagonal planes in the cavity. A single frequency interval, 1400–1800 Hz, is considered. As can be seen the ratio is everywhere nearly constant and close to unity, except along a cavity side, edge and, especially, at a cavity corner. On theoretical grounds the ratio is expected to be, asymptotically,

side:	2
edge:	4
corner:	8

To see how these expected asymptotes are approached, con-

sider Fig. 7. One corner point, A, and three edge points, B, C, D, are considered. The ratio, CMA/AMA, is shown as a function of center frequency for a fixed bandwidth. As expected the ratio approaches 8 for the corner point and 4 for the edge points.

Conclusions

Several points were brought out in the text that bear emphasis. When spatially averaged, the Classical Modal Analysis (CMA) response approaches the Asymptotic Modal Analysis (AMA) response more rapidly as the number of modes increases, $\Delta N_A \to \infty$. However, information about local response intensification is lost in the averaging process. Examination of local response as $\Delta N_A \to \infty$ revealed an almost uniform response throughout the interior cavity field with the exception of peaks at the boundaries, i.e., sides, edges, and corners.

Although a larger bandwidth at a given center frequency contains more excited modes than a smaller bandwidth, AMA is often modestly more accurate in the smaller bandwidth. This is because the increased variation of natural frequencies from one mode to the next in the larger bandwidth decreases the accuracy of the AMA result. Finally it is noted that all AMA asymptotes were approached from below by CMA with fixed bandwidth and increasing center frequency.

Future Work

- **Basic Theory for Asymptotic Modal Analysis**

  $\Delta M \equiv$ number of structural modes
  $\Delta N_A \equiv$ number of cavity acoustic modes

  The theory for
  $\Delta M \to \infty$, ΔN_A finite
  and $\Delta M \to \infty$, $\Delta N_A \to \infty$
  has been worked out as has been discussed in the text. The case ΔM finite and $\Delta N_A \to \infty$ has yet to be considered. Of course the case, ΔM finite and ΔN_A finite, is simply classical modal analysis.
- **Numerical Studies.** Further work might include studies of the reduction of the moving portion of the wall to a point source. In this paper an entire wall is taken as the moving area. It would also be interesting to consider more complex cavity geometries. The rectangular cavity shape was chosen for this study because its modal characteristics are well known and therefore comparison of CMA with AMA was a readily feasible task.
- **Experimental Studies.** An experimental study should be undertaken to assess the predictions of the numerical studies. A rectangular box with a portion of one wall vibrating might be considered.

References

1 Dowell, E. H., "Vibration Induced Noise in Aircraft: Asymptotic Modal Analysis and Statistical Energy Analysis of Dynamical Systems," R82-112447, United Technologies Research Center, January 1983.

2 Lyon, R. H., *Statistical Energy Analysis of Dynamical Systems: Theory and Applications*, the MIT Press, Cambridge, MA, 1975.

3 Dowell, E. H., and Kubota, Y., "Asymoptotic Modal Analysis and Statistical Energy Analysis of Dynamical Systems," ASME *Journal of Applied Mechanics*, Vol. 107, 1985, pp. 949-957.

4 Kubota, Y., and Dowell, E. H., "Experimental Investigation of Asymptotic Modal Analysis and for a Rectangular Plate," *Journal of Sound and Vibration*, Vol. 106, No. 2, 1986, pp. 203-216.

5 Crandall, S. H., "Random Vibration of One- and Two-Dimensional Structures," *Developments in Statistics*, Vol. 2, Krishnaiah, P. R., ed., Academic Press, New York, 1979, pp. 1-82.

6 Crandall, S. H., "Structured Response Patterns Due to Wide-Band Random Excitation," *Stochastic Problems in Dynamics*, Clarkson, B. L., ed., Pitman, London, 1977, pp. 366-389.

7 Itao, K., and Crandall, S. H., "Wide-Band Random Vibration of Circular Plates," ASME *Journal of Mechanical Design*, Vol. 100, 1978, pp. 690-694.

8 Crandall, S. H., and Zhu, W. -Q., "Wide Band Random Excitation of Square Plates," *Random Vibrations and Reliability, Proc. IUTAM Symp.* Frankfurt/Oder, Akademic-Verlag, Berlin, 1983, pp 231-243.

9 Kubota, Y., "Asymptotic Modal Analysis for Sound Fields of a Reverberant Chamber," *Journal of Acoustical Society Japan*, to be published in Japanese. An English version of this paper is in preparation.

10 Crandall, S. H., and Mark, W. D., *Random Vibration in Mechanical Systems*, Academic Press, New York, 1963.

Appendix B:

Peretti, L. F. and E. H. Dowell, "Asymptotic Modal Analysis of a Rectangular Acoustic Cavity Excited by Wall Vibration," AIAA Journal, **30**, 1191-1198, 1991.

AIAA JOURNAL
Vol. 30, No. 5, May 1992

Asymptotic Modal Analysis of a Rectangular Acoustic Cavity Excited by Wall Vibration

Linda F. Peretti* and Earl H. Dowell†
Duke University, Durham, North Carolina 27706

Asymptotic modal analysis, a method that has recently been developed for structural dynamical systems, has been applied to a rectangular acoustic cavity. The cavity had a flexible vibrating portion on one wall, and the other five walls were rigid. Banded white noise was transmitted through the flexible portion (plate) only. Both the location along the wall and the size of the plate were varied. The mean square pressure levels of the cavity interior were computed as a ratio of the result obtained from classical modal analysis to that obtained from asymptotic modal analysis for the various plate configurations. In general, this ratio converged to 1.0 as the number of responding modes increased. Intensification effects were found due to both the excitation location and the response location. The asymptotic modal analysis method was both efficient and accurate in solving the given problem. The method has advantages over the traditional methods that are used for solving dynamics problems with a large number of responding modes.

Nomenclature

A = area
c = speed of sound
F = cavity acoustic modal function
L = cavity dimension
M = generalized mass
p = pressure
r = modal index
V = volume
w = displacement
X,Y,Z = acoustic modal function component dependent on x,y,z
x,y,z = spatial position coordinates
ΔN = number of acoustic modes
ζ = damping ratio
ρ = density
Φ = power spectrum
ω = frequency
$\langle\ \rangle$ = spatially averaged quantity
$\cdot$ = time derivative
$-$ = rms

Subscripts

c = center frequency
f = flexible
o = reference value
r = acoustic modal index
w = pertaining to the flexible wall

Superscripts

A = acoustic

Introduction

COUPLED structural-acoustic systems are encountered often in aeronautical applications. Accurate, efficient means of analysis are central to the design of structures with the desired sound transmittal properties. Two analytical methods that are commonly used to solve such coupled systems are classical modal analysis (CMA) and statistical energy analysis (SEA). Recently, Dowell[1] and others[2-4] have developed an additional method, asymptotic modal analysis (AMA), which can also be applied to structural-acoustic systems.

AMA incorporates the advantages of the other two methods. Providing there are a large number of modes, the CMA result and the AMA result are nearly identical. Since it does not need to take the individual modal contributions into account, the computation cost of AMA is significantly less. An added advantage of AMA is that the degree of generality in the final result can be controlled by adjusting the types of assumptions and/or simplifications made in the derivation. This feature allows the use of AMA to obtain results identical to SEA or, for example, to relax the averaging simplifications and obtain local response results of which SEA is not capable.

To explore the capabilities of AMA, the interior sound field of a rectangular acoustic cavity was analyzed mathematically. The ratio of response predicted by CMA to that predicted by AMA was calculated either as a spatial average or at particular locations inside the cavity. Five of the cavity walls were rigid. A random white noise sound field passed through a portion of the sixth wall into the interior of the cavity. The flexible vibrating portion was varied in size and location, and the resulting sound pressure levels (mean square pressures) in the interior were calculated using AMA and CMA and then compared.

Local response peaks, or intensification zones, were observed at boundary points, while the response in the interior region was nearly uniform. Sound pressure levels were affected by the location and size of the flexible vibrating portion of the wall (sound source). In general, sound pressure levels increased by a factor of 4 when a point was placed in the corner. Also, for small sound sources (smaller than an acoustic wavelength) that are placed in the center of the wall, lines of symmetry become regions of increased sound pressure level.

Background

SEA has been used to study the high-frequency interaction between large, complex, multimodal structures and acoustic spaces. The basic assumption underlying SEA is that the dynamic parameters in the system behave stochastically. SEA relates the power of the applied forces to the energy of the coupled systems and produces a set of linear equations that can be solved for the energy in each system. The energy in the system is the variable of primary interest, and other variables such as displacement, pressure, etc., are found from the energy of vibration. SEA has its advantages, as well as its limitations.

Received Jan. 2, 1991; revision received June 18, 1991; accepted for publication June 26, 1991.

*Research Assistant Professor, Department of Mechanical Engineering and Materials Science, School of Engineering.
†Professor and Dean, Department of Mechanical Engineering and Materials Science, School of Engineering. Fellow AIAA.

The main advantage of SEA is its ability to describe the sound field without having to consider the individual modes. Statistical energy analysis also allows for a much simpler description of the system, requiring only parameters such as modal density, average modal damping, and certain averages of modal impedance to sound sources. The most significant disadvantage of using a statistical approach is that it is only valid for systems whose order is sufficiently high that the stochastic assumptions apply. Certain frequency bandwidths may not contain enough modes to allow the underlying assumptions to hold, rendering the SEA result unreliable. In addition, the local response information is lost in the SEA treatment. The text by Lyon[5] is the standard reference on SEA.

Dowell[1] has shown that results identical to those calculated using SEA can be obtained by studying the asymptotic behavior of CMA for a general, linear (structural) system; this asymptotic approach is AMA. AMA is basically a modal sum method. It possesses all of the computational advantages of SEA, in that the individual modal characteristics do not play a role in the asymptotic analysis. Additionally, AMA has advantages that SEA does not. Since AMA results can be derived systematically from CMA, AMA allows an assessment of the assumptions and consequent simplifications that are made to obtain such results. Also, by using a combination of CMA and AMA, results can be obtained for all frequency bandwidths of interest, not just those with a sufficiently high number of modes. And finally, AMA has predicted local response peaks, or intensification zones, results unobtainable using SEA.[3,4]

Previous work for structural systems has shown that the asymptotic behavior of AMA depends on the number of modes in a frequency interval of interest and the location of point forces. In the limit of an infinite number of modes, all points on the structure have the same response except for some special areas. The exceptional areas (intensification zones) are near the points of excitation and near the structural system boundary.[3,4] Numerical examples were presented for a beam in Ref. 2. Crandall,[6] Itao and Crandall,[7] and Crandall and Kulvets[8] experimentally found intensification zones in their work with structures. The response of a rectangular plate under a point random force was investigated by Kubota and Dowell,[3] and AMA calculations were found to agree closely with experimental measurements.

Work has also been done using AMA for structural-acoustic systems. Kubota et al.[4] examined a rectangular acoustic cavity with one vibrating wall (the other five rigid). They assumed that the vibrating wall had an infinite number of structural modes responding and that the entire wall was oscillating. The results obtained from the numerical study indicated that the spatially averaged CMA response approaches the AMA response as the number of modes increases. The local asymptotic response revealed an almost uniform distribution in the cavity interior, with peaks at the boundaries (sides, edges, and corners) of the cavity. Here, an AMA method is presented and new results obtained for structural-acoustic systems where only a portion of the wall vibrates rather than the entire wall, and both the size and location of the oscillating portion are varied.

Theory

Most coupled structural acoustic problems are modeled using either CMA, summing for the response of each mode, or SEA, which combines the predicted energies of the subsystems and coupling loss factors to obtain a final result. In this work, a comparison is made between the CMA result and the AMA result as the number of acoustic modes and the number of structural modes approaches infinity. Note that the spatially averaged AMA result is identical to the SEA result.

In order to calculate the response of the interior acoustic cavity to the transmission of noise through a structural wall on its boundary, both the structural modes of the wall and the acoustic modes of the interior must be considered. As derived in Ref. 4, the CMA result for the mean square pressure at a point (x,y,z) in a structural-acoustic enclosure is

$$\frac{\bar{p}^2}{(\rho_o c_o^2)^2} \cong \frac{\pi}{4}\frac{A_f}{V^2}\Phi_{\ddot{w}}(\omega_c)\sum_r \frac{F_r^2(x,y,z)}{(M_r^A)^2(\omega_r^A)^3\zeta_r^A} \times \iint_{A_f} F_r^2(x,y,z_o)\,dx\,dy \tag{1}$$

Implicit in this result are the following assumptions: the number of structural modes within the frequency band of interest is large (i.e., approaches infinity), and the power spectrum of the wall response is slowly varying with respect to frequency relative to the rapidly varying acoustic modal transfer function. As a result of these assumptions, the modal dynamics of the structure are effectively removed from the problem. In other words, the structural system is described in the AMA limit, whereas the acoustic system is taken in the CMA limit. Further, it is assumed that the modal damping ratio is small ($\ll 1$), which removes the coupling between acoustic modes (see Ref. 9 for justification).

To obtain the AMA result for the acoustic cavity, further assume that the acoustic generalized mass squared $(M_r^A)^2$, the frequency of the acoustic mode cubed $(\omega_r^A)^3$, and the acoustic damping (ζ_r^A) do not vary rapidly with respect to modal number r and can therefore be replaced by their values at the center frequency, $(M_c^A)^2$, $(\omega_c^A)^3$, and (ζ_c^A). Moreover, the expression

$$\sum_r F_r^2(x,y,z)\iint_{A_f} F_r^2(x,y,z_o)\,dx\,dy$$

is approximately equal to the average of $F_r^2(x,y,z)$ times

$$\sum_r \iint F_r^2(x,y,z_o)\,dx\,dy \qquad \text{as } r\to\infty$$

(i.e., a large number of acoustic modes). The previous expression can be further simplified by

$$\sum_r \iint_{A_f} F_r^2(x,y,z_o)\,dx\,dy = \sum_r A_f\langle X_r^2\rangle_{A_f}\langle Y_r^2\rangle_{A_f}\langle Z_r^2(z_o)\rangle_{A_f}$$

where the right-hand side reduces to

$$A_f\Delta N^A\frac{\langle F_c^2\rangle}{\langle Z_c^2\rangle}$$

where $\langle Z_c^2\rangle = \langle F_c^2\rangle/\langle F_c^2\rangle_{A_f}$. Here, $\langle F_c^2\rangle$ is a volume average, and $\langle F_c^2\rangle_{A_f}$ is an average over the vibrating structural wall area. Then,

$$\frac{\bar{p}^2}{(\rho_o c_o^2)^2} \cong \frac{\pi\Phi_{\ddot{w}}(\omega_c)A_f^2\langle F_c^2\rangle\sum_r F_r^2(x,y,z)}{4V^2(M_c^A)^2(\omega_c^A)^3\zeta_c^A\langle Z_c^2\rangle} \tag{2}$$

This result is the AMA representation for the acoustic cavity, which assumes that there are both a large number of acoustic modes and a large number of structural modes. It is valid at any point x,y,z inside the acoustic cavity and is not a spatial average. The spatial average of Eq. (2) is

$$\frac{\langle\bar{p}^2\rangle}{(\rho_o c_o^2)^2} \cong \frac{\pi}{4}\left(\frac{A_f}{V}\right)^2\frac{\Delta N}{\Delta\omega^A}\frac{\langle\bar{\ddot{w}}^2\rangle_{\Delta\omega}}{(\omega_c^A)^3\zeta_c^A\langle Z_c^2\rangle} \tag{3}$$

This expression is referred to as the spatially averaged AMA result (⟨AMA⟩) and is used as the denominator throughout the analysis.

The effect of the source position is included in the term $\langle Z_c^2\rangle$, which is a ratio of the spatially averaged modal functions over the volume to that over the flexible wall area. Except for this term, the expression in Eq. (3) is independent of the

cavity geometry. The $\langle Z_c^2 \rangle$ ratio will always be of order 1. Specifically, for a rectangular geometry when the flexible portion is well removed from a corner or an edge, or for a cylindrical cavity with a vibrating portion on one of the ends (but away from the edge), $\langle Z_c^2 \rangle = 1/2$. The usual AMA result assumes this value of $\langle Z_c^2 \rangle$; however, the cases where the flexible portion is placed at a corner or an edge are easily accounted for in the $\langle Z_c^2 \rangle$ term and result in an additional multiplicative factor of 1/4 or 1/2, respectively.

In order to separate the effects of the response position inside the cavity from the position of the flexible portion A_f of the wall (source position), two ratios were used, $\langle \text{CMA} \rangle / \langle \text{AMA} \rangle$ and $\text{CMA}_{\text{local}} / \langle \text{AMA} \rangle$. Several combinations of CMA and AMA, spatially averaged and local results, were possible. The motivation for the choice of these particular ratios is presented in the Discussion section of this paper. The first ratio, comparing the spatial averages computed by the two methods, is used to demonstrate the convergence of the CMA results toward AMA as a function of frequency. The spatially averaged results are also used to demonstrate the overall effect of excitation position on sound pressure level. The second ratio is used to study local behavior at particular points inside the acoustic cavity. This ratio is therefore used to demonstrate the effect of response position independent of source position, as well as the combined effects of source position and local response position.

The ratio of the spatial average of CMA to the spatial average of AMA is

$$\frac{\text{CMA}}{\langle \text{AMA} \rangle} = \sum_r \frac{\langle F_r^2(x,y,z) \rangle}{(M_r^A)^2(\omega_r^A)^3} \frac{\iint_{A_f} F_r^2(x,y,z_o)\,dx\,dy (\omega_c^A)^3 \langle Z_c^2 \rangle}{\Delta N^A A_f} \tag{4}$$

This expression is derived in Ref. 4 and can be obtained from Eqs. (1) and (3). Equation (4) was used to assess the effect of excitation size and location due to area change and position of the vibrating portion of the wall.

The separate effect of response position was studied by taking the ratio of the local mean square pressure predicted with CMA to the spatially averaged mean square pressure predicted by AMA:

$$\frac{\langle \text{CMA} \rangle}{\langle \text{AMA} \rangle} = \frac{(\omega_c^A)^3 \langle Z_c^2 \rangle}{\Delta N^A A_f} \sum_r \frac{F_r^2(x,y,z) \iint_{A_f} F_r^2(x,y,z_o)\,dx\,dy}{(M_r^A)^2(\omega_r^A)^3} \tag{5}$$

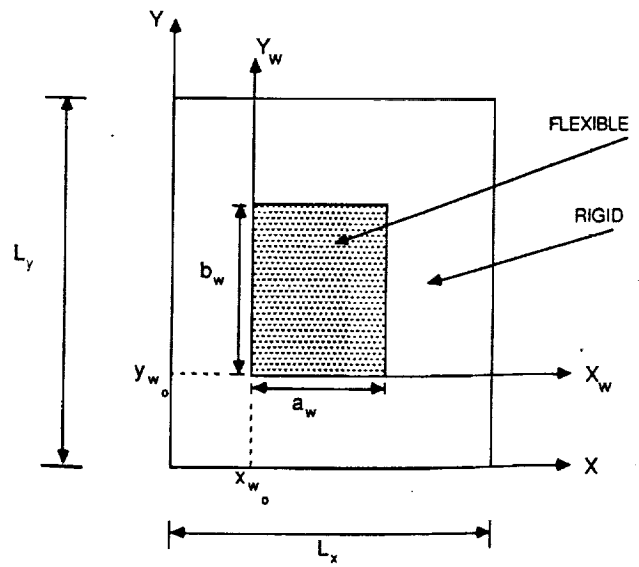

Fig. 1 Flexible vibrating portion of one wall of the cavity.

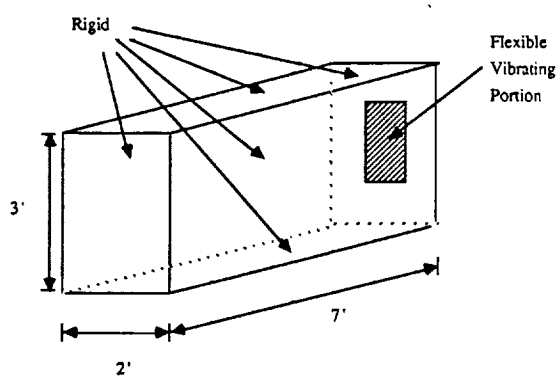

Fig. 2 Rectangular acoustic cavity with a portion of one wall flexible and vibrating.

Equations (1-5) hold for any cavity geometry.

Rectangular Cavity

Dowell et al.[10] have shown that the acoustic pressure for a rectangular cavity with a flexible wall (all others rigid) can be described by the well-known rigid wall expansion or hard box modes for the structure:

$$F_r(x,y,z) = \cos\left(\frac{r_x \pi x}{L_x}\right) \cos\left(\frac{r_y \pi y}{L_y}\right) \cos\left(\frac{r_z \pi z}{L_z}\right)$$

In this analysis, the flexible portion of the structural wall is allowed to vary both in size and position. Therefore, the integral

$$\iint_{A_f} F_r^2(x,y,z_o)\,dx\,dy$$

in Eqs. (4) and (5) becomes

$$\int_0^{a_w} \int_0^{b_w} \cos^2\left[\frac{r_x \pi (x_{w_o} + x_w)}{L_x}\right] \cos^2\left[\frac{r_y \pi (y_{w_o} + y_w)}{L_y}\right] \times \cos^2\left(\frac{r_z \pi z_o}{L_z}\right) dx_w\,dy_w$$

where r_x, r_y, and r_z are modal indices, and x_{w_o}, y_{w_o}, x_w, y_w, L_x, and L_y are defined in Fig. 1. This integral can then be evaluated analytically in terms of the parameters x_{w_o}, y_{w_o} and a_w, b_w. In the previous work by Kubota et al.,[4] which assumed that the entire wall was flexible, this integral over the flexible area A_f divided by A_f evaluated simply to 1/4, which, in general, is not true here since in most cases only a portion of the wall is flexible.

Numerical Study

Description

For the numerical study, a rectangular cavity was considered (Fig. 2). One of its walls, or a portion thereof, was assumed to vibrate in an infinite number of structural modes. The wall was driven with banded white noise. The effects of varying both the size and position of the vibrating portion of the wall were studied. The size of the wall varied from full wall (100% wall area) down to a point (0.004% wall area).

The quantities used in the study were ratios of mean square pressure predicted by CMA to that predicted by AMA. Initially, spatial averages using both CMA and AMA were taken in order to avoid introducing the response location within the cavity as an additional parameter. Later, the local acoustic pressure responses at corner points, edge points, points on the face, and points in the interior were considered for these cases.

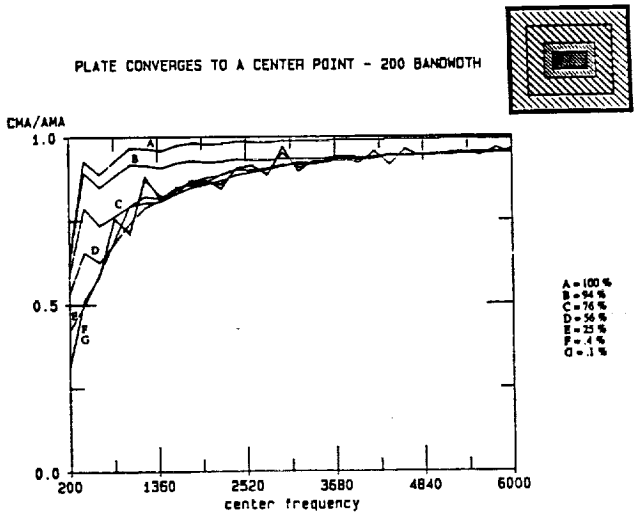

Fig. 3 ⟨CMA⟩/⟨AMA⟩ vs center frequency, 200-Hz fixed bandwidth, flexible area shrinks to center.

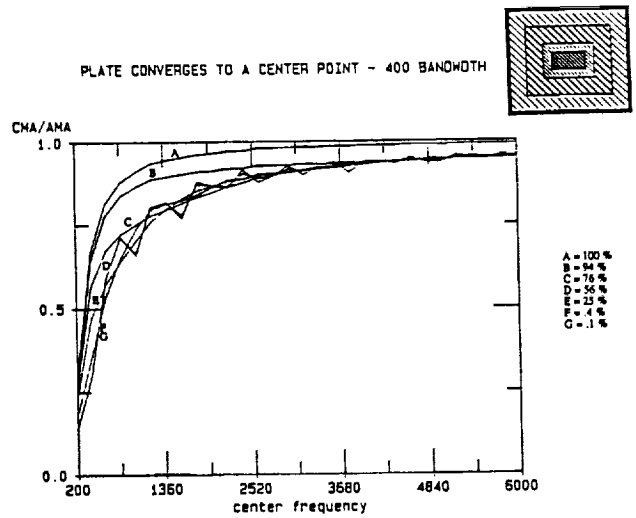

Fig. 4 ⟨CMA⟩/⟨AMA⟩ vs center frequency, 400-Hz fixed bandwidth, flexible area shrinks to center.

Results

Spatially Averaged Case

The ratio of the spatial average of CMA to the spatial average of AMA [Eq. (4)] for the case where the oscillating portion of the wall converges to a center point is shown in Figs. 3–5. Each figure shows the spatially averaged CMA to spatially averaged AMA ratio for a different frequency bandwidth (200, 400, and 600 Hz) as a function of center frequency. The bandwidth $\Delta\omega$ is defined as $\Delta\omega = \omega_{max} - \omega_{min}$, and the center frequency ω_c as $\omega_c^2 = (\omega_{max} \cdot \omega_{min})$, where ω_{max} and ω_{min} are the maximum and minimum frequencies of the frequency interval. All acoustic modes are assumed to have the same modal critical damping ratio ζ ($\zeta \ll 1$).

As can be seen from Figs. 3–5, all results approach unity as the center frequency becomes large. The larger bandwidths yield smoother curves, and the smaller bandwidths approach the asymptote slightly more rapidly. Kubota et al.[4] found similar trends regarding bandwidth effects in the related work. However, what was not expected was that departure from the entire wall oscillating caused litle change in the spatially averaged CMA/AMA ratio for the cavity. This was most likely due to the fact that the oscillating plate was centered about the midpoint on the wall and that all modes are symmetric or antisymmetric about that point.

In Fig. 6, the result of the spatially averaged CMA/AMA ratio [Eq. (4)] for the oscillating plate of variable area and convergence to a point in the corner are shown. Again, plots that correspond to different frequency bandwidths yield similar results, and so only the 400-Hz fixed bandwidth plot is shown. In this case, there is a family of curves that approaches unity as center frequency (and therefore, number of modes) increases, as expected. However, the asymptote is approached from above rather than below for all plates smaller than the quarter wall. The quarter-wall case is equivalent, in terms of the CMA/AMA ratio, to the full wall due to symmetry. The cases where the plate is larger than a quarter panel approach from below as did the center point cases. For those cases in which the vibrating wall is smaller than a quarter panel, not only does the curve approach the asymptote from above, but as the oscillating portion of the wall better approximates a point, the peak of the curve approaches 4 and is slower to drop off to the asymptotic limit of 1. This region of elevated sound pressure level is similar to the intensification zones for structural systems discussed in Crandall,[6] Itao and Crandall,[7] and Crandall and Kulvets[8] and for structural-acoustic systems in Kubota et al.[4] However, the intensification is due to excitation location rather than response location.

It may first apear as if the AMA result does not account for this intensification. However, it was assumed that the excita-

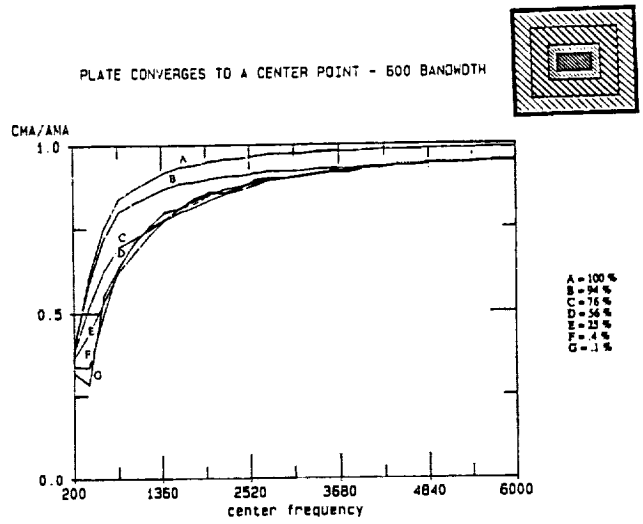

Fig. 5 ⟨CMA⟩/⟨AMA⟩ vs center frequency, 600-Hz fixed bandwidth, flexible area shrinks to center.

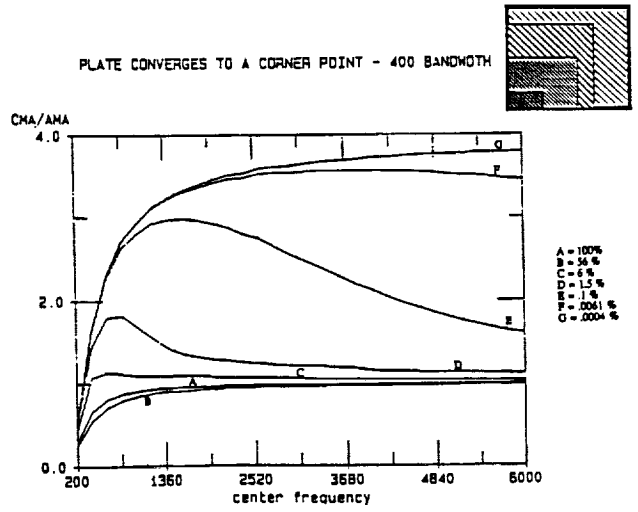

Fig. 6 ⟨CMA/⟨AMA⟩ vs center frequency, 400-Hz fixed bandwidth, flexible area shrinks to corner.

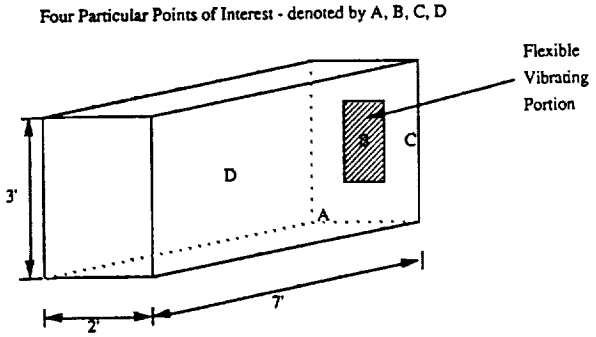

Fig. 7 Points at which the local response was predicted.

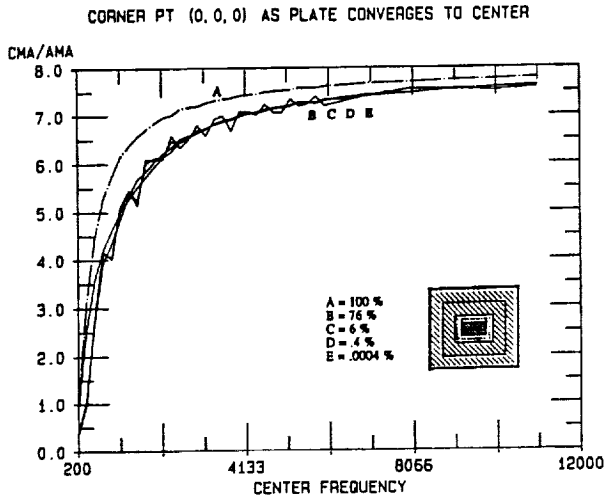

Fig. 8a Local CMA to ⟨AMA⟩ ratio vs center frequency for point A, flexible area shrinks to center.

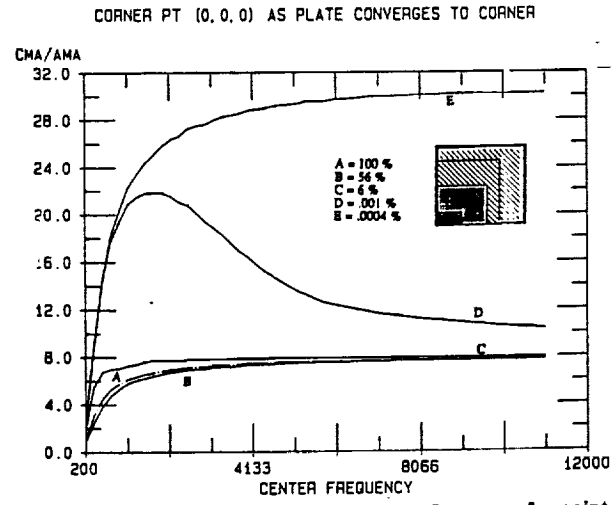

Fig. 8b Local CMA to ⟨AMA⟩ ratio vs center frequency for point A, flexible area shrinks to corner.

tion occurs away from a corner or an edge of the wall in computing the integral over the flexible area in the AMA expression. The effect of excitation intensification can be included in the AMA expression and, for corner excitation, would provide a factor of 4 increase. In addition to studying the effects of varying size and position of the oscillating portion of the wall in a spatially averaged sense, the local response was also calculated.

Local Response

The effect of position in the cavity was determined by considering the local response. This was again done for both convergence of the vibrating plate from a full vibrating wall down to a vibrating point in the center and convergence to a point in a corner of the wall. The results are presented as a ratio of the mean square pressure evaluated at particular points in the cavity using CMA to the spatially averaged mean square pressure predicted by AMA. This ratio was computed for many center frequencies at a constant bandwidth of 400 Hz. There was no need to vary the bandwidth since Figs. 3-5 show little variation with bandwidth. The result was computed for various center frequencies in 200-Hz bandwidth increments up to a center frequency of 6000 Hz. Beyond 6000 Hz, 1000-Hz bandwidth increments were taken up to 11,000 Hz. This produces a smoother looking curve beyond 6000 Hz due to the larger frequency bandwidth increments.

Initially, four special response points were considered (see Fig. 7): the corner point (0,0,0), the midpoint of the flexible wall, the midpoint of the entire cavity, and a point on the wall along the centerline (1.8,1.5,0). For these four points, the ratio of CMA to spatially averaged AMA was plotted as a function of center frequency in Figs. 8-11.

Taking the corner point first (point A in Fig. 7), Fig. 8a shows that, as the plate converges to the center of the wall, the response of the corner approaches a pseudoasymptote of 8, whereas for convergence of the plate to the corner (Fig. 8b), this same point has a pseudoasymptote of 32, a factor of 4 greater. The idea of a pseudoasymptote will be discussed in the following section. The factor of 4 comes from the excitation

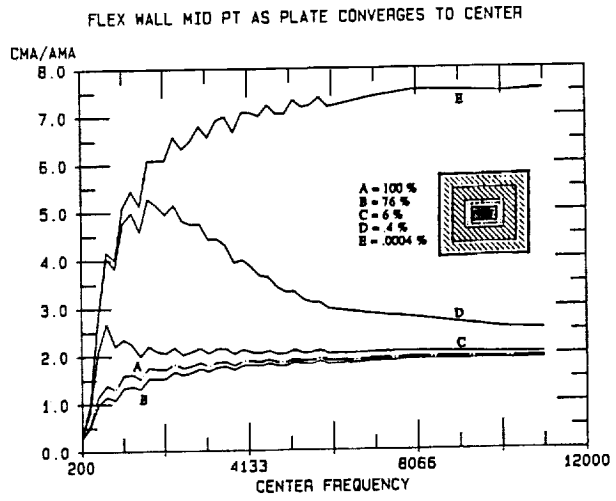

Fig. 9a Local CMA to ⟨AMA⟩ ratio vs center frequency for point B, flexible area shrinks to center.

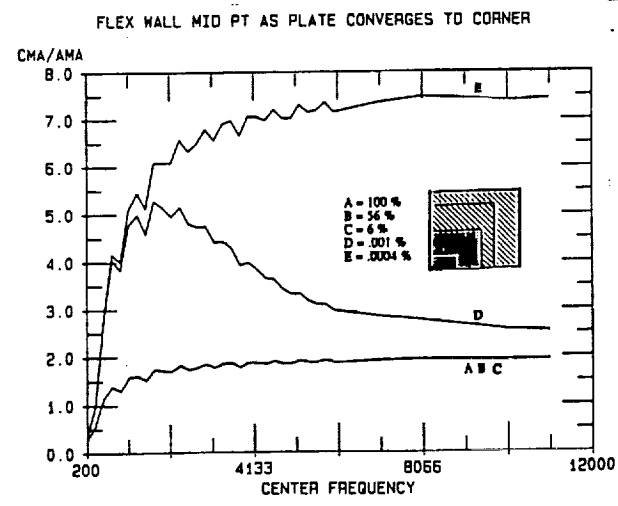

Fig. 9b Local CMA to ⟨AMA⟩ ratio vs center frequency for point B, flexible area shrinks to corner.

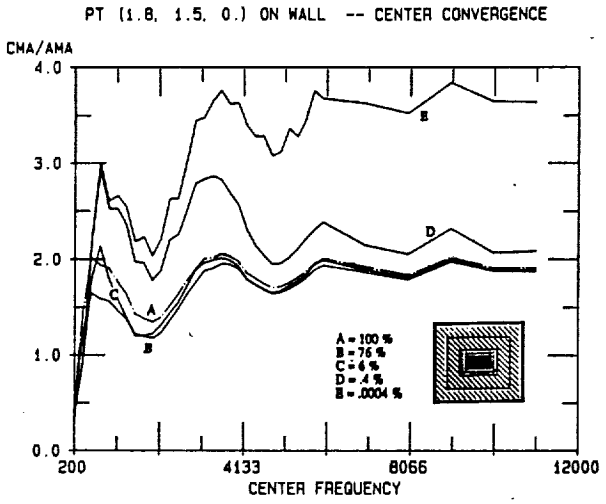

Fig. 10 Local CMA to ⟨AMA⟩ ratio vs center frequency for point C, flexible area shrinks to center.

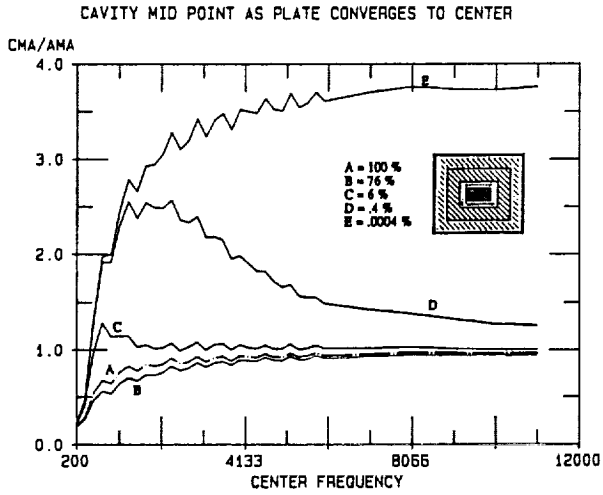

Fig. 11 Local CMA to ⟨AMA⟩ ratio vs center frequency for point D, flexible area shrinks to center.

location (i.e., the location of the point source rather than the point of evaluation being in the corner), as was seen in the spatially averaged cases. Recall that when a point source was in the corner the spatial average was 4 times greater than when the point source was in the center of the wall.

Figures 9a and 9b show that, at the midpoint of the flexible wall (point B in Fig. 7), both types of convergence yield a pseudoasymptote of 8. Since this point is on the wall, its expected pseudoasymptote is 2. However, when the excitation is in the corner (Fig. 9b), this is increased by a factor of 4, hence the value 8. Five curves are actually plotted; only the curves representing the smallest plate areas (0.01 and 0.004%) deviate significantly from the others. On the other hand, when the excitation location and the response location are at the center of the wall (Fig. 9a), the response there is also increased by a factor of 4. This phenomenon is similar to the intensification observed by Kubota and Dowell[3] in experiments where point loads are applied to a rectangular plate. They found that, in the limit of a large number of responding modes on the plate, the response of the plate as measured by the plate acceleration at various places on the plate surface was nearly uniform. The accelerations were significantly higher near the application points of the point loads. Because of symmetry, the effect of a point sound source acting at the center of the wall is to divide the rectangular cavity into quadrants (defined by cutting perpendicular planes through the point source). In the newly defined subcavities, this point where the source is located is now a corner point. The response at a corner point is eight times greater than the interior region, and so the pseudoasymptote of 8 is appropriate for this case.

Kubota and Dowell[3] also found hot lines running perpendicularly through the point force. To test for these in this acoustic cavity analysis, a point along one of the anticipated hot plates was studied (point C in Fig. 7). Since this point is on the face, it is expected to have a pseudoasymptote of 2.0, which is indeed the case if the full wall is moving (dotted line in Fig. 10). However, in the case of center convergence (i.e., analogous to a point load acting at the center of the structural wall), this point lies on a hot plane, and Fig. 10 shows a pseudoasymptote of 4. Assuming that the hot planes divide the cavity into subcavities, this point is on an edge of a subcavity. Therefore, the value of 4 is appropriate since the response at an edge is four times greater than the interior. When the oscillating portion of the wall converges to the corner, the pseudoasymptote is 8. This is consistent with previous findings for

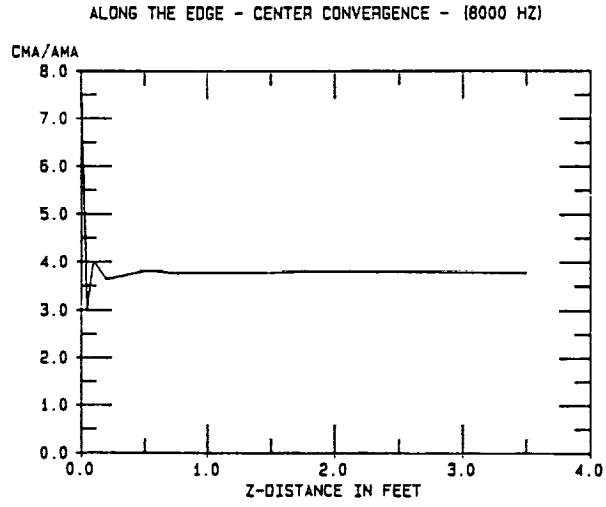

Fig. 12 Local CMA to ⟨AMA⟩ ratio vs distance along an edge of the cavity away from a corner, with a point sound source in the center of the wall.

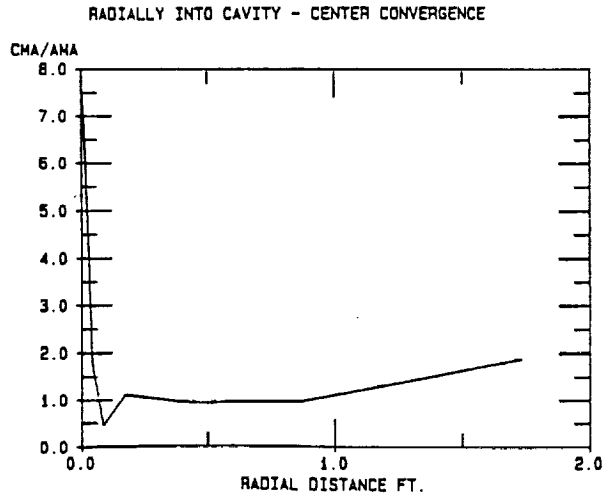

Fig. 13 Local CMA to ⟨AMA⟩ ratio vs distance radially into the cavity away from a corner, with a point sound source in the center of the wall.

corner convergence since it represents a factor of 4 increase over the expected value for a point on a wall.

Response at the midpoint of the entire cavity (point D in Fig. 7) was also considered. At an interior point such as this, the expected asymptote is 1.0. However, when the plate converges to the center of the wall (Fig. 11), this point lies on a plane of symmetry resulting in a factor of 4 increase. Similar to the previous case, this point now lies on an edge of a newly defined subcavity. The edge point response is four times greater than the interior, and so the center convergence case is consistent. When the plate converges to a corner of the wall, again a fourfold increase is expected, due to the previous results for the spatially averaged cases, and the result is a pseudoasymptote of 4 (see curve E in Fig. 11).

Points A–D were studied as the plate size was allowed to vary, for the two cases (sound source shrinking from a full wall to a point sound source in a corner of the wall, and to a point in the center of the wall) as a function of center frequency (for a fixed bandwidth). Next, the plate size was fixed at 0.004% of the wall area, corresponding to a vibrating point. The center frequency was fixed at a value at which the pseudoasymptotes had previously been reached (8000 Hz), and the bandwidth was fixed at 400 Hz. The distance into the cavity from the vibrating wall was varied. Sample plots of local CMA to spatially averaged AMA vs distance into the cavity are shown in Figs. 12 and 13.

In Fig. 12, the sound source (vibrating point) is located in the center of the wall, and the response is plotted along an edge. The peak response in the corner is 8. Moving away from the corner, the response then oscillates before approaching the asymptote for an edge, which is 4.0. The data are symmetric in the z direction, as can be shown analytically. Therefore, only half of the edge length is plotted (3.5 out of 7.0 ft). The purpose of this plot is to show that there is a region where the transition is made from the increased (intensification) value to the nearly uniform value farther away. Further studies are needed to examine this transition zone and the parameters that determine its thickness.

Figure 13 is a plot of the response in a radial direction away from the corner of the cavity for the sound source in the center of the wall. The radial direction is defined by the line $x=y=z$, and the radial distance is equal to the square root of $(x^2+y^2+z^2)$. Since the point source is in the center of the wall, hot lines exist that run down the center of the cavity. Because of these hot lines, which redefine new effective boundary points, the cavity interior is no longer uniform, as is shown in Fig. 13. After the radial distance of 1.0, the response begins to increase, and approaches a value of 2.0, as if there were a wall or face there. This is not a physical boundary created by the cavity geometry, but rather an artificial boundary created by the point source. If the same radial trajectory is taken with the point source located in the corner, the response of the interior is uniform. The peak value in the corner is 32; the response then oscillates and eventually approaches a uniform interior value of 4.0. This plot shows the theoretical existence of hot planes or surfaces inside the cavity that are created by a point source acting at the center of the wall.

In summary, for a vibrating point at the center of the wall, the asymptotic limit for points that do not lie on hot planes is 1.0 for interior points, 2.0 for points on a face, 4.0 for points on an edge, and 8.0 for corner points. Also, the corner convergence cases yield the same relationships between locations but the magnitudes are increased by a factor of 4. Hot planes can be thought of as dividing the cavity into subcavities or quadrants along lines of symmetry. Each subcavity then produces its own corner, edge, and face points, with the respective sound pressure levels relative to each other, thereby redefining effective boundary points. The intensification results that were obtained here were through the use of CMA; however, AMA is capable of predicting intensification as well, as is pointed out in the next section. In subsequent work,[11] intensification zones are studied using an extension of the AMA method.

Discussion

The term in the CMA/AMA equation [Eq. (4) or (5)] that is affected by changing the flexible area size and location of the flexible portion is

$$\iint_{A_f} F_r^2(x,y,z_o)\,dx\,dy/A_f$$

This can be thought of as a spatial average of the acoustic modal function in two dimensions (x and y). The expected result would be ¼, unless the argument of one or both cosine functions (in F_r) is always zero or a multiple of π. When the plate converges to a point in the corner, the x and y values are essentially zero; therefore, the value for the cosine is equal to 1 and the spatial average would then be 1.0 rather than ¼. Mathematically, the effect of shrinking the area down to a point in the corner yields a fourfold increase in the relative mean square pressure locally or spatially averaged.

However, one can imagine driving the frequency up so high that the approximated corner point no longer behaves like a point compared to an acoustic wavelength. This occurs when the acoustic wavelength becomes so small that the fixed physical size of the sound source is much larger than the wavelength of sound at that frequency. It is for this reason that the term pseudoasymptote has been used rather than asymptote. As the center frequency becomes sufficiently large (i.e., wavelength sufficiently small), the true asymptote will always be 1.0 for the spatially averaged CMA/AMA ratio.

Throughout this study, the numerical results have been presented either as the ratio of spatially averaged CMA to spatially averaged AMA, $\langle \text{CMA}\rangle/\langle \text{AMA}\rangle$, or for the ratio of local CMA response to spatially averaged AMA response. Other possible ratios could have been used. An alternative choice could have been the ratio of local CMA to local AMA. However, this ratio would not show any variation between points on a boundary and points in the interior. It would approach 1.0 at high center frequencies for all points if the excitation were in the center, or 4.0 if the excitation were in the corner, as is shown in the following analysis.

The local AMA result is [Eq. (2)]

$$\frac{\bar{p}^2}{(\rho_o c_c^2)^2} \cong \frac{\pi}{4}\frac{A_f}{V^2}\Phi_{\ddot{w}}(\omega_c)\frac{A_f \Delta N^A \langle F_c^2\rangle}{(M_c^A)^2(\omega_c^A)^3\zeta_c^A\langle Z_c^2\rangle}\sum_r \frac{F_r^2(x,y,z)}{\Delta N^A}$$

whereas the spatially averaged AMA result (derived in Ref. 4) is

$$\frac{\langle \bar{p}^2\rangle}{(\rho_o c_c^2)^2} \cong \frac{\pi}{4}\frac{\Delta N^A}{\Delta\omega^A}\left(\frac{A_f}{V}\right)^2\frac{\Delta\omega\Phi_{\ddot{w}}(\omega_c)}{(\omega_c^A)^3\zeta_c^A\langle Z_c^2\rangle} \tag{6}$$

Therefore, the ratio of local AMA to spatially averaged AMA is

$$(\text{AMA})_{\text{local}}/\langle \text{AMA}\rangle_{\text{spatial average}} = \left[\sum F_r^2(x,y,z)/\Delta N^A\right]\Big/\langle F_c^2\rangle$$

The numerator

$$\left[\sum F_r^2(x,y,z)/\Delta N^A\right]$$

is equal to ⅛ when x, y, and z are not zero or L_x, L_y, L_z. It is equal to ¼ when one of the values of x, y, or z is equal to 0 or the length of the cavity in the appropriate direction, which is true on any face. Similarly, the numerator becomes ½ for an edge point and 1 for a corner point.

The spatially averaged acoustic modal function evaluated at the center frequency $\langle F_c^2\rangle$, which comprises the denominator of the $(\text{AMA})_{\text{local}}/\langle \text{AMA}\rangle_{\text{spatial average}}$ ratio, is always equal to ⅛. Therefore, the $(\text{AMA})_{\text{local}}/\langle \text{AMA}\rangle_{\text{spatial average}}$ is summarized in Table 1.

Table 1 Local to spatial average-AMA ratios

Location	$AMA_{local}/\langle AMA\rangle$
Corner	$(1)/(1/8) = 8$
Edge	$(1/2)/(1/8) = 4$
Face	$(1/4)/(1/8) = 2$
Interior	$(1/8)/(1/8) = 1$

Recall that the local CMA to spatially averaged AMA ratio for the center convergence case yields pseudoasymptotes of 8 in the corner, 4 on an edge, 2 on a face, and 1 in the interior. These ratios are four times greater if the excitation is in a corner.

This indicates that, for a large number of modes, the AMA results agree locally with the exact (CMA) results predicted when the oscillating wall is a full wall or converging toward the center. For corner convergence, the difference is a factor of 4. In deriving the AMA result used in this study, it was assumed that the excitation occurs at a location other than in a corner or on an edge, which accounts for the factor of 4 difference between center excitation and corner excitation, as explained previously. It is possible to incorporate the excitation location effect into the AMA result, if desired.

Conclusions

An AMA approach has been developed and applied to a coupled structural-acoustic problem. It is broadly applicable to any linear dynamic system at high frequency regardless of geometry, assuming that the damping is small. Further work is needed to develop an AMA result that is applicable for cases involving large damping.

It is an extremely flexible approach and can be developed in accord with the nature of the system under study through inclusion of a series of simplifying assumptions. This technique can thereby bridge the gap between CMA and SEA in terms of computational requirements and predictive capability. In that AMA is developed from CMA, it retains the capability to predict spatial variations (intensification) in sound pressure levels or other relevant responses, something of which SEA is not capable. On the other hand, simplifications arising from the nature of the forces and the number of structural and acoustic modes involved result in a process that does not require individual modal characteristics. This greatly reduces the number of calculations required relative to CMA.

A rectangular acoustic cavity, with five rigid walls, was chosen to investigate the capabilities of AMA. Spatial averages and local behavior for sound pressure levels were calculated for a number of cases involving the location and size of the sound source on the wall. For the spatially averaged cases, intensification due to source location was observed. In particular, when a point sound source was located in the corner as opposed to the center of a wall, the spatially averaged sound pressure ratio was increased by a factor of 4.

In addition to the spatial average, the local response was also calculated. The local response of the cavity interior is nearly uniform, with the exception of points on the structural boundary (walls, edges, and corners), when one entire wall of the rectangular cavity is vibrating. However, when only a portion of one wall vibrates, and particularly when this portion approaches a vibrating point, there are further exceptions. Perpendicular planes (hot planes) that run through the vibrating point were found to divide the cavity into subcavities, which have new corners, edges, and walls. New subcavity corners, edges, and walls exhibit the same relative increase as the original corners, edges and walls, which is eight, four, and two times greater than the interior, respectively.

Acknowledgments

This work was supported by the Structural Acoustics Branch of NASA Langley Research Center through Grant NAG-1-709 and NASA Graduate Student Researchers Program Fellowship NGT-50342. The authors would like to thank Donald B. Bliss of Duke University for his insightful comments and discussions related to this work.

References

[1]Dowell, E. H., "Vibration Induced Noise in Aircraft: Asymptotic Modal Analysis and Statistical Energy Analysis of Dynamical Systems," United Technologies Research Center, R82-112447, 1983.

[2]Dowell, E. H., and Kubota, Y., "Asymptotic Modal Analysis and Statistical Energy Analysis of Dynamical Systems," *Journal of Applied Mechanics,* Vol. 52, No. 4, 1985, pp. 949–957.

[3]Kubota, Y., and Dowell, E. H., "Experimental Investigation of Asymptotic Modal Analysis for a Rectangular Plate," *Journal of Sound and Vibration,* Vol. 106, No. 2, 1986, pp. 203–216.

[4]Kubota, Y., Dionne, H. D., and Dowell, E. H., "Asymptotic Modal Analysis and Statistical Energy Analysis of an Acoustic Cavity," *Journal of Vibration, Acoustics, Stress and Reliability in Design,* Vol. 110, No. 3, 1988, pp. 371–376.

[5]Lyon, R. H., *Statistical Energy Analysis of Dynamical Systems: Theory and Applications,* MIT Press, Cambridge, MA, 1975.

[6]Crandall, S. H., "Random Vibration of One- and Two-Dimensional Structures," *Developments in Statistics,* Vol. 2, edited by P. R. Krishnaiah, Academic, New York, 1979, pp. 1–82.

[7]Itao, K., and Crandall, S. H., "Wide-Band Random Vibration of Circular Plates," *Journal of Mechanical Design,* Vol. 100, 1978, pp. 690–695.

[8]Crandall, S. H., and Kulvets, A. P., "Source Correlation Effects on Structural Response," *Application of Statistics,* edited by P. R. Krishnaiah, North-Holland, New York, 1977, pp. 168–182.

[9]Dowell, E. H., "Reverberation Time, Absorption, and Impedance," *Journal of the Acoustical Society of America,* Vol. 64, No. 1, 1978, pp. 181–191.

[10]Dowell, E. H., Gorman, G. F., III, and Smith, D. A., "Acoustoelasticity: General Theory, Acoustic Natural Modes and Forced Response to Sinusoidal Excitation, Including Comparisons with Experiment," *Journal of Sound and Vibration,* Vol. 52, No. 4, 1977, pp. 519–542.

[11]Peretti, L. F., and Dowell, E. H., "Study of Intensification Zones in a Rectangular Acoustic Cavity," *AIAA Journal*, Vol. 30, No. 5, pp. 1199–1206.

Appendix C:

Peretti, L. F. and E. H. Dowell, "Study of Intensification Zones in a Rectangular Acoustic Cavity," AIAA Journal, **30**, 1199-1206, 1991.

AIAA JOURNAL
Vol. 30, No. 5, May 1992

Study of Intensification Zones in a Rectangular Acoustic Cavity

Linda F. Peretti* and Earl H. Dowell†
Duke University, Durham, North Carolina 27706

The interior acoustic field of a rectangular acoustic cavity, which is excited by the structural vibration of one of its walls, or a portion of the wall, has been studied. Particularly, the spatial variations of sound pressure levels from the peak levels at the boundaries (intensification zones) to the uniform interior are considered. Analytical expressions, which describe the intensification zones, are obtained using the methodology of asymptotic modal analysis. These results agree well with results computed by a discrete summation over all of the modes. The intensification zones were also modeled as a set of oblique waves incident upon a surface. The result for a rigid surface agrees with the asymptotic modal analysis result. In the presence of an absorptive surface, the character of the intensification zone is dramatically changed. The behavior of the acoustic field near an absorptive wall is described by an expression containing the rigid wall result plus additional terms containing impedance information. The important parameter in the intensification zone analysis is the bandwidth to center frequency ratio. The effect of bandwidth is separated from that of center frequency by expanding the expression about the center frequency wave number. The contribution from the bandwidth is second order in bandwidth to center frequency ratio.

Nomenclature

A	= area
c	= speed of sound
F	= cavity acoustic modal function
f	= frequency
k	= wave number
L	= cavity dimension
M	= generalized mass
n	= modal index
p	= pressure
r_b	= real part of impedance
V	= volume
w	= displacement
x,y,z	= spatial position coordinates
x_b	= imaginary part of impedance
z_b	= impedance at the boundary
ΔN	= number of acoustic modes
ζ	= damping ratio
ρ	= density
Φ	= power spectrum
ω	= frequency
$\langle\ \rangle$	= spatially averaged quantity

Subscripts

b	= bandwidth
c	= center frequency
f	= flexible
o	= reference value
r	= acoustic modal index

Superscripts

A	= acoustic
$\cdot$	= time derivative
$\bar{}$	= (overbar on pressure) rms
$\bar{}$	= (overbar on impedance quantities) nondimensionalized by ρc

Received March 11, 1991; revision received July 8, 1991; accepted for publication July 9, 1991.

*Research Assistant Professor, Department of Mechanical Engineering and Materials Science, School of Engineering.
†Dean and Professor, Department of Mechanical Engineering and Materials Science, School of Engineering.

Introduction

In structural-acoustic coupled systems, such as the interior of an automobile or an aircraft fuselage, an acoustic field is created by the structural vibration of a wall or walls of the enclosure. This problem has been studied previously using asymptotic modal analysis (AMA) on a rectangular acoustic cavity.[1,2] The cavity was assumed to be entirely rigid except for a vibrating portion of one of its walls. The vibrating portion contained a large number of structural modes, which in turn generated a large number of acoustic modes in the interior space. Acoustic theory predicts, and the previous numerical work has shown, that there are intensification zones in the acoustic field near the cavity boundary and an otherwise uniform response in the interior region. This is due to the lack of spatial correlation in the interior and the imposition of spatial correlation at the boundaries. For a rectangular acoustic cavity, it is well known that the mean square pressures are eight, four, and two times the uniform interior pressure levels at the corners, edges, and faces, respectively.[3-5]

In designing acoustic spaces, allowances must be made for these intensification zones. Therefore, it is important to determine the characteristic distance over which the response levels change from their peak values at the boundary to the uniform interior level. If the distance from a boundary is nondimensionalized by the center frequency wave number k_c, then the intensification zone can be described by the nondimensionalized spatial variable $k_c x$ and the bandwidth to center frequency ratio f_b/f_c. Significantly, the parametric dependence is independent of cavity dimensions. The spatial variation of mean-square pressure is also independent of cavity dimensions. The spatial variation of mean-square pressure is also independent of the size of vibrating or absorptive surfaces on the cavity wall, provided that the surfaces are very large compared to an acoustic wavelength (high-frequency limit) and provided that the damping is small.

The dependence on bandwidth can be separated mathematically from the dependence on center frequency through a Taylor series expansion in f_b/f_c taken about the center frequency wave number. It is found that the bandwidth dependence is a higher order effect. The resulting mathematical expression for mean-square pressure consists of a term that is dependent only on the center frequency, plus terms that contain the bandwidth to center frequency ratio; but these terms are of order $\mathcal{O}[(f_b/f_c)^2]$ and higher.

Using AMA, the spatial variation of mean-square pressure was found to be independent of cavity dimensions. This suggests that the problem can also be analyzed as a local problem consisting of an infinite number of oblique acoustic waves incident upon a rigid surface from all possible angles. The solution to that problem is equivalent to that derived from AMA.

In the same manner, an expression can be obtained for the spatial variation of mean-square pressure, which describes the intensification zone near a boundary for a case where the incident wall is nonrigid (i.e., finite impedance cases). This result can be written in terms of a hard wall component plus an absorption correction term, which contains the impedance information.

The purpose of this research is to determine the structure of these intensification zones and their relation to the entire acoustic field. It is hoped that this work will lead to better design and analysis of acoustic spaces by providing a more thorough understanding of intensification zones for both rigid and absorptive walls.

Background

Intensification zones for structures have been studied extensively by Crandall[6] and others for random vibrations of plates (see, e.g., Refs. 6–8). They have found that the response of the plate at high frequency is relatively uniform, with exceptions occurring at the point of application of a force and/or at the boundaries, depending on loading conditions and boundary conditions. Kubota and Dowell[9] found similar intensification phenomena for a rectangular plate excited by random vibration of a point force. They used AMA to predict the response of the plate, and they verified their results with experimental data.

The study of intensification zones in acoustic spaces was first begun by Waterhouse[10] in the 1950s. His pioneering work on interference patterns in reverberant sound fields was followed by further research by Chu,[11,12] Tohyama and Suzuki,[13] and others [14,15] who were specifically interested in the placement of microphones in reverberation chambers. The results presented here for rigid wall boundaries agree with the earlier work, although the derivations are different. References 10–15 were restricted to rigid walls only. Later work by Waterhouse and Cook[16] included the treatment of pressure release ($p = 0$) boundary conditions.

Parameterization of Intensification Zone

Asymptotic Modal Analysis Approach

A rectangular acoustic cavity with five rigid walls and one vibrating wall has been studied previously using AMA. A diagram of this problem is shown in Fig. 1. The vibrating wall was driven by white noise such that a large number of structural modes was excited in a particular bandwidth. It was assumed that a large number (approaching infinity) of acoustic modes was present in the interior acoustic cavity, and that these modes were temporally uncorrelated. Although it is not assumed in the AMA derivation, a consequence of the previous assumptions is that the acoustic modes are spatially uncorrelated as well. From Refs. 1 and 2, the expression for the mean-square pressure for a finite number of acoustic modes and an infinite number of structural modes is

$$\frac{\bar{p}^2}{(\rho_o c_o^2)^2} \cong \frac{\pi}{4}\frac{A_f}{V^2}\Phi_w(\omega_c)\sum_r \frac{F_r^2(x,y,z)}{(M_r^A)^2(\omega_r^A)^3\zeta_r^A} \times \iint_{A_f} F_r^2(x,y,z_o)\,dx\,dy \tag{1}$$

As in AMA, M_r^A and ζ_r^A can be treated as constant in a band and can therefore be evaluated at the center frequency. Thus, for example, M_r^A becomes M_c^A, etc. Normalizing $\bar{p}^2$ by the spatially averaged $\bar{p}^2$ yields the following expression for the nondimensionalized mean-square pressure in the rigid cavity with one entire wall flexible and vibrating:

$$\frac{\bar{p}^2}{\langle\bar{p}^2\rangle} \cong \frac{\sum_r F_r^2(x,y,z)/(\omega_r^A)^3}{\sum_r \langle F_r^2(x,y,z)\rangle/(\omega_r^A)^3} \tag{2}$$

where the quantities in $\langle\,\rangle$ are spatially averaged values. This is the expression that describes the intensification zone near a boundary; it is a ratio of the local mean-square pressure to the spatially averaged (or uniform interior value) mean-square pressure. At interior points, this ratio will asymptotically (for $r \to \infty$) approach 1.0, whereas at the boundaries, the ratio will be 2.0, 4.0, or 8.0 for walls, edges, or corners, respectively. There are several possible transitions to study: from a corner to an edge, a wall, or the interior; from an edge to a wall or the interior; and from a wall to the interior. For each case, there are one-, two-, and three-dimensional modes to consider.

For the rectangular acoustic cavity, Dowell et al.[17] have shown that hard-box modes can be used to describe the interior acoustic field, even when all six walls are not rigid. Therefore,

$$F_r^2(x,y,z) = \cos^2\left(\frac{n_x\pi x}{L_x}\right)\cos^2\left(\frac{n_y\pi y}{L_y}\right)\cos^2\left(\frac{n_z\pi z}{L_z}\right)$$

$$(\omega_r^A)^2 = \left(\frac{n_x\pi c}{L_x}\right)^2 + \left(\frac{n_y\pi c}{L_y}\right)^2 + \left(\frac{n_z\pi c}{L_z}\right)^2$$

One-Dimensional

Considering one-dimensional modes only, $F_r = \cos(n\pi x/L_x)$ and $\omega_r^A = n\pi c/L_x$. Assuming there are a large number of acoustic modes, which is consistent with the AMA approach, the discrete variable n can be treated as a continuous variable. Equation (2) becomes,

$$\frac{\bar{p}^2}{\langle\bar{p}^2\rangle} \cong \frac{\int_n \cos^2\left(\frac{n\pi x}{L_x}\right)\Big/ n^3\,dn}{\frac{1}{2}\int_n 1/n^3\,dn} \tag{3}$$

This integration can be done analytically, and the result is,

$$1 + \frac{f_c^2}{f_u^2 - f_t^2}\left\{\frac{f_c^2}{f_t^2}\cos\theta_t - \frac{f_c^2}{f_u^2}\cos\theta_u + \frac{4\pi x f_c}{c} \times \left(\frac{f_c}{f_u}\sin\theta_u - \frac{f_c}{f_t}\sin\theta_t\right) + \left(\frac{4\pi x f_c}{c}\right)^2 [Ci(\theta_t) - Ci(\theta_u)]\right\} \tag{4}$$

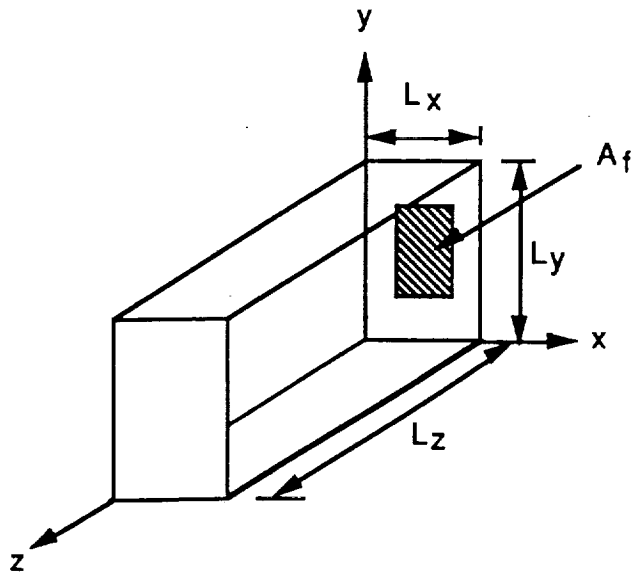

Fig. 1 Rectangular acoustic cavity that was studied.

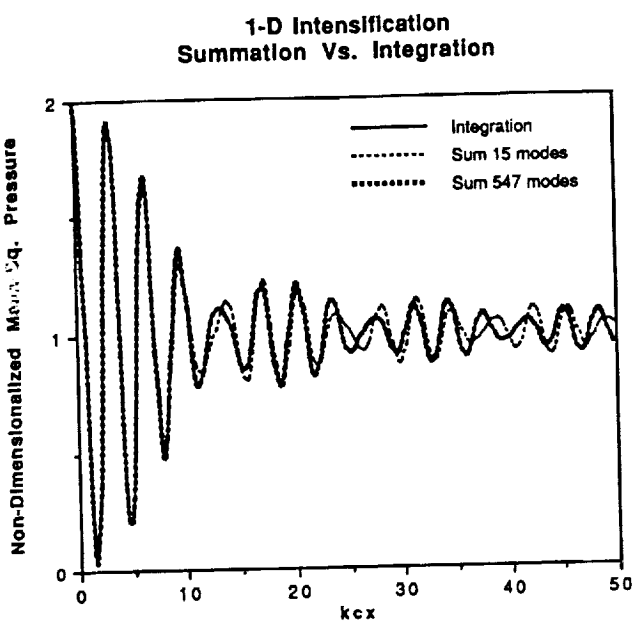

Fig. 2 Nondimensionalized mean-square pressure vs $k_c x$ computed three ways: as an integration in wave-number space, as a summation over 15 modes, and as a summation over 567 modes.

where f_c is the center frequency, f_b the frequency bandwidth, and f_l and f_u are defined as the lower and upper frequencies, respectively, of the frequency interval as follows: $f_u - f_l = f_b$, and $f_c = \sqrt{f_u \cdot f_l}$. The arguments of the cosines and the cosine integral function Ci are defined by $\theta_l = 2^* k_c x^* f_l / f_c$, $\theta_u = 2^* k_c x^* f_u / f_c$, where the nondimensional distance $k_c x$ is equal to $(2\pi f_c)x/c$.

The ratios f_l/f_c and f_u/f_c can be obtained from f_b/f_c using these definitions. In fact, the entire expression (8) can be written in terms of f_b/f_c and $k_c x$, where $k_c x$ is the product of the wave number associated with the center frequency and the distance from the endpoint. Knowing the ratio of frequency bandwidth to center frequency (f_b/f_c) allows the pressure function in the transition zone to be plotted as a function of nondimensionalized distance $k_c x$ away from the endpoint. Note that the dimensions of the cavity do not appear in this result.

If we assume that the frequency is approximately constant over the interval, and allow ω to equal ω_c, the result would be

$$\frac{\bar{p}^2}{\langle \bar{p}^2 \rangle} \cong 1 + \frac{1}{2}\frac{1}{(k_c x)(f_b/f_c)} \{\sin(\theta_u) - \sin(\theta_l)\} \tag{5}$$

This is a decaying function that beats with some predictable frequency, as is shown in Fig. 2. In Fig. 2, both the previous approximation (5) and the discrete sum are plotted. The summation is performed for two different center frequencies, one in which 15 modes are present and the other in which 567 modes are present. The summation expression requires an additional parameter that is dependent on cavity dimension. Although the AMA (integration) approximation is theoretically valid when there are a large number of modes, here the approximation works well for relatively few modes. However, the agreement is not as good in the two- and three-dimensional cases.

Two-Dimensional Case

The transition zone for the two-dimensional case is slightly more complicated. In this case, $F_r = \cos(n\pi x/L_x)\cos(m\pi y/L_y)$ and $(\omega_r^A)^2 = c^2[(n\pi x/L_x)^2 + (m\pi y/L_y)^2]$. Assuming there are a sufficiently large number of modes, m and n can be treated as continuous variables and the summation can be replaced by integration. Converting to wave-number space ($n\pi x/L_x = k_x$, etc.) and transferring k_x and k_y into polar coordinates by the relations $k_x = k\cos\alpha$ and $k_y = k\sin\alpha$, Eq. (2) can be written for the two-dimensional case as,

$$\frac{\bar{p}^2}{\langle \bar{p}^2 \rangle} = \frac{\int\int_0^{\pi/2} [\cos^2(kx\cos\alpha)][\cos^2(ky\sin\alpha)]/k^2 \, d\alpha \, dk}{\tfrac{1}{4}\int\int_0^{\pi/2} \frac{1}{k^2} \, d\alpha \, dk} \tag{6}$$

To show that this integral is dependent only on $k_c x$ and f_b/f_c, let $\xi = kx$. Then $ky = \xi\, y/x$ and $d\xi = x\, dk$. The nondimensionalized pressure ratio becomes

$$\frac{\bar{p}^2}{\langle \bar{p}^2 \rangle} \cong \frac{\int\int_{(k_l/k_c)k_c x}^{(k_u/k_c)k_c x} [\cos^2(\xi\cos\alpha)][\cos^2(\xi y/x \sin\alpha)]/\xi^2 \, d\xi \, d\alpha}{\int\int_{(k_l/k_c)k_c x}^{(k_u/k_c)k_c} \frac{1}{4}\frac{1}{\xi^2} \, d\xi \, d\alpha} \tag{7}$$

In Eq. (7), the only independent parameters are $k_c x$ and the ratios k_u/k_c and k_l/k_c, which can be derived from f_b/f_c. The ratio y/x is known from the desired location within the cavity. The geometry of the cavity itself (i.e., the cavity dimensions) is not an important parameter in determining the nondimensionalized pressure ratio of the cavity interior.

If we assume that k is a constant (i.e., $\Delta k/k \ll 1$), this expression can be integrated explicity with the result that

$$\frac{\bar{p}^2}{\langle \bar{p}^2 \rangle} \cong 1 + J_0(2k_c x) + J_0(2k_c y) + J_0(2k_c x)\cdot J_0(2k_c y) + \frac{8}{\pi}\sum_{m=1}^{\infty}\sum_{n=1}^{\infty}(-1)^n J_{2n}(2k_c x) J_{2m}(2k_c y) \times \begin{cases} \dfrac{\sin(m-n)\pi/2}{2(m-n)} + \dfrac{\sin(m+n)\pi/2)}{2(m+n)} & m \neq n \\ (\pi/4) & m = n \end{cases}$$

Notice in the limit as $k_c x$ and $k_c y$ asymptotically approach infinity, the Bessel functions decay and the nondimensionalized pressure ratio asymptotically approaches 1, whereas the k_c and $k_c y$ approach zero (i.e., near the corner), the higher-order Bessel functions decay, but $J_0(0) = 1$ and so the nondimensionalized pressure ratio asymptotically approaches 4.

Three-Dimensional Case

For the three-dimensional case, $F_r = \cos(n\pi x/L_x)\cos(m\pi y/L_y)\cos(\ell\pi z/L_z)$ and $\omega_r^2 = c^2[(n\pi/L_x)^2 + (m\pi/L_y)^2 + (\ell\pi/L_z)^2]$. Substituting these expressions into Eq. (2), making the appropriate assumptions to allow the summation to be replaced by integration (large number of modes, etc.), and transforming from modal index space to wave-number space yields the following expression in spherical wave-number coordinates:

$$\frac{\bar{p}^2}{\langle \bar{p}^2 \rangle} \cong \frac{8\int\int\int_{k,\phi,\theta} [\cos^2(kx\sin\theta\cos\phi)\cdot\cos^2(ky\sin\theta\sin\phi)\cdot\cos^2(kz\cos\theta)/k]\sin\theta \, d\theta \, d\phi \, dk}{\int\int\int_{k,\phi,\theta}(1/k)\sin\theta \, d\theta \, d\phi \, dk} \tag{8}$$

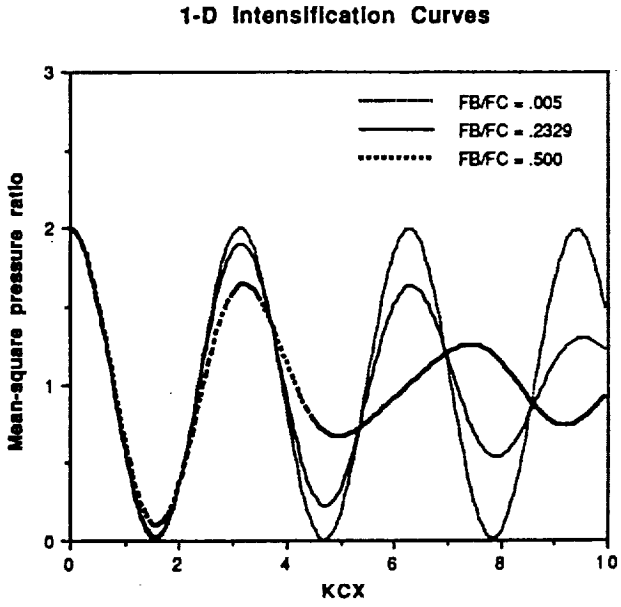

Fig. 3 Nondimensionalized mean-square pressure vs $k_c x$, one-dimensional case, three f_b/f_c ratios plotted: f_b/f_c = 0.005, 0.23, and 0.50.

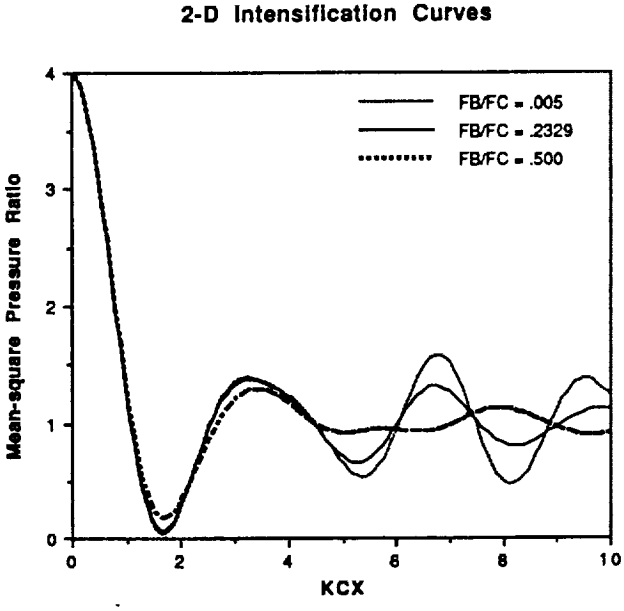

Fig. 4 Nondimensionalized mean-square pressure vs $k_c x$, two-dimensional case, three f_b/f_c ratios plotted: f_b/f_c = 0.005, 0.23, and 0.50.

Again, it can be shown that the nondimensional pressure ratio is independent of cavity geometry and is, in fact, only dependent on the parameters $k_c x$, y/x, z/x, and f_b/f_c by performing a change of variables, as in the two-dimensional case. When the spatial variables are nondimensionalized by wave number, the transition zone can be plotted as a function of mean-square pressure vs position if the bandwidth to center frequency ratio is specified.

As the number of dimensions increases, the ratio f_b/f_c plays a less significant role in the shape of the transition zone, as can be seen upon comparison of Figs. 3-5. In each of the three figures, curves corresponding to three different f_b/f_c ratios are overlayed. The three f_b/f_c ratios are f_b/f_c = 0.005 (which corresponds to a narrow bandwidth at a high center frequency), f_b/f_c = 0.23 (corresponding to a ⅓ octave band), and $f_b f_c$ = 0.500 (which corresponds to an octave band). For the one-dimensional case, Fig. 3 shows three distinct curves for the three different ratios. In the two-dimensional case, the three separate curves are beginning to converge (Fig. 4), whereas in the three-dimensional case (Fig. 5), convergence occurs more rapidly. This trend is due to the large number of two- and three-dimensional modes for a given center frequency at fixed bandwidth.

Oblique-Wave Approach

Alternatively, the problem of intensification near boundaries can be analyzed as a local problem. At the walls, for example, the problem can be modeled as an infinite number of sound waves incident upon a rigid surface from infinitely many directions. The expression for the pressure at a point in the x,y plane due to a single sound wave, as shown in Fig. 6, is $p(x,y,t) = P\, e^{i(\omega t - k_y y)}$, where $P = 2A \cos k_x x$, and A is the amplitude of the incident pressure wave. Assuming equal amplitude incident waves with random phase and random incidence angles (all equally probable), the summation of the mean-square pressures is

$$\sum_{\Delta\omega,\theta} \bar{p}^2 = \sum_{\Delta k,\theta} 2A^2 \cos^2(kx \cos\theta)$$

where k_x has been replaced by $k \cos\theta$.

Assuming there are a large number of frequencies in a particular bandwidth, as in AMA, the mean-square pressure in the band is

$$\bar{p}^2 = \int_{-\pi/2}^{\pi/2} 2A^2 \int_{k\ \text{lower}}^{k\ \text{upper}} \cos^2(kx\cos\theta)\, dk\, d\theta$$

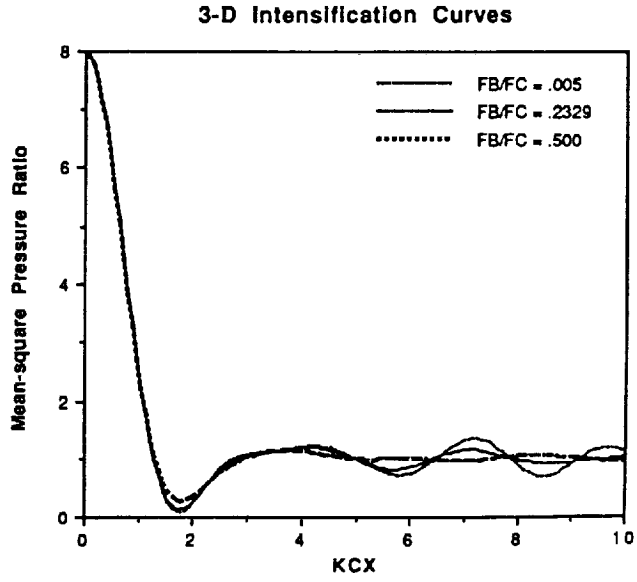

Fig. 5 Nondimensionalized mean-square pressure vs $k_c x$, three-dimensional case, three f_b/f_c ratios plotted: f_b/f_c = 0.005, 0.23, and 0.50.

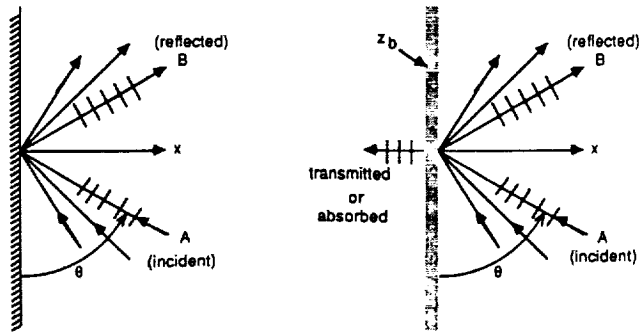

Fig. 6 Reflection from a rigid surface (left) or from an absorptive surface (right).

In order to compare this result to the AMA result, it must be nondimensionalized by its asymptotic far-field value (i.e., large $k_c x$), which is $2\pi A^2 (k_u - k_l)$. The corresponding result derived from AMA is Eq. (6). However, Eq. (6) contains variation in both the y and x directions. The nondimensionalized mean-square pressure ratio is equivalent to Eq. (6) for the two-dimensional AMA intensification from a wall providing that the y variable is held constant and the wave number is assumed large, such that the product ky approaches infinity. Note that the $1/k^2$ terms in Eq. (6) are contained in the pressure amplitude P for the oblique waves. These results also agree with the earlier result of Waterhouse[10] which was derived using methods similar to the oblique-wave formulation.

Similar relations can be derived for the two- and three-dimensional incident sound fields with reflections from one, two, or three rigid surfaces. The methodology is similar to that presented here, and the results are in agreement with the AMA results.

Absorptive Wall Intensification

Using the oblique-wave approach outlined earlier, the effect of an absorptive wall can also be analyzed. Assume that an infinite number of oblique waves are incident upon an absorptive surface (of finite impedance, z_b) from infinitely many directions. Figure 6 shows one such pressure wave. The expression for the pressure from one wave is

$$p = Pe^{i(\omega t - k_y y)} = 2A\left\{\cos k_x x - \frac{e^{-ik_x x}}{\overline{z_b}\cos\theta + 1}\right\} e^{i(\omega t - k_y y)}$$

and

$$\overline{z_b} = z_b/\rho_o c$$

Rewriting, $p = |P| e^{i(\omega t - k_y y + \phi_p)}$, where $P = |P| e^{i\phi_p}$. Then $p_{\text{real}} = |P| \cos(\omega t - k_y y + \phi_p)$. The mean-square pressure is equal to

$$\bar{p}^2 = \sum_{j=1}^{\text{No. of waves}} \frac{|P_j|^2}{2}$$

As in the previous analysis, assume that there are a large number of modes and replace the summation with integration. For equal amplitude waves, the expression for the mean-square pressure is

$$\bar{p}^2 = 2|A|^2 \int_{-\frac{\pi}{2}}^{\frac{\pi}{2}} \left\{\cos^2(k_c x\cos\theta) - 2\cos(k_c x\cos\theta)\left[\frac{(\overline{r_b}\cos\theta + 1)\cos(k_c x\cos\theta) - \overline{x_b}\cos\theta\sin(k_c x\cos\theta)}{(\overline{r_b}\cos\theta + 1)^2 + (\overline{x_b}\cos\theta)^2}\right] + \frac{1}{(\overline{r_b}\cos\theta + 1)^2 + (\overline{x_b}\cos\theta)^2}\right\} d\theta$$

Consistent with the assumptions of AMA, the wave number has been replaced by its value at the center frequency, assuming a narrow band with many modes. The first term in the expression is the same as in the rigid wall case. The far-field value (i.e., the limit for large $k_c x$) is

$$\bar{p}^2 = 2|A|^2 \int_{-\frac{\pi}{2}}^{\frac{\pi}{2}} \left\{1 - \frac{\overline{r_b}\cos\theta}{(\overline{r_b}\cos\theta + 1)^2 + (\overline{x_b}\cos\theta)^2}\right] d\theta$$

After dividing by the expression for the far-field mean-square pressure, the end result is an expression that is equivalent to the rigid wall mean-square pressure result, but with a set of terms added to include the effects of absorption.

These expressions can be extended to three dimensions by integrating in spherical coordinates around both angular directions. If desired, inclusion of the bandwidth effect is also easy to implement. This involves changing k_c from a constant, evaluated at the center frequency, to a k, a variable, and integrating the expression over the band Δk.

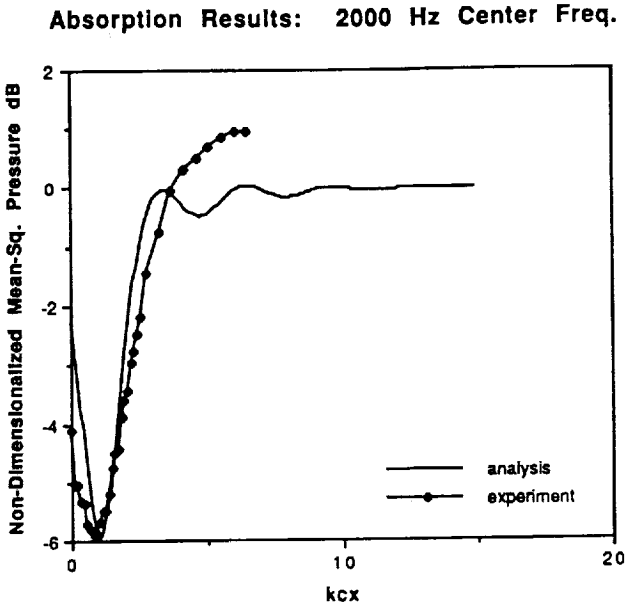

Fig. 7 Comparison of theoretically computed and experimentally measured nondimensionalized mean-square pressure in dB vs $k_c x$: 2000-Hz center frequency, ⅓ octave band.

Comparisons between theoretically calculated results and experimentally measured data are shown in Figs. 7–9 for three different center frequencies: 2000, 3250, and 4000 Hz, respectively. The impedance of the foam is different at each center frequency. At 2000 Hz, the normalized resistence ($\overline{r_b}$) is 1.17 and the normalized reactance ($\overline{x_b}$) is -0.84. These impedance characteristics correspond to an equivalent random incidence absorption coefficient α of 0.85. At 3250 Hz, $\overline{r_b} = 1.44$, $\overline{x_b} = 0.15$, and the corresponding $\alpha = 0.95$. At 4000 Hz, $\overline{r_b} = 1.47$, $\overline{x_b} = 0.64$, and the equivalent value for α is 0.91.

The theoretical results are for the three-dimensional case with bandwidth included. These three examples are plotted for a ⅓ octave bandwidth. The experimental data were taken as an extension of an experiment that was used to validate the asymptotic modal analysis method for a rectangular acoustic cavity with rigid walls. The apparatus and details of the experiment are described in Ref. 18. However, the original apparatus was modified by placing an open-cell acoustic foam on one wall of the cavity. The experimental data were taken by moving a microphone into the cavity from the foam-covered wall and recording the measured sound pressure levels.

The theoretical curves show clear asymptotic behavior, whereas the experimental curves settle down less rapidly. The physical system in the experiment was a three-dimensional enclosure with rigid walls. Provided that the rigid walls were in the far field of the microphone, so that their intensification zones were not penetrated by the microphone, the experiment should be analogous to the theoretical model. Although this condition was satisfied, it appears from the experimental data that the interior of the cavity was not uniform. Previous work, both analytical[1,2] and experimental[18] have shown that, when

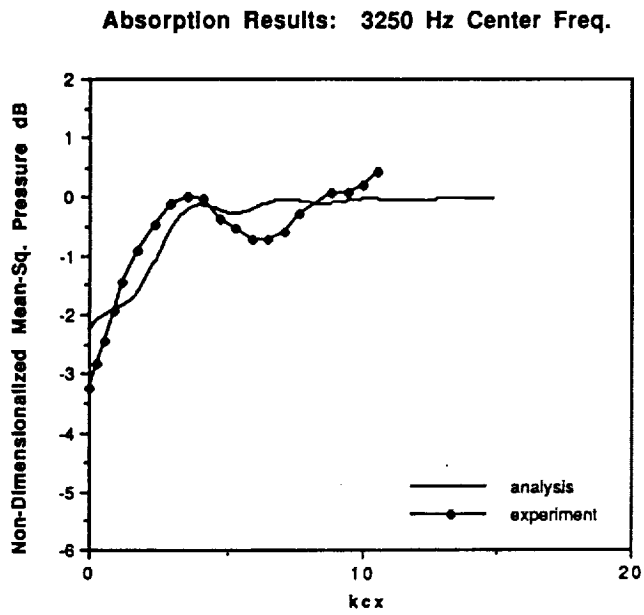

Fig. 8 Comparison of theoretically computed and experimentally measured nondimensionalized mean-square pressure in dB vs $k_c x$: 3250-Hz center frequency, ⅓ octave band.

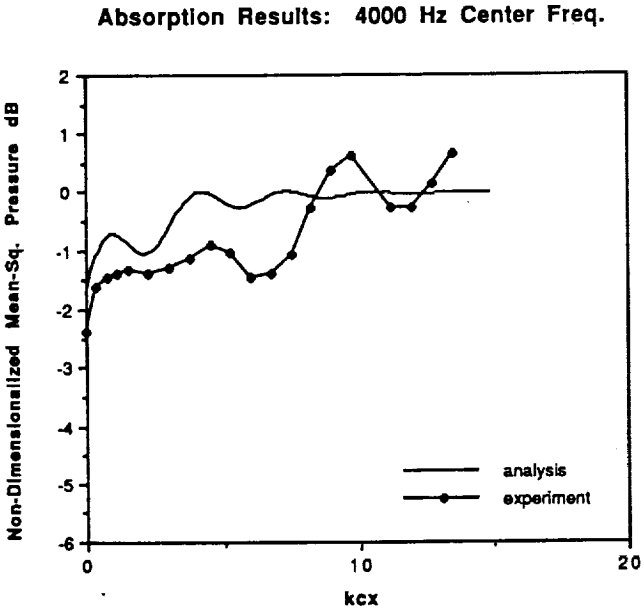

Fig. 9 Comparison of theoretically computed and experimentally measured nondimensionalized mean-square pressure in dB vs $k_c x$: 4000-Hz center frequency, ⅓ octave band.

the damping in the cavity is small, the cavity interior is uniform except in the intensification regions. Covering one wall with the absorptive foam apparently added enough damping to prevent the interior sound pressure levels from becoming uniform.

The wall impedance dramatically changes the character of the intensification region. In fact, as Figs. 7–9 show, the sound pressure levels at the wall can be reduced well below the interior levels if the wall is sufficiently absorptive. Despite the discrepancies away from the wall, the curves show reasonable qualitative agreement between the analytical and experimental results near the wall, as is consistent with the local nature of the intensification process.

Bandwidth Effect

The key parameter in all of the previous studies was the bandwidth to center frequency ratio f_b/f_c. In order to isolate the contribution of the bandwidth from that of the center frequency, a Taylor series expansion was performed. For example, Eq. (6) for the two-dimensional waves in the intensification zone is a double integral in k and α. It can be written as a Taylor series expansion about the center frequency wave number k_c as follows:

$$\int_0^{\frac{\pi}{2}}\int_{k_l}^{k_u} F(k,\alpha)\,dk\,d\alpha = \int_0^{\frac{\pi}{2}}\int_{k_l}^{k_u} F(k_c,\alpha)\,dk\,d\alpha + \int_0^{\frac{\pi}{2}}\int_{k_l}^{k_u} \frac{\partial F(k,\alpha)}{\partial k}\bigg|_{k_c}(k-k_c)\,dk\,d\alpha + \int_0^{\frac{\pi}{2}}\int_{k_l}^{k_u} \frac{\partial^2 F(k,\alpha)}{\partial k^2}\bigg|_{k_c}\frac{(k-k_c)^2}{2!}\,dk\,d\alpha + \cdots \tag{9}$$

Using the arithmetic definition of center frequency, i.e., $k_c = (k_u + k_l)/2$, the integrals of odd powers of $(k-k_c)$ will equal zero, leaving only the integrals of even powers of bandwidth. Nondimensionalizing introduces a factor of bandwidth in the denominator. Therefore, the resulting function will consist of a term that is dependent only on center frequency plus higher-order terms that contain bandwidth squared and the higher even powers of bandwidth.

An illustrative example, which can be solved in closed form, is the intensification in a corner approaching along an edge, where the motion of the wall is such that the displacement is relatively constant (white noise) in the bandwidth. For this case, the nondimensional mean-square pressure expression is

$$\frac{\bar{p}^2}{\langle \bar{p}^2\rangle} \cong \frac{\iiint_{k,\phi,\theta} \cos^2(kz\cos\theta)\,k\sin\theta\,d\theta\,d\phi\,dk}{\frac{1}{3}\iiint_{k,\phi,\theta} k\sin\theta\,d\theta\,d\phi\,dk} \tag{10}$$

This equation differs from Eq. (8) by a factor of k^2 in the integrals, since Eq. (8) is for the case where the white noise assumption is applied to the acceleration of the moving wall, rather than its displacement. The z axis is taken as the edge along which the intensification is studied. This expression has the closed-form solution:

$$\frac{\bar{p}^2}{\langle \bar{p}^2\rangle} = \frac{4 + 2\sin(2k_c z)\sin[(k_b/k_c)k_c z)]}{(k_c z)^2(k_b/k_c)} \tag{11}$$

All center frequency subscripts here refer to the arithmetic center frequency. Alternatively, the Taylor series expansion procedure outlined in Eq. (9) and performed on Eq. 10 yields

$$\frac{\bar{p}^2}{\langle \bar{p}^2\rangle} = 4 + 4\frac{\sin(2k_c z)}{2k_c z} - \frac{1}{3}\left(\frac{k_b}{k_c}\right)^2 (k_c z)\sin(2k_c z) + \text{higher order terms} \tag{12}$$

Expanding the sine $(k_b/k_c\ k_c z)$ term in Eq. (11) in a Taylor series about the center frequency wave number produces an identical result. This approximate solution is only valid in the region where the sine function is closely approximated by a two-term Taylor series. For greater accuracy, the solution would have to include higher-order bandwidth to center frequency ratio terms. The two-term Taylor series for sine is only valid up to arguments approximately equal to 1.25. Therefore, in this example, the combination $(k_b/k_c)(k_c z)$ must be ≤ 1.25, or conservatively ≤ 1.0, which means that $k_c z \leq 1/(k_b/k_c)$ for the approximate solution to be accurate. Typically, intensification occurs close to the wall, edge, or corner where the

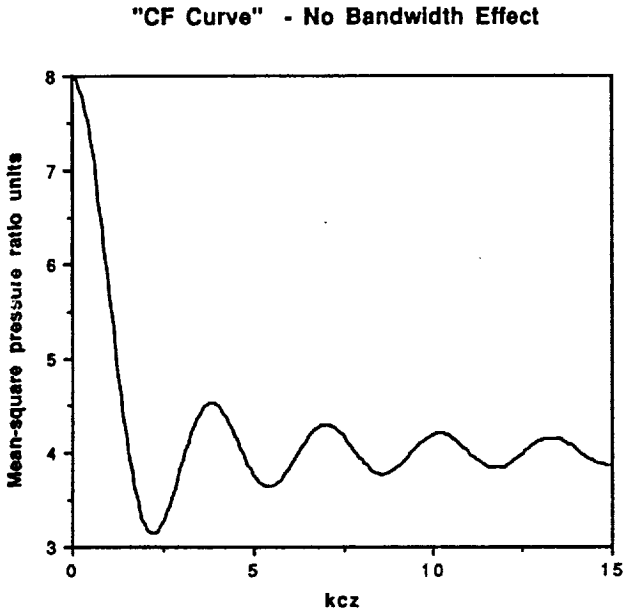

Fig. 10 CF curve that is dependent upon $k_c z$ only: nondimensionalized mean-square pressure ratio vs $k_c z$ for the example problem.

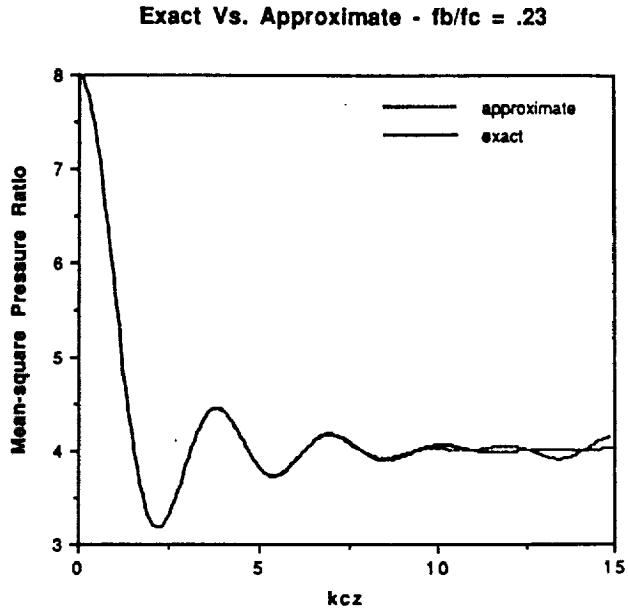

Fig. 12 Comparison of exact solution vs the approximate solution consisting of CF curve + $(f_b/f_c)^2$ correction curve, for $f_b/f_c = 0.23$ (⅓ octave band).

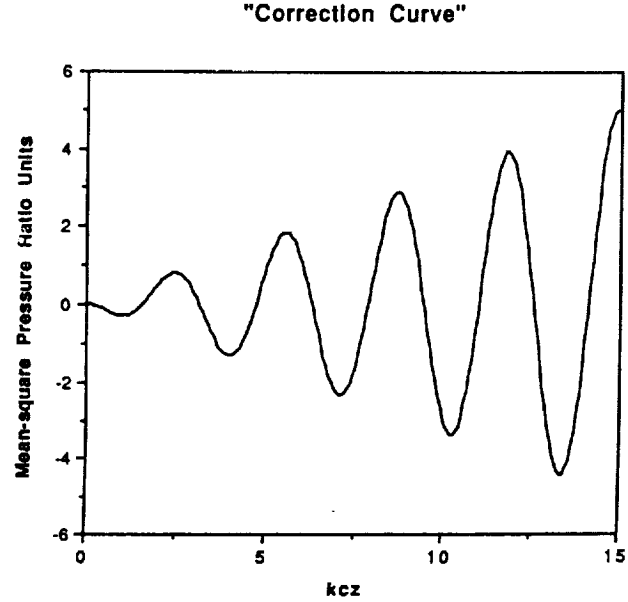

Fig. 11 Correction curve that is to be multiplied by f_b/f_c ratio squared: this curve by itself is also independent of bandwidth.

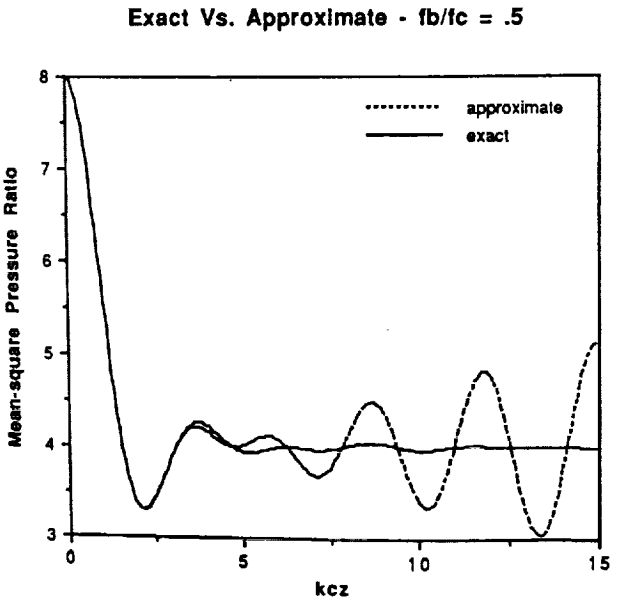

Fig. 13 Comparison of exact solution vs the approximate solution consisting of CF curve + $(f_b/f_c)^2$ correction curve, for $f_b/f_c = 0.500$.

values of $k_c x$, $k_c y$, or $k_c z$ are small. In fact, usually, $k_c x$, $k_c y$, and/or $k_c z \leq 2\pi/3$. Therefore, in most cases, the two-term solution should be sufficient. For a ⅓ octave band, for example k_b/k_c is 0.23, which satisfies the requirement that $k_c z < 1/(k_b/k_c)$.

Since the bandwidth correction is second order in bandwidth, the mean-square pressure can be approximated by a simple curve that is dependent on center frequency (CF) only for small bandwidths. This curve (the CF curve) for the current example problem is plotted in Fig. 10. It is a function of $k_c x$ alone, and is independent of bandwidth. The effects of increasing bandwidth can be taken into account by adding another function of center frequency that has been multiplied by the ratio $(f_b/f_c)^2$. This function, called the correction curve, is shown in Fig. 11 [before multiplication by $(f_b/f_c)^2$] for this example.

In Fig. 12, the correction curve has been multiplied by $(0.23)^2$ and then added to the CF curve. The results are expected to be accurate up to $k_c z$ around 4.0, as explained earlier. However, the exact solution and the approximate solution agree with each other well beyond 4.0. In Fig. 13, a similar comparison between the approximate solution and the exact solution is made for $f_b/f_c = 0.5$. Here, good agreement is expected up to 2.0. Once again, the agreement actually extends beyond that predicted. From the plot, it is also easy to see that the approximate solution fails for large $k_c z$.

Conclusions

In previous work, asymptotic modal analysis was used to predict interior sound pressure levels in a rectangular acoustic cavity. Local response peaks in sound pressure level were found at the boundaries; otherwise, the interior levels were nearly constant. In the present work, the spatial variation of sound pressure level between the boundary and the uniform interior was studied, i.e., the intensification zone.

It was found that using such AMA techniques as treating the discrete summation as an integration, and evaluating certain parameters at the center frequency, etc., provides accu-

rate results even when the number of modes is relatively few. In addition, the AMA formulation allows estimation of the mean-square pressure ratio as a function of nondimensionalized distance into the cavity, without knowing the cavity dimensions. The family parameter for the curves of nondimensionalized mean-square pressure vs nondimensionalized distance (distance multiplied by the center frequency wave number) is the bandwidth to center frequency ratio f_b/f_c. Plots of one-, two-, and three-dimensional intensification zones have shown that the dependence on f_b/f_c is less important as the number of modal dimensions increases, i.e., the effect is least important in the three-dimensional case.

The bandwidth dependence was separated from the center frequency dependence through a Taylor series expansion about the center frequency wave number, which was performed on the expression for mean-square pressure. As a result, the mean-square pressure can be expressed as a function of center frequency plus terms that are of order bandwidth to center frequency ratio squared, and higher (even powers). Therefore, if the bandwidth to center frequency ratio is sufficiently small, the expression can be simplified. If several bandwidth to center frequency ratios are to be considered, their effects can be added on as corrections that are of order $(f_b/f_c)^2$.

The intensification zones were also analyzed as local problems consisting of an infinite number of oblique incidence sound waves impinging upon a rigid or an absorptive surface. The result for the spatial average of the sound pressure levels in the rigid wall case was identical to that obtained from the AMA methods. The result for the absorptive wall was found to contain the rigid wall result as well as additional terms that contain the impedance information. The shape of the intensification zone is strongly affected by the choice of wall impedance and can be remarkably different from that near a rigid wall. In particular, minimum rather than maximum levels may occur in this zone. The absorptive wall analytical result was compared with experimental results and found to agree qualitatively near the wall.

The results of this work provide physical insight into the intensification zone behavior in acoustic cavities by providing analytical expressions that describe the sound field in terms of universal components that show the importance of various parameters. The analytical techniques that were used here provide efficient and accurate methods for predicting sound pressure levels in rooms with intensification zones.

Acknowledgments

This work was supported by the Structural Acoustics Branch of NASA Langley Research Center through Grant NAG-1-709 and NASA Graduate Student Researchers Program Fellowship NGT-50342. The authors also wish to thank Donald Bliss of Duke University for his comments, suggestions, and stimulating discussions regarding this work.

References

[1]Kubota, Y., Dionne, H. D., and Dowell, E. H., "Asymptotic Modal Analysis and Statistical Energy Analysis of an Acoustic Cavity," *Journal of Vibration, Acoustics, Stress and Reliability in Design*, Vol. 110, No. 3, 1988, pp. 371–376.

[2]Peretti, L. F., and Dowell, E. H., "Asymptotic Modal Analysis of a Rectangular Acoustic Cavity Excited by Wall Vibration," *AIAA Journal*, Vol. 30, No. 5, pp. 1191–1198.

[3]Pierce, A. D., "Room Acoustics," *Acoustics: An Introduction to Its Physical Principles and Applications*, Acoustical Society of America, Woodbury, NY, 1989, Chap. 6.

[4]Kinsler, L. E, and Frey, A. R., "Architectural Acoustics," *Fundamentals of Acoustics*, 2nd Ed., Wiley, New York, 1962, Chap. 14.

[5]Morse, P. M., and Ingard, K. U., "Room Acoustics," *Theoretical Acoustics*, McGraw-Hill, New York, 1968, Chap. 9.

[6]Crandall, S. H., "Random Vibration of One- and Two-Dimensional Structures," *Developments in Statistics*, Vol. 2, edited by P. R. Krishnaiah, Academic, New York, 1979, pp. 1–82.

[7]Itao, K., and Crandall, S. H., "Wide-Band Random Vibration of Circular Plates," *Journal of Mechanical Design*, Vol. 100, No. 4, 1978, pp. 690–695.

[8]Crandall, S. H., and Kulvets, A. P., "Source Correlation Effects on Structural Response," *Application of Statistics*, edited by P. R. Krishnaiah, North-Holland, New York, 1977, pp. 168–182.

[9]Kubota, Y., and Dowell, E. H., "Experimental Investigation of Asymptotic Modal Analysis for a Rectangular Plate," *Journal of Sound and Vibration*, Vol. 106, No. 2, 1986, pp. 203–216.

[10]Waterhouse, R. V., "Interference Patterns in Reverberant Sound Fields," *Journal of the Acoustical Society of America*, Vol. 27, No. 2, 1955, pp. 247–258.

[11]Chu, W. T., "Eigenmode Analysis of the Interference Patterns in Reverberant Sound Fields," *Journal of the Acoustical Society of America*, Vol. 68, No. 1, 1980, pp. 184–190.

[12]Chu, W. T., "Comments on the Coherent and Incoherent Nature of a Reverberant Sound Filed," *Journal of the Acoustical Society of America*, Vol. 69, No. 6, 1981, pp. 1710–1715.

[13]Tohyama, M., and Suzuki, A., "Space Variances in the Mean-Square Pressure at the Boundaries of a Rectangular Reverberation Room," *Journal of the Acoustical Society of America*, Vol. 80, No. 3, 1986, pp. 828–832.

[14]Waterhouse, R. V., "Noise Measurement in Reverberant Rooms," *Journal of the Acoustical Society of America*, Vol. 54, No. 4, 1973, pp. 931–934.

[15]Waterhouse, R. V., and Cook, R. K., "Diffuse Sound Fields: Eigenmode and Freewave Models," *Journal of the Acoustical Society of America*, Vol. 59, No. 3, 1976, pp. 576–581.

[16]Waterhouse, R. V., and Cook, R. K., "Interference Patterns in Reverberant Sound Fields. II," *Journal of the Acoustical Society of America*, Vol. 37, No. 3, 1965, pp. 424–428.

[17]Dowell, E. H., Gorman, G. F., III, and Smith, D. A., "Acoustoelasticity: General Theory, Acoustic Natural Modes and Forced Response to Sinusoidal Excitation, Including Comparisons with Experiment," *Journal of Sound and Vibration*, Vol. 52, No. 4, 1977, pp. 519–542.

[18]Peretti, L. F., and Dowell, E. H., "Experimental Verification of the Asymptotic Modal Analysis Method as Applied to a Rectangular Acoustic Cavity Excited by Structural Vibration," *Journal of Vibrations and Acoustics* (to be published).

Appendix D:

Peretti, L. F. and E. H. Dowell, "Experimental Verification of the Asymptotic Modal Analysis Method as Applied to a Rectangular Acoustic Cavity Excited by Structural Vibration," ASME Journal of Vibration and Acoustics, to appear 1992. (Galley proofs).

Experimental Verification of the Asymptotic Modal Analysis Method as Applied to a Rectangular Acoustic Cavity Excited by Structural Vibration

L. F. Peretti

E. H. Dowell
Duke University,
Durham, NC 27706

An experiment was performed on a rigid wall rectangular acoustic cavity driven by a flexible plate mounted in a quarter of one end wall and excited by white noise. The experiment was designed so that the assumptions of Asymptotic Modal Analysis (AMA) were satisfied for certain bandwidths and center frequencies. Measurements of sound pressure levels at points along the boundaries and incrementally into the interior were taken. These were compared with the theoretical results predicted with AMA, and found to be in good agreement, particularly for moderate (1/3 octave) bandwidths and sufficiently high center frequencies. Sound pressure level measurements were also taken well intot he cavity interior at various points along the 5 totally rigid walls. The AMA theory, including boundary intensification effects, waw shown to be accurate provided the assumption of large number of acoustic modes is satisfied, and variables such as power spectra of the wall acceleration, frequency, and damping are slowly varying in the frequency bandwidth.

Introduction

Enclosed spaces such as the interiors of airplanes or automobiles, in which the enclosure itself or portions of a wall vibrate, are most often subject to interior noise problems. This structural vibration induces an acoustic field in the interior space, and the wall flexibility allows external sound fields to be transmitted to the interior. Two methods which are traditionally used to predict the interior noise levels are Classical Modal Analysis (CMA) and Statistical Energy Analysis (SEA). Another method, Asymptotic Modal Analysis (AMA) which contains aspects of both CMA and SEA, has recently been developed for structural-acoustic applications.

Classical Modal Analysis involves consideration of each individual mode of the system: the structural modes of the enclosure, the acoustic modes of the cavity, as well as the coupled structural-acoustic modes. Recent work by Pan and Bies (1990), studying the effect of fluid-structural coupling on sound waves in an enclosure is an example of a CMA-type approach. Other CMA-based methods include finite element analysis (for example, Sung and Nefske, 1984), and boundary element methods (for example, Seybert and Cheng, 1987). Because individual modal contributions are considered, these methods are cumbersome for systems with large numbers of modes.

The SEA method is often a good alternative method when there is a large number of modes involved, since only statistical quantities regarding the system need to be known. The SEA method gives accurate results, when the underlying stochastic assumptions are met in the frequency range considered. However, because the results are given in terms of statistical quantities only (e.g., spatially-averaged mean-square pressures), detailed information cannot be obtained using SEA. The standard reference on SEA is the textbook by Lyon (1975).

A new method, Asymptotic Modal Analysis (AMA), which was developed by Dowell (1983), is a hybrid of the previous methods. It is systematically derived from Classical Modal Analysis, and therefore contains several levels of approximation and generality. The accuracy and simplicity of the results obtained from AMA are adjusted by determining the level of approximation in the derivation. In this work, the accuracy and limitations of the AMA method for a structural-acoustic system are explored experimentally.

Peretti and Dowell (1992a) analyzed the acoustic field inside a rectangular cavity where five walls were rigid and the sixth wall, or a portion of that wall, was vibrating. In their work, the interior noise levels were studied through a comparison of the results obtained by Asymptotic Modal Analysis (AMA) and those obtained by Classical Modal Analysis (CMA). It was found that AMA, which in theory is valid in the limit when there is an infinite number of modes responding, gave

Contributed by the Technical Committee on Vibration and Sound for publication in the JOURNAL OF VIBRATION AND ACOUSTICS. Manuscript received March 1991.

suprisingly good results when the number of modes was infinite and only moderately large. Peretti and Dowell (1992a) studied the case where the vibrating wall was excited with a white noise time history and assumed to respond with an infinite number of structural modes. Their theoretical study found that the sound pressure levels in the interior of the rectangular acoustic cavity were nearly constant, with the exceptions occurring at the boundaries. In particular, these boundary areas or "intensification zones" exhibited levels which were 8, 4, and 2 times higher than the interior level for the corners, edges and walls, respectively. The intensification effect is caused by the existence of spatially correlated modes at the boundaries due to enforcement of the wall boundary conditions, while the modes in the interior are uncorrelated.

Peretti and Dowell (1992b) also analyzed the transition between the intensification at the boundaries and the uniform interior region. They found that the pressure field can be described in terms of a nondimensional parameter, which scalesthe distance into the cavity with the wavenumber corresponding to the center frequency, for different values of the bandwidth to center frequency ratio. This result is independent of the cavity dimensions for frequencies sufficiently high to achieve the AMA limit, and suggests that it is effectively a local solution near the boundary. In fact, similar intensification results were obtained for a uniform distribution of oblique waves incident on an infinite wall, which is the equivalent problem in the nearfield.

The purpose of this work is to compare these previous analytical results with experimental data and to test the practical limitations of the theory. To this end, an experiment was performed in which a portion of one wall of an otherwise rigid rectangular cavity was excited structurally with a white noise time history. The experimented design was chosen to best match the assumptions which were made in the theoretical study of Peretti and Dowell (1992a). The principal findings of the earlier theoretical study which were further investigated by the present experimental study are: that the response in the interior of the cavity is uniform, that at the corners, edges and walls the sound pressure levels are 8, 4, and 2 times greater than the levels in the interior; and that the thickness of the intensification zone is independent of the cavity dimensions.

Previous Theoretical Results and Experimental Goals

This section summarizes the previous theoreticals results in relation to the goals of current experimental work.

When both the number of structural modes and the number of acoustic modes are large then, from Peretti and Dowell (1992a) the nondimensionalized mean square pressure locally (i.e., as a function of position in the cavity (can be expressed as:

$$\frac{\overline{p}^2}{(\rho_o c_o^2)^2} \equiv \frac{\pi}{4}\frac{A_f}{V^2}\Phi_w(\omega_c)\frac{A_f\langle F_c^2\rangle}{(M_c^A)^2(\omega_c^A)^3\zeta_c^A\langle Z_c^3\rangle}\sum_r F_r^2(x,y,z). \quad (1)$$

From, (1), the quantities which are needed to predict the local mean-square pressure are: the flexible wall area (A_f), the volume of the cavity (V), the acoustic modal function, ($F_r(x,y,z)$, cosines for the rectangular cavity), as well as quantities which are evaluated at the center frequency of the band. The acoustic generalized mass (M_c^A), the center frequency (ω_c), the acoustic modal damping (ζ_c^A), and the power spectra of the wall acceleration (Φ_w) are all evaluated at the center frequency only and are not determined for each individual mode. F_c stands for the modal average of the acoustic modal function. $\langle Z_c^2\rangle$is the ratio of the volume average of F_c^2 to the average of F_c^2 over the flexible wall area. The following assumptions are implicit in this equation: the power spectra of the wall response is uncorrelated in space, which is a consequence of having a large number of structural modes; and the power spectrum of the wall response is slowly varying with respect to frequency relative to the rapidly varying acoustic cavity transfer function. Also, it is assumed that the generalized mass, the frequency in the band of interest, and the damping ratio vary slowly, and can be approximately by their values at the at the center frequency of the band. A complete derivation of Eq. (1) is given in the Appendix.

Increasing the bandwidth, and therefore increasing the number of modes at a given center frequency, should improve the agreement between the experimental results and the asymptotic modal analysis results. However, beyond a certain bandwidth size, the assumptions that frequency, damping, etc. are constant are violated, and this tends to negate the positive effect on analytical/experimental correlation which is due to the increased number of modes. One goal of the experiment was to investigate the bandwidth effect.

When there is a large number of acoustic modes in the cavity, i.e., when the index r in Eq. (1) goes to infinity, the mean square pressure levels in the interior approach a uniform value. The only term in the AMA expression for mean square pressure which contains spatial variation is inside the summation over acoustic modes. However, for very large r, the summation of F_r^2 equals a constant, which is the same for all x, y, and z, unless x, y, or z are close (within an acoustic wavelength) to the cavity boundaries. The condition, x, and/or y, and/or z equal to 0, L_x, L_y, or L_z, corresponds to a wall, an edge or a corner location.

For a rectangular enclosure, substituting $F_r^2 = \text{cosine}^2(r_x\pi x/L_x)^*\text{cosine}^2(r_y\pi y/L_y)^*\text{cosine}^2(r_z\pi z/L_z)$ into Eq. (1), and setting either x, y, or z equal to 0 or L_x, L_y, or L_z, for a wall, the term $\Sigma F_r^2/\Delta N^A$ for large r becomes 1/4. In the interior region, where neither x, y, nor z are equal to 0 or the cavity dimensions in their respective directions, this ratio is 1/8. Therefore, the ratio of wall mean square pressure to the uniform interior pressure is 2 to 1. Similarly, the ratio of mean square pressure in a corner to the uniform level is 8 to 1, and for an edge it is 4 to 1. These intensification zones at the boundaries are due to the spatial correlation of the modes there (enforced by the rigid wall boundary conditions) as opposed to the random distribution (spatially and temporally) in the interior. Vali-

Nomenclature

A	= area	X, Y, Z	= acoustic modal function component dependent on x, y, z	$\cdot$	= time derivative
c	= speed of sound	ΔN	= number of acoustic modes	$\bar{}$ (overbar)	= RMS
F	= cavity acoustic modal function	ω	= frequency	**Subscripts**	
L	= cavity dimension	Φ	= power spectrum	c	= center frequency
M	= generalized mass	ρ	= density	f	= flexible
p	= presure	ζ	= damping ratio	r	= acoustic modal index
V	= volume	$\langle\ \rangle$	= spatially averaged quantity	w	= pertaining to the flexible wall
w	= displacement			0	= reference value
x, y, z	= spatial position coordinate			A	= acoustic

dation of the uniformity of the interior sound level as well as the intensification levels at the walls, edges and corners was another goal of the experiment.

The intensification zones exhibit boundary layer behavior, and are relatively flat in the interior region. Peretti and Dowell (1992b) studied the transition from the peak boundary levels to the uniform interior level for the rectangular acoustic cavity previously considered. They define the nondimensional parameter, $k_c d$, as the center frequency wavenumber multiplied by the distance into the cavity. The mean square pressure as a function of $k_c d$ is independent of cavity dimensions and is only dependent on the bandwidth to center frequency ratio and direction from the cavity boundary. The thickness of the intensification zone scales with the center frequency wavenumber and is such that for different bandwidth to center frequency ratios the intensification thickness is relatively constant. A further goal of the experiment was to measure the sound pressure levels as they transition from the peak levels at the boundaries to the nearly uniform levels inside the cavity.

Experimental Design and Description of Apparatus

The experiment was designed to match as closely as possible the theoretical assumptions. These assumptions include: a rigid rectangular cavity with only a flexible portion of of one wall vibrating, a large (infinite) number of structural modes responding on the vibrating wall portion, and a large number of acoustic modes containing all frequencies in the band ("white noise"). In the theoretical work, the width, height, and length dimensions were in the proportions 2 to 3 to 7. These dimensions were chosen so that they would not be integer multiples of each other.

A rectangular box was constructed almost entirely of 1 in. thick Plexiglass. The interior dimensions of the box were 408 mm X 610 mm X 1520 mm. One of the 408 mm by 610 mm walls was constructed of Bakelite and was removable. This feature allows the flexible plate location and dimensions to be varied in subsequent experiments. The portion of the Bakelite wall that was rigid was 25.4 mm (1 in.) thick, and the thickness of the portion which was flexible varied according to its other dimensions. The requirement of having a large number of structural modes responding on the flexible Bakelite plate dictated the thickness to area ratio of the plate; the smaller the plate area, the thinner the plate needed to be. For the experimental data reported here, the flexible area was positioned in the lower left corner of the wall, its area was 622.2 square cm, which corresponds to 1/4 of the entire wall area for that face, and its thickness was 1.5875 mm (1/16 in.).

The flexible portion was driven by white noise which was supplied by a B&K Noise Generator connected to an amplifier and then to a 2 lb. shaker. The sting of the shaker was attached to the flexible portion of the wall by wax at a position which was off-center, so as to excite both symmetric and antisymmetric modes. Previous work by Kubota and Dowell (1986) has shown that when a plate is driven in this manner, a large number of (structural) modes respond, and the response characteristics are nearly spatially uniform; exceptions occur at the structural boundaries and at the point of excitation. For this type of behavior, at least fifteen structural modes must be present in the bandwidth. Figure 1 shows a plot of the number of structural modes for the flexible plate used in this study as well as the number of acoustic modes in the cavity versus frequency for various frequency bandwidths divided by center frequency, i.e, .005, .2329, .500.

An accelerometer was used to measure the acceleration of the vibrating plate. The accelerometer was carefully positioned so as not to be near a boundary or the force application point.

Microphone probe tubes were used to take sound pressure level measurements inside the cavity and they were approximately 20 cm (8 in.) long. Holes of approximately 4 mm in diameter were drilled at various locations on the 5 rigid walls to accommodate the microphone probe tubes. In order to keep the cavity "rigid," the holes where plugged when not in use. The end of each plug was aligned with the interior of the cavity. A schematic drawing of the cavity is shown in Fig. 2.

The microphone probe tubes possessed standing waves which were damped out using open cell foam strips, which were inserted into each tube. Figure 3 shows a diagram of a microphone probe tube. The effect of the damping was accounted for in the final pressure measurements by calibrating accordingly. The calibration was done by comparing the outputs of two microphones: a half-inch microphone without a probe tube, and a half-inch microphone with a probe tube. The two microphones were placed in front of a loudspeaker which was driven with white noise, such at that the mouth of the probe

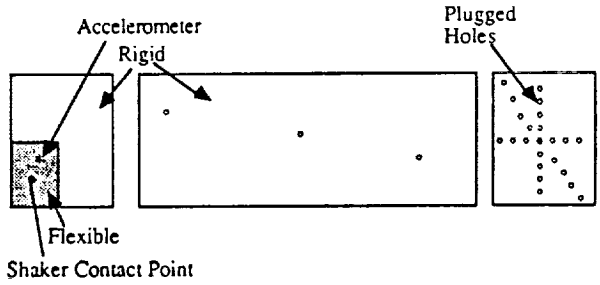

Fig. 2 Schematic of the rectangular cavity

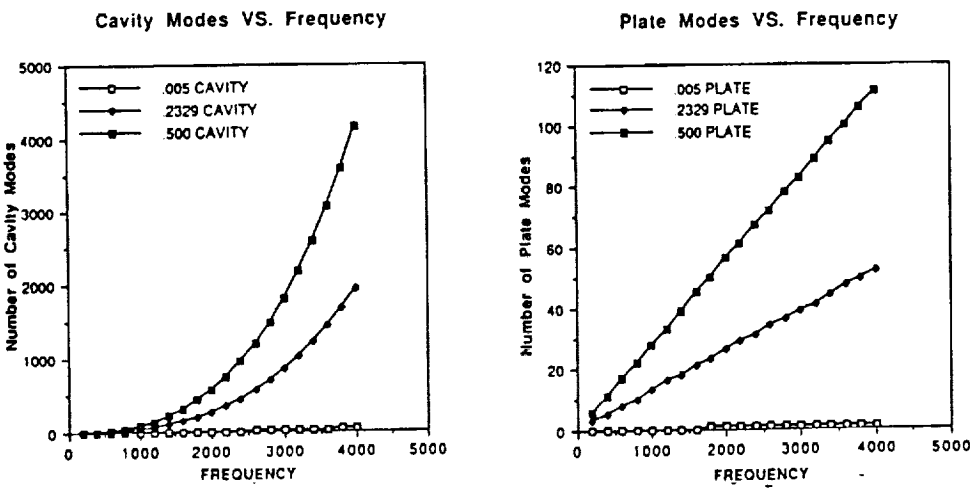

Fig. 1 Number of modes vs. frequency

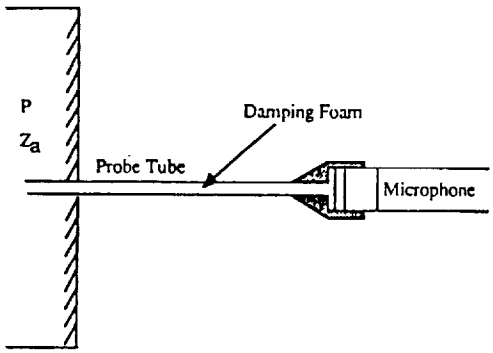

Fig. 3 Schematic of microphone probe tube

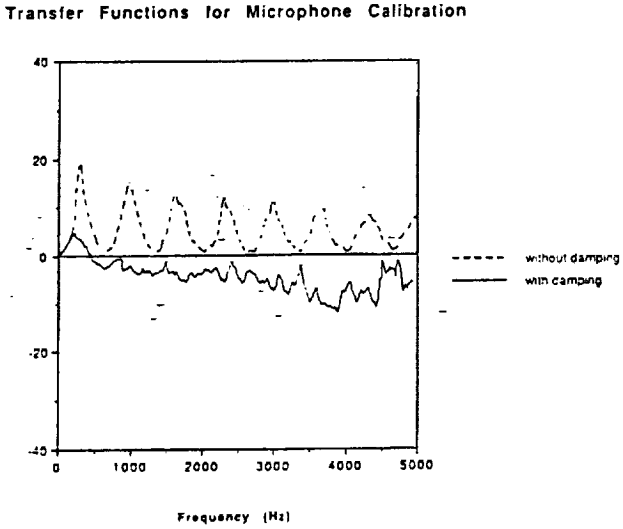

Fig. 4 Transfer function of the response of microphone probe tube without damping to a bare microphone, and transfer function of the response of microphone probe tube with damping to a bare microphone

tube was flush with the face of the bare microphone. The transfer function between the two microphone outputs was taken on a spectrum analyzer and stored on a computer for future use in calibrating the data. Figure 4 shows transfer functions, with and without damping. The added damping has the effect of removing the standing wave peaks without a large reduction in signal to noise ratio.

The ratio of the output (in volts) from the two microphones (without probe tubes) subject to a fixed pressure input was also needed for the calibration. This ratio was assumed to be independent of frequency in the frequency range of interest, and therefore, could be obtained from two pistonphone measurements. Since the system is linear, the raw data could be corrected for the damping effect in the probe tube by using the ratio of the two microphones without probe tubes, and the transfer function (which varied with frequency) for a microphone with a probe tube to one without.

During the experiment, two microphone/probe setups (both calibrated as described earlier) were used to measure sound pressure levels at two interior points simultaneously while the accelerometer measured the motion of the wall. These three data samples were input to a spectrum analyzer (4-channel Scientific Atlanta SD-380), from which power spectra could be plotted on a compatible Hewlett-Packard plotter directly, or the raw data could be stored on the VAX computer via an IEEE connection, and later post-processed. The plotter option was convenient for checking measurements in the early stages of the experiment. However, the bulk of the experimental data was stored on a computer as raw data (i.e., volts) and later

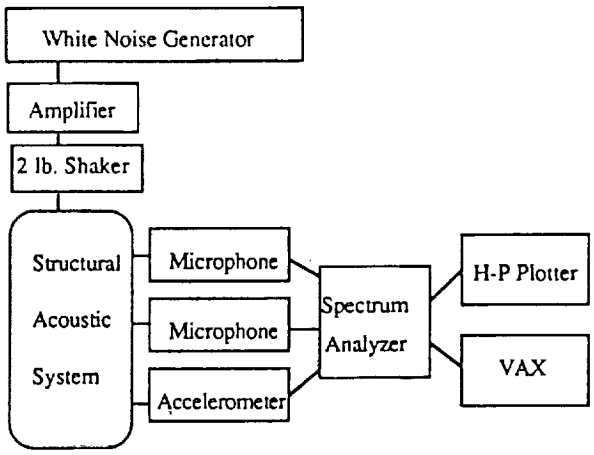

Fig. 5 Experimental set-up schematic

post-processed, since the goal was to compare with the earlier analytical study in which nondimensional groupings were used.

Results and Discussion

Experimental Procedure and Data Processing. Microphones with probe tubes were used to measure sound pressure levels at different locations inside the rectangular acoustic cavity while an accelerometer measured the shaker input to the wall. For each fixed microphone probe tube location, three independent readings were taken for both the microphones and the accelerometer. The microphone and accelerometer data were read into a spectrum analyzer and converted to power spectra densities. The power spectra ranged from 0 to 5000 Hz and consisted of 400 data points. Therefore, the narrow bandwidths for the raw data were 12.5 Hz. The power spectra data in volts were stored on a computer for later post-processing.

The first step in the post-processing was to read in the three independent measurements for a fixed spatial coordinate inside the cavity and average them. The measurements were checked by plotting the three samples and their average. These data were then converted from volts into mean square pressures in Newtons per meter squared by using the earlier microphone calibration data and the conversion factors from the pistonphone measurements . The second post-processing step was to take the average of the three narrow band power spectral densities (12.5 Hz spacing), and create new spectra with different bandwidth to center frequency ratios. For this, a computer program was written which stepped through center frequency, computed the bandwidth for a desired bandwidth to center frequency ratio, and summed the squares of the data in that desired band. The outputs of this computer program were power spectral densities (in dB) in continous bands, typically from 200 Hz to 4000 Hz with spacing every 20 Hz, for a particular bandwidth to center frequency ratio (f_b/f_c). Typical plots for a microphone and an accelerometer are shown in Fig. 6.

The third and final step in post-processing introduced the probe location into the data. Here, a series of power spectral densities for a given f_b/f_c ratio were read into a computer program, along with their associated position (x, y, and z coordinates) in the cavity. The output of this program was mean square pressure level versus $k_c d$, where $k_c d$ is the wavenumber (k_c) for a particular center frequency times the distance (d) into the cavity with respect to a reference point. Upon completion of the final step, the data have been transformed from power spectral densities in volts to mean-square pressures as a function of a nondimensional parameter $k_c d$ for a given

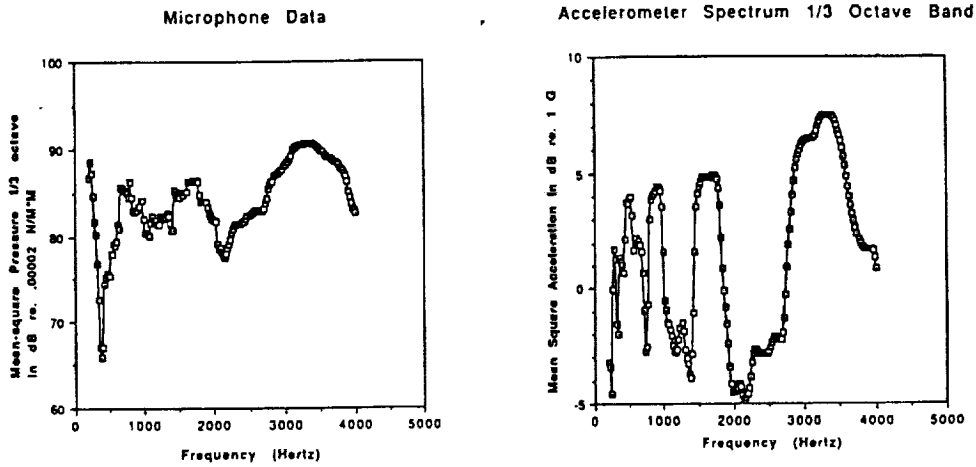

Fig. 6 Typical accelerometer and microphone data for psd's with 1/3 octave band

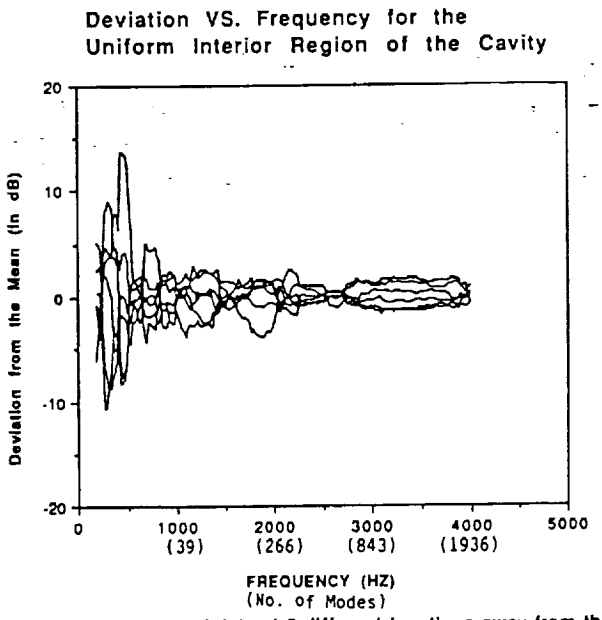

Fig. 7 Scatter of the psd data at 6 different locations away from the boundaries of the cavity. Numbers in parenthesis indicate the number of modes in a 1/3 octave band at that center frequency

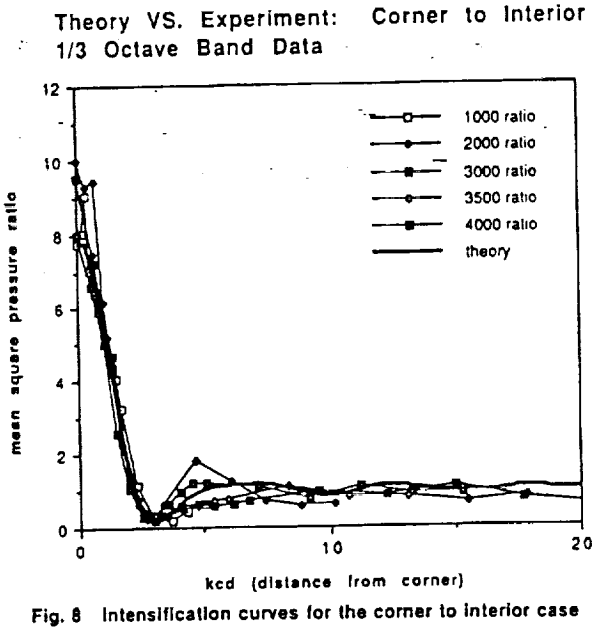

Fig. 8 Intensification curves for the corner to interior case

center frequency and given bandwidth to center frequency ratio.

Uniform Interior. When there is a large number of spatially uncorrelated acoustic modes in the cavity, the theory predicts that the interior sound pressure levels in a band will be uniformly spatially distributed. To test this hypothesis, microphone probe tubes were inserted into the cavity to their maximum extension (approx. 20 cm) at various locations on the five rigid walls. The power spectral densities (in dB re. 2 X 10^{-5} N/M^2) were plotted versus frequency (Hz) for a 1/3 octave band. The scatter of this data is shown in Fig. 7, where the deviation from the mean is plotted versus frequency. Note that above 2000 Hz, the data contain little scatter, while below 2000 Hz the scatter in the data is as much as ±10 dB. This suggests that the region above 2000 Hz will be in the AMA limit, that is, the theoretical conditions are met regarding the large number of acoustic modes. For this geometrical configuration, a frequency of 2000 Hz corresponds to 26 plate (structural) modes and 266 cavity (acoustic modes in a 1/3 octave band. This compares to 16 plate modes and 64 cavity modes at 1000 Hz. (Figure 1 shows the growth in the number of modes versus frequency for various bandwidth to center frequency ratios.)

Intensification Zones Near The Cavity Boundaries. Theoretically, response peaks occur at the boundaries of the cavity, due to the imposition of the boundary conditions. These peaks are 8, 4, and 2 times higher than the spatially uniform values that exist further into the cavity; the level of intensification depends upon whether the boundary point is on a corner, edge or a wall, respectively. Analytically, these intensification zones have been studied by Peretti and Dowell (1992b) by plotting the mean-square pressure as a function of nondimensional distance into the cavity ($k_c d$). The two main points for comparison between theory and experiment for the intensification zone study were the ratio of the levels at the boundaries to those in the uniform region and the thickness of the intensification zone (as determined by the distance to the first minimum).

Figures 8, 9, and 10 show intensification curves coming from a corner, an edge, and a wall into the interior. In the cases of the corner and the edge, the trajectory was at an oblique angle, whereas for the wall, the trajectory was perpendicular to the wall. The three cases shown here are for a 1/3 octave bandwidth. Several center frequencies are plotted for the experimental data; the theoretical data is only dependent upon the ratio of bandwidth to center frequency which is .2329 for a 1/3 octave band. The ordinate is the ratio of mean-square

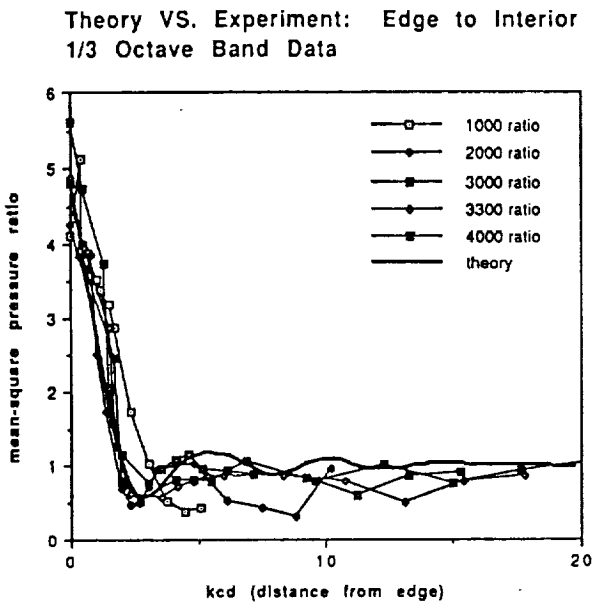

Fig. 9 Intensification curves for the edge of interior case

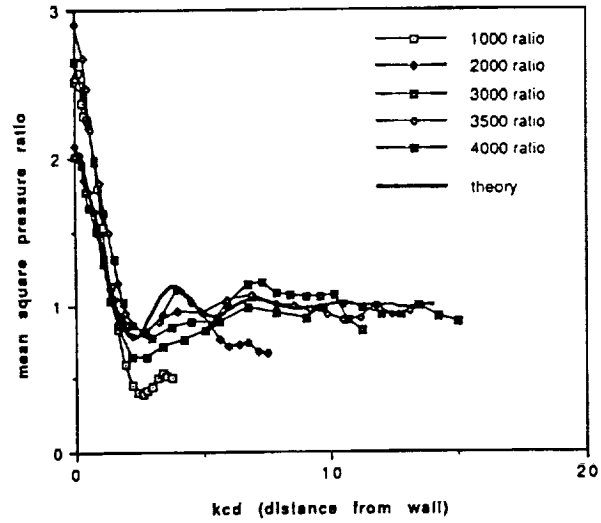

Fig. 10 Intensification curves for the wall to interior case

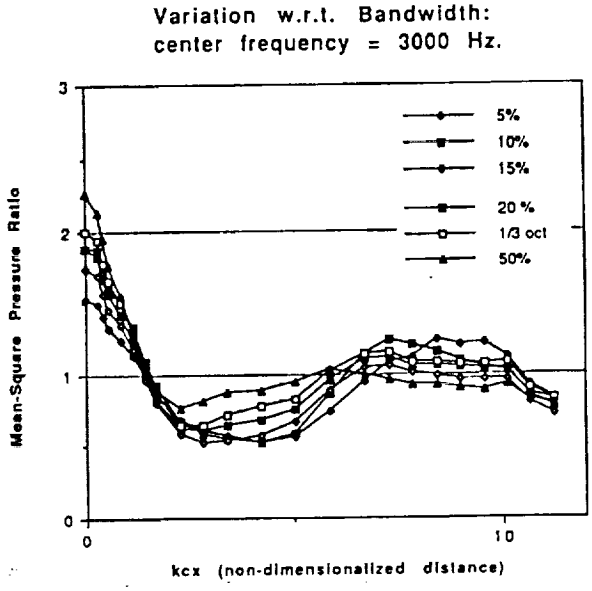

Fig. 11 Effect of bandwidth for a fixed center frequency

pressure at the x, y, z point to mean-square pressure of the interior region. The abscissa is the nondimensional distance into the cavity.

The theoretical curve in Fig. 8, for the case where $k_c d$ starts in the corner (0, 0, 0) and proceeds into the cavity at an angle which is approximately 33 deg in one direction and 56° in the other, starts with a ratio of 8 in the corner, and then becomes flat with a level of 1 for large values of $k_c d$. Also, the first minimum occurs around $k_c d = \pi$, which corresponds to $d = \lambda_c/2$, where λ_c is the center frequency wavelength. The experimental curves which best fit the theoretical curve are for frequencies above 2000 Hz. This was expected since 20000 Hz seemed to be the lower bound on the AMA regime from the earlier results evaluating the uniformity of the interior sound levels. Therefore, at 2000 Hz, there are not enough modes for the theory to hold, although the agreement is still fairly good. The experimental data show better agreement with theory as the center frequency and, therefore, the number of modes increases, up to a point, and then it is slightly worse. At 4000 Hz, the ratio of mean-square pressure in a corner to that in the interior is almost 10 to 1. The deterioration of the theory at higher center frequency is due to the fact that the bandwidth is proportional to the center frequency. Therefore the bandwidth gets wider as the center frequency. Therefore the bandwidth gets wider as the center frequency increases. In large bandwidths, the assumptions that the frequency, power spectra of the wall acceleration, damping, etc. are essentially constant may break down.

Similar results are shown in Figs. 9 and 10. In Fig. 9, the theoretical curve has a value of 4 at $k_c d$ equal 0(at the edge), reaches its first minimum around 3 oscillates slightly and asymptotes to 1 for large values of $k_c d$. Here, $k_c d$ is the nondimensional distance from the edge along a line which makes an angle of 33 deg. with the wall. Experimental results agree well for center frequencies above 3000 Hz. At 3000 Hz, the value of mean-square pressure at the edge is more than 5 times higher than the interior.

The mean-square pressure ratio in the intensification zone near a wall (away from its corners or edges) is shown in Fig. 10. Theoretically, the ratio is 2 to 1 at the wall. Again, agreement is good, although the experimental levels are higher than the predicted levels at the wall, for the highest center frequency values.

In all three cases, the experimental data show asymptotic behavior, that is, the mean-square pressure levels approach a constant for large $k_c d$. In almost all instances, the theory predicts the thickness of the intensification zone well.

Effect Of Bandwidth. The previous data suggest that the theory holds when the center frequency is large such that there is a large number of acoustic modes in the cavity. However, it also suggests that when the bandwidth is too large the theory breaks down. In Fig. 11, the center frequency is held constant at 3000 Hz, and the bandwidth to center frequency ratio is varied from 5 percent to 50 percent. The experimental data which are used here are for the wall intensification zone. Six experimental curves are shown. A corresponding theoretical curve for each experimetnal curve is not shown in order not to crowd the plot. Although there are six different theoretical curves to compare to, all the theoretical curves have a value of two at the wall, and asymptote to one away from the wall. Therefore, qualitatively this data can be judged on how well it agrees at the wall and asymptotically. The worst cases are the data corresponding to the 5 percent and the 50 percent f_b/f_c ratios, but for different reasons. For small bandwidths, there

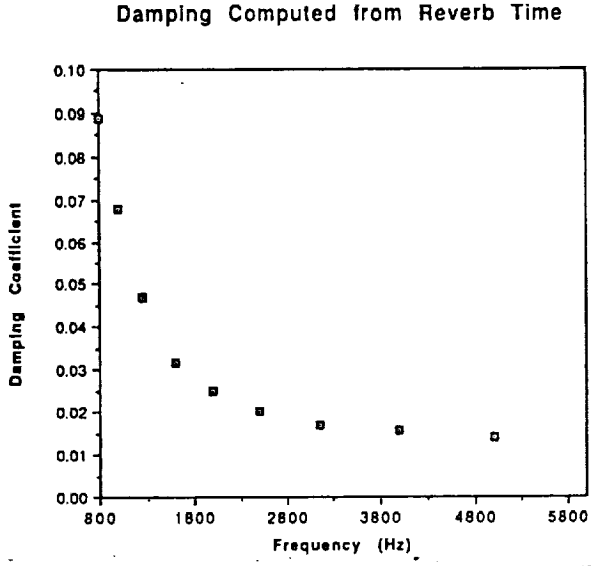

Fig. 12 Damping coefficient, ζ_c^A, predicted from reverberation time measurements

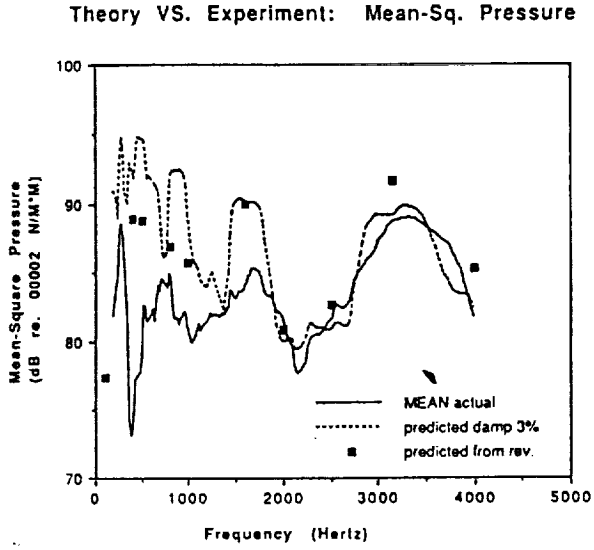

Fig. 13 Comparison of experimental and theoretically predicted values for spatially-averaged mean-square pressure

may not be enough modes to satisfy the condition that the number of acoustic modes be very large. However, for large bandwidths, the condition that certain variables be considered constant in the band is violated.

Prediction of Interior Levels using AMA vs. Experimental Results. The spatially-averaged mean-square pressure of the interior is described by AMA theory (see the Appendix) as:

$$\frac{\langle \bar{p}^2 \rangle}{(\rho_o c_o^2)^2} \cong \frac{\pi}{4} \left(\frac{A_f}{V}\right)^2 \frac{\Delta N^A \Phi_w}{(\omega_c^A)^3 \zeta_c^A \langle Z_c^2 \rangle} \qquad (2)$$

The quantities A_f (the flexible wall area) and V (the volume of the interior) are known from the geometry of the rectangular acoustic cavity. The number of modes ΔN^A in the desired bandwidth can be estimated using the standard formula from architectural acoustics (in any of the textbooks referenced). The term $\langle Z_c^2 \rangle$ is a ratio of the acoustic modal functions evaluated at the center frequency spatially averaged over the entire volume to that spatially averaged over the flexible wall area. For this example, the acoustic modal functions are products of cosines. The damping ratio evaluated at the center frequency, ζ_c^A can be estimated from independent measurements of the reverberation time in the acoustic cavity, which were performed as part of the overall experimental effort.

The reverberation time was measured using a B&K sound level meter with a reverbation module attached, (B&K Sound Level Meter Type 2231 Plus Reverberation Processor Module BZ 7104) which sends 1/3 octave band bursts and then measures decay as a function of time. It calculates and displays the reverberation time in each 1/3 octave band. The damping ratio was predicted from reverberation time measurements through the relationship described by Dowell (1978) and are plotted in Fig. 12. The remaining unknown parameter in Eq. (2) is the power spectra of the wall acceleration, Φ_w. This information can be obtained from the accelerometer measurements shown, for example, in Fig. 6, which were taken concurrently with the microphone readings for sound pressure levels. The accelerometer was moved around on the flexible portion of the wall, and the response was found to be nearly spatially uniform above 2000 Hz, i.e., the flexible plate, itself, was in the AMA limit for structural vibration above 2000 Hz (approximately 26 modes in a 1/3 octave band).

A comparison between experimentally obtained results and theoretically predicted values for spatially averaged mean square pressures are shown in Fig. 13. The solid line corresponds to data which were measured experimentally with microphones and then averaged. The spatially-averaged sound pressure levels which are predicted using AMA, with the input to the AMA formula being the accelerometer measurement from the flexible wall and the predicted damping ratio from reverberation time measurements, are represented by discrete points. An additional curve is also shown in the figure, it corresponds to the AMA predicted values for the mean-square pressure assuming a constant damping ratio of 3 percent. The agreement shown is quite good, particularly above 2000 Hz, where the flexible plate is in the AMA limit. Below this value, one accelerometer reading is not sufficient to represent the power spectra of the wall acceleration. It is believed that better agreement could be obtained by using a spatial average of the output from several accelerometers on the flexible wall for Φ_w. However, below a certain value of center frequency, the assumptions for AMA, both in the acoustics as well as the structural dynamics, break down and good agreement can never be reached.

Conclusions

When there is a large number of structure modes responding on the vibrating portion of the wall and when there is a large number of acoustic modes in the cavity, the AMA theory predicts that the sound pressure levels in the interior are uniform. This was verified by the experiment performed here, which showed that for this cavity configuration, an AMA regime exists above 2000 Hz for power spectral densities taken in 1/3 octave bands. The AMA theory also predicts that intensification occurs at the cavity boundaries, and that the respective ratios relative to the interior level are 8, 4, and 3 for corner, edge, and wall intensification. The theory and experiment showed reasonable agreement with respect to the levels of intensification at the boundaries as well as the thickness of the intensification zone. The combination of bandwidth and center frequency must be carefully chosen to give optimal results from the AMA theory. If the bandwidth is too narrow, or the center frequency too low there may not be enough modes for the assumption of infinite number of acoustic modes to be valid. Whereas, if the bandwidth is too wide, other AMA assumptions break down, such as that the modal properties are slowly varying over the bandwidth.

Acknowledgments

The authors wish to thank Dr. Kevin Shepherd and Dr. C. A. Powell of the Structural Acoustics Branch at NASA Langley Research center for their guidance and sharing of experimental expertise while this work was being conducted. This work was supported by the Structural Acoustics Branch of NASA Langley Research Center through Grant No. NAG-1-709 and NASA Graduate Student Researchers Program fellowship NGT-50342. We also wish to thank to Dr. Donald B. Bliss at Duke University for sharing his technical expertise with us regarding this experiment.

References

Dowell, E. H., 1978, "Reverberation Time, Absorption, and Impedance," *Journal of the Acoustical Society of America*, Vol. 64, pp. 181-191.

Dowell, E. H., 1983, "Vibration Induced Noise in Aircraft: Asymptotic Modal Analysis and Statistical Energy Analysis of Dynamical Systems," United Technologies Research Center., R82-112447.

Kinsler, L. E., and Frey, A. R., 1962, "Chapter 14: Architectural Acoustics," *Fundamentals of Acoustics*, Second Edition, John Wiley & Son, New York.

Kubota, Y., and Dowell, E. H., 1986, "Experimental Investigation Of Asymptotic Modal Analysis For A Rectangular Plate," *Journal of Sound and Vibration*, Vol. 106, pp. 203-216.

Kubota, Y., and Dionne, H. D., and Dowell, E. H., 1988, "Asymptotic Modal Analysis and Statistical Energy Analysis of an Acoustic Cavity," ASME JOURNAL OF VIBRATION, ACOUSTICS, STRESS, AND RELIABILITY IN DESIGN, Vol. 119, pp. 371-376.

Lyon, R. H., 1975, *Statistical Energy Analysis of Dynamical Systems: Theory and Application*, MIT, Cambridge, MA.

Morse, P. M., and Ingard, K. U., 1968, "Chapter 9: Room Acoustics," *Theoretical Acoustics*, McGraw Hill, New York.

Pan, J., and Bies, D. A., 1990, "The Effect of Fluid-Structural Coupling on Sound Waves in an Enclosure-Theoretical Part," *J. Acoust. Soc. Am.*, Vol. 87, pp. 691-707.

Peretti, L. F., and Dowell, E. H., 1992a, "Asymptotic Modal Analysis of a Rectangular Acoustic Cavity Excited by Wall Vibration," *AIAA Journal*, January.

Peretti, L. F., and Dowell, E. H., 1992b, "A Study of Intensification Zones in a Rectangular Acoustic Cavity," *AIAA Journal*, January.

Pierce, A. D., 1989, "Chapter 6: Room Acoustics," *Acoustics: An Introduction to Its Physical Principles and Applications*, Acoustical Society of America, Woodbury, New York.

Seybert, A. F., and Cheng, C. Y. R., 1987, "Application of the Boundary Element Method to Acoustic Cavity Response and Muffler Analysis," ASME JOURNAL OF VIBRATION, ACOUSTICS, STRESS, AND RELIABILITY IN DESIGN, Vol. 109, pp. 15-21.

Sung, S. H., and Nefske, D. J., 1984, "A Coupled Structural-Acoustic Finite Element Model for Vehicle Interior Noise Analysis," ASME JOURNAL OF VIBRATION, ACOUSTICS, STRESS, AND RELIABILITY IN DESIGN, Vol. 106, pp. 314-318.

APPENDIX

The following is a derivation of Eq. (1) in the text. Equation (2) is a spatial average of Eq. (1). A Similar derivation can be found in Kubota, Dionne and Dowell (1988).

The structural wall modal equation of motion is

$$M_m[\ddot{q}_m + 2\zeta m\omega m\dot{q}_m + \omega_m{}^2 q_m] = Q_m{}^E \tag{1}$$

where the modal expansion for the wall deflection is

$$w = \sum_m q_m(t)\Psi_m(x,y) \tag{2}$$

and the structural generalized mass is

$$M_m \equiv \int\int_{A_f} m_p \Psi_m{}^2(x,y)dxdy \tag{3}$$

and the generalized force due to a given external pressure is

$$Q_m{}^E \equiv \int\int_{A_f} p^E \Psi_m(x,y)dxdy \tag{4}$$

The acoustic cavity modal equation is

$$\ddot{p}_r + 2\zeta_r{}^A\omega_r{}^A\dot{p}_r + \omega_r{}^{A2}p_r = Q_r{}^W \tag{5}$$

where the modal expansion for the acoustic cavity pressure is

$$p = \rho_0 c_0{}^2 \sum_r \frac{p_r(t)F_r(x,y,z)}{M_r^A} \tag{6}$$

and the acoustic generalized mass is

$$M_r^A \equiv \frac{1}{V}\int\int\int_v F_r^2(x,y,z)dxdydz \tag{7}$$

and the generalized acceleration due to the structural wall is

$$Q_r^W \equiv \frac{1}{V}\int\int\int_{A_f} \ddot{w}F_r(x,y,z)dxdy. \tag{8}$$

Define f, a nondimensional cavity pressure,

$$f(t,x,y,z) \equiv \frac{p}{\rho_0 c_0{}^2}$$

From (6) and the defintion of auto-power spectrum, the auto-power spectrum of f is:

$$\Phi_f(\omega;x,y,z) = \sum_r\sum_s \frac{F_r(x,y,z)}{M_r^A}\frac{F_s(x,y,z)}{M_s^A}\Phi_{p_rp_s} \tag{9}$$

where the cross-spectra are defined as:

$$\Phi_{p_rp_s} \equiv \frac{1}{\pi}\int_{-\infty}^{\infty} R_{p_rp_s}(\tau)e^{i\omega\tau}d\tau \tag{10}$$

and the cross-correlations of the modal generalized pressure coordinates are:

$$R_{prps} \equiv \lim_{T-\infty}\frac{1}{2T}\int_{-T}^{T} P_r(t)P_s(t+\tau)d\tau. \tag{11}$$

Similarly from (8) the cross-power spectra $Q_r{}^W$ and $Q_s{}^W$ are:

$$\Phi_{Q_r{}^WQ_s{}^W}(\omega) = \frac{1}{V^2}\int\int\int\int F_r(x,y,z)F_s(x^*,y^*,z^*)\Phi_w(\omega;x,y,x^*,y^*)\,dxdydx^*dy^*. \tag{12}$$

The transfer function for the acoustic modal Eq. (5) is:

$$H_r^A(\omega) = \frac{1}{-\omega^2 + 2i\zeta_r{}^A\omega_r^A\omega + \omega_r^{A2}} \tag{13}$$

From standard random response theory and Eq. (5), the relationship between $\Phi_{p_rp_s}$ and $\Phi_{r^WQ_s{}^W}$ is:

$$\Phi_{p_rp_s}(\omega) = H_r^A(\omega)H_s^A(-\omega)\Phi_{Q_r{}^WQ_s{}^W}(\omega). \tag{14}$$

From (9), (12), and (14):

$$\Phi_f(\omega;x,y,z) = \frac{1}{V^2}\sum_r\sum_s \frac{F_r(x,y,z)}{M_r^A}\frac{F_s(x,y,z)}{M_s^A}H_r^A(\omega)H_s^A(-\omega) \tag{15}$$

$$\cdot\int\int\int\int F_r(x,y,z)F_s(x^*,y^*,z^*)\Phi_w(\omega;x,y,x^*,y^*)dxdydx^*dy^*$$

This is the basic expression for the power spectra of the cavity pressure in terms of the power spectra of the wall acceleration. The double summation over r and s can be reduced to a single summation by ignoring the off-diagonal coupling. This is called "joint acceptance" theory, and it entails omitting all terms in the double sum except those for which $r=s$, This theory is applicable because $H_r(\omega)\cdot H_s(-\omega) << |H_r(\omega)|^2$ and $H_s(\omega)\cdot H_r(-\omega) << |H_s(\omega)|^2$ for typical small damping values. Equation (15) is then simplified to:

$$\Phi_f(\omega;x,y,z) = \frac{1}{V^2}\sum_r \frac{F_r^2(x,y,z)}{(M_r^A)^2}|H_r^A(\omega)|^2 \tag{15*}$$

$$\cdot\int\int\int\int F_r(x,y,z)F_r(x^*,y^*,z^*)\Phi_n(\omega;x,y,x^*,y^*)dxdydx^*dy^*$$

Since,

$$\Phi_w(w;x,y,x^*,y^*) \cong \sum_{m,n} \Psi_m(x,y)\Psi_n(x^*,y^*)\omega^2 H_m(\omega)^2 H_m(\omega)\omega^2 H_n(-\omega)\cdot$$

$$\sum_{i,j} \Psi_m(x_i,y_i(\Psi_n(x_j^*,y_j^*)\Phi_{F_{ij}}(\omega)$$

then, for a large number of excited structural modes ($\Delta M \to \infty$),

$$\Phi_w(\omega;x,y,x^*,y^*) \cong \begin{matrix} 0 & \text{if} x \neq x^*, y \neq y^* \\ \text{constant} & \text{if} (x = x^*, y = y^* \end{matrix}$$

Therefore, $\Phi_w(\omega;x,y,x^*,y^*) \cong A_f \Phi_w(\omega)\delta(x-x^*)\delta(y-y^*)$.

Assuming the power spectra is smoothly varying with respect to the transfer function ("white noise assumption"), then $\Phi_w(\omega) \cong \Phi_w(\omega_c)$. Equation (15*) then becomes:

$$\Phi_f(\omega;x,y,z) = \frac{A_f}{V^2}\Phi_w(\omega_c)\sum_r \frac{F_r^2(x,y,z)}{(M_r^A)^2}|H_r^A(\omega)|^2$$

$$\cdot \int\int_{A_f} F_r^2(x,y,z)dxdy \quad (16)$$

Integrating over frequency to obtain mean-square pressure gives:

$$\bar{f}^2 = \frac{\bar{p}^2}{(\rho_o c_o^2)^2} \cong \frac{\pi}{4}\frac{A_f}{V^2}\Phi_w(\omega_c)\sum_r \frac{F_r^2(x,y,z)}{(M_r^A)^2(\omega_r^A)^3(\zeta_r^A)}$$

$$\cdot \int\int_{A_f} F_r^2(x,y,z_o)dxdy \quad (17)$$

This is the equation for mean-square pressure in the cavity when there is a large number of structural modes and a moderate number of acoustic modes. Assuming M_r^A, ω_r^A, and ζ_r^A do not vary rapidly in the bandwidth, and can be replaced by their values at the center frequency of the band (subscripted by "c"), Eq. (17) becomes:

$$\frac{\bar{p}^2}{(\rho_o c_o^2)^2} \cong \frac{\pi}{4}\frac{A_f}{V^2}\frac{\Phi_w(\omega_c)}{(M_c^A)^2(\omega_c^A)^3(\zeta_c^A)}\sum_r F_r^2(x,y,z)$$

$$\cdot \int\int_{A_f} F_r^2(x,y,z_o)dxdy \quad (18)$$

The integral over the flexible area can be expressed as a spatial average over the flexible area times the area, F_f. The acoustic modal function, F_r, can be written in terms of spatially independent functions, $X_r(x)\cdot Y_r(y)\cdot Z_r(z)$. Assuming that the flexible wall area is in the $z = z_o$ plane, $F_r(x,y,z_o) = X_r(x)Y_r(y)Z_r(z_o)$. Mathematically,

$$\frac{\int\int F_r^2(x,y,z_o)dxdy}{A_f} = \frac{\langle X_r^2\rangle\langle Y_r^2\rangle\langle Z_r^2\rangle}{\langle Z_r^2\rangle} = \frac{\langle F_r^2\rangle_{\text{volume}}}{\langle Z_r^2\rangle}. \quad (19)$$

When there is a large number of acoustic modes, ($r \to \infty$) and when the acoustic wavelengths are small compared to the size of the flexible area, then $\langle F_r^2\rangle$ and $\langle Z_r^2\rangle$ are independent of modal number, r, and can be taken outside the summation. If these conditions do not apply, then $\langle F_r^2\rangle$ and $\langle Z_r^2\rangle$ should be modally averaged over the frequency band. Subscripting F and Z by "c" to denote that they are independent of r, and taking them outside the summation, Eq. (19) becomes:

$$\frac{\bar{p}^2}{(\rho_o c_o^2)^2} \cong \frac{\pi}{4}\frac{A_f^2}{V^2}\frac{\Phi_w(\omega_c)}{(M_c^A)^2(\omega_c^A)^3(\zeta_c^A)}\frac{\langle F_c^2\rangle}{\langle Z_c^2\rangle}\sum_r F_r^2(x,y,z) \quad (20)$$

Equation (20) is identical to Eq. (1) in the text. Equation (2) in the main text is simply a spatial average of this equation. Using the following relations,

$$(M_c^A)^2 = \langle F_c^2\rangle^2 \text{ and } \sum_r \langle F_r^2(x,y,z)\rangle \cong \Delta N^A \cdot \langle F_c^2\rangle$$

in the above equation leads to the spatially averaged result:

$$\frac{\langle \bar{p}^2\rangle}{(\rho_o c_o^2)^2} \cong \frac{\pi}{4}\left(\frac{A_f^2}{V}\right)^2 \frac{\Delta N^A \Phi_w}{(\omega_c^A)^3\zeta_c^A\langle Z_c^2\rangle}$$

which is the same as Eq. (2) in the text.

Appendix E:

Peretti, L. F. "Chapter 4: Asymptotic Modal Analysis for Structural-Acoustic Systems with Finite Structural and Infinite Acoustic Modes," Asymptotic Modal Analysis for Structural-Acoustic Systems, Ph.D. Thesis, Duke University, 1991.

CHAPTER 4

Asymptotic Modal Analysis for Structural-Acoustic Systems with Finite Structural and Infinite Acoustic Modes

Introduction

When part of an enclosure vibrates, it often excites a large number of acoustic modes in its interior. Such is the case when part of an automobile vibrates, creating unpleasant acoustic responses in the interior, or when the sidewall of an airplane fuselage vibrates, transmitting annoying sound pressure levels to the interior. The results presented here are directly applicable to these vehicular noise and other interior noise problems.

Previously, Asymptotic Modal Analysis has been used to study a similar class of problems in structural-acoustics [Ref. 4, 11, 22, 23]. In the previous works, it was always assumed that the number of structural modes was large, and the number of acoustic modes was either large or small. Here, it is assumed that the number of acoustic modes is large (approaches infinity), and the result will be derived for the case where the number of structural modes is finite.

This result, in the limit where the number of structural modes approaches infinity, will be compared to the result derived previously for an infinite number of both structural and acoustic modes. In the previous result, it was initially assumed that the number of structural modes was infinite, and then the number of acoustic modes was allowed to go to infinity.

Asymptotic Modal Analysis (AMA) is a recent method, which is systematically derived from classical modal analysis. AMA was originally developed by Dowell [1] as a way to demonstrate the relationship between statistical energy analysis and classical modal analysis. The book by Richard Lyon [5] is the classic reference on statistical energy

analysis. The AMA method has many advantages. Since it is systematically derived from CMA, the generality of the final result can be modified by changing assumptions which are made in the derivation. For instance, AMA can predict spatially averaged sound pressure levels in the interior of an acoustic cavity, and it also has the capability to predict local sound pressure levels. The AMA method requires less information about the system than a traditional CMA approach. Parameters, such as modal damping ratio, frequency, generalized mass, etc. for each individual mode are needed for CMA, whereas in AMA, only the values at the center frequency are required.

The AMA method is useful for solving linear dynamical systems where there are a large number of modes and has been proven accurate for both structural dynamics and acoustics problems. The method has been verified experimentally by Kubota [3] for a rectangular plate excited by point forces as well as a vibrating plate with a concentrated mass or masses [24, 25]. Experimental verification of the AMA method applied to a rectangular acoustic cavity in which part of one wall vibrated was reported by Peretti & Dowell [22]. In all of the previous AMA analyses it was assumed that the number of structural modes was large. Conversely, for the structural-acoustic system studied here, a small number of structural modes will be assumed initially. The underlying assumption in this analysis is that the number of acoustic modes approaches infinity.

Theoretical Development

Derivation of the Result for a Finite Number of Structural Modes, and an Infinite Number of Acoustic Modes

The expression for mean-square pressure as a function of wall acceleration for a rigid wall acoustic cavity with a flexible vibrating portion is derived below. This derivation is similar to the derivation found in Ref. 4. However, in Ref. 4 the initial assumption is that the number of structural modes is infinite. Here, the underlying assumption is that the number of acoustic modes is infinite. The derivations are identical up to Equation (4.14), but all of the steps are included here for completeness.

The structural wall modal equation of motion is

$$M_m\left[\ddot{q}_m+2\zeta_m\omega_m\dot{q}_m+\omega_m^2 q_m\right] = Q_m^E \tag{4.1}$$

where the modal expansion for the wall deflection is

$$w = \sum_m q_m(t)\,\Psi_m(x,y) \tag{4.2}$$

and the structural generalized mass is

$$M_m \equiv \int\int_{A_f} m_p \Psi_m^2(x,y)\,dxdy \tag{4.3}$$

and the generalized force due to a given external pressure is

$$Q_m^E \equiv \int\int_{A_f} p^E \Psi_m(x,y)\,dxdy \tag{4.4}$$

The acoustic cavity modal equation is

$$\ddot{p}_r + 2\zeta_r^A \omega_r^A \dot{p}_r + \omega_r^{A^2} p_r = Q_r^W \tag{4.5}$$

where the modal expansion for the acoustic cavity pressure is

$$p = \rho_o c_o^2 \sum_r \frac{p_r(t)F_r(x,y,z)}{M_r^A} \tag{4.6}$$

and the acoustic generalized mass is

$$M_r^A \equiv \frac{1}{V}\int\int\int_v F_r^2(x,y,z)\, dxdydz \tag{4.7}$$

and the generalized acceleration due to the structural wall is

$$Q_r^W \equiv \frac{1}{V}\int\int_{A_f} \ddot{w} F_r(x,y,z)\, dxdy\ . \tag{4.8}$$

Define f, a non-dimensional cavity pressure,

$$f(t,x,y,z) \equiv \frac{p}{\rho_o c_o^2}\ .$$

From (4.6) and the definition of auto-power spectrum, the auto-power spectrum of f is:

$$\Phi_f(\omega;x,y,z) = \sum_r\sum_s \frac{F_r(x,y,z)}{M_r^A}\frac{F_s(x,y,z)}{M_s^A}\Phi_{P_rP_s} \tag{4.9}$$

where the cross-spectra are defined as:

$$\Phi_{P_rP_s} \equiv \frac{1}{\pi}\int_{-\infty}^{\infty} R_{P_rP_s}(\tau)\, e^{i\omega\tau} d\tau \tag{4.10}$$

and the cross-correlations of the modal generalized pressure coordinates are:

$$R_{P_rP_s} \equiv \lim_{T\to\infty} \frac{1}{2T}\int_{-T}^{T} P_r(t)P_s(t+\tau)\, d\tau\ . \tag{4.11}$$

Similarly from (4.8) the cross-power spectra of Q_r^W and Q_S^W are:

$$\Phi_{Q_r^W Q_s^W}(\omega) = \frac{1}{V^2}\int\int\int\int F_r(x,y,z)F_s(x^*,y^*,z^*)\Phi_{\ddot{w}}(\omega;x,y,x^*,y^*)\, dxdydx^*dy^*. \tag{4.12}$$

The transfer function for the acoustic modal equation (4.5) is:

$$H_r^A(\omega) = \frac{1}{-\omega^2 + 2i\zeta_r^A\omega_r^A\omega + \omega_r^{A^2}} \tag{4.13}$$

From standard random response theory and equation (4.5), the relationship between $\Phi_{P_rP_S}$ and $\Phi_{Q_r^W Q_S^W}$ is:

$$\Phi_{P_r P_s}(\omega) = H_r^A(\omega) H_s^A(-\omega)\, \Phi_{Q_r^w Q_s^w}(\omega) \ . \tag{4.14}$$

From (4.9), (4.12), and (4.14):

$$\Phi_f(\omega;x,y,z) = \frac{1}{V^2}\sum_r\sum_s \frac{F_r(x,y,z)}{M_r^A}\frac{F_s(x,y,z)}{M_s^A} H_r^A(\omega) H_s^A(-\omega) \tag{4.15}$$

$$\cdot \iiiint F_r(x,y,z) F_s(x^*,y^*,z^*) \Phi_{\ddot{w}}(\omega;x,y,x^*,y^*)\, dxdydx^*dy^*$$

This is the basic expression for the power spectra of the cavity pressure in terms of the power spectra of the wall acceleration. The double summation over r and s can be reduced to a single summation by ignoring the off-diagonal coupling. This is called "joint acceptance" theory, and it entails omitting all terms in the double sum except those for which r=s, This theory is applicable because $H_r(\omega)H_s(-\omega) << |H_r(\omega)|^2$ and $H_s(\omega)H_r(-\omega) << |H_s(\omega)|^2$ for typical damping values. Equation (4.15) is then simplified to:

$$\Phi_f(\omega;x,y,z) = \frac{1}{V^2}\sum_r \frac{F_r^2(x,y,z)}{(M_r^A)^2} \left|H_r^A(\omega)\right|^2 \tag{4.15*}$$
$$\cdot \iiiint F_r(x,y,z) F_r(x^*,y^*,z^*) \Phi_{\ddot{w}}(\omega;x,y,x^*,y^*)\, dxdydx^*dy^*$$

Further, $\ddot{w} = \sum_m \ddot{q}_m(t)\Psi_m(x,y)$, from (2)

$$R_{\ddot{w}} = \lim_{T\to\infty} \frac{1}{2T}\int_{-T}^{T} \ddot{w}_r(x,y,t)\ddot{w}_s(x^*,y^*,t+\tau)\, dt$$

$$= \lim_{T\to\infty} \frac{1}{2T}\int_{-T}^{T} \sum_m \ddot{q}_m(t)\Psi_m(x,y)\sum_n \ddot{q}_n(t+\tau)\Psi_n(x^*,y^*)dt$$

or, $$R_{\ddot{w}}(\tau,x,y,x^*,y^*) = \sum_m\sum_n \Psi_m(x,y)\Psi_n(x^*,y^*) R_{\ddot{q}_m\ddot{q}_n}(\tau) \ .$$

Taking a Fourier transform ($\tau \to \omega$, $R \to \Phi$)

$$\Phi_{\ddot{w}}(\omega,x,y,x^*,y^*) = \sum_m\sum_n \Psi_m(x,y)\Psi_n(x^*,y^*)\Phi_{\ddot{q}_m\ddot{q}_n}(\omega) \tag{4.16}$$

Again, ignoring the off-diagonal coupling by "joint acceptance" arguments, and noting that the point pairs x, y and x*, y* correspond to the same points and are therefore, superfluous:

$$\Phi_f(\omega;x,y,z) = \frac{1}{V^2}\sum_r \frac{F_r^2(x,y,z)}{(M_r^A)^2}\left|H_r^A(\omega)\right|^2 \cdot \left[\iint_{A_f} F_r(x,y,z_o)\Psi_m(x,y)\,dxdy\right]^2 \cdot \Phi_{\ddot{q}_m\ddot{q}_m}(\omega) \quad (4.17)$$

Equation (4.17) is for one structural mode (m). The total mean-square pressure can be computed by summing the individual contribution from each mode. The mean square pressure response is found by:

$$\bar{f}^2 \equiv \frac{\bar{p}^2}{(\rho_o c_o^2)^2} \equiv R_f(\tau=0;x,y,z) = \int_0^{\infty} \Phi_f(\omega;x,y,z)\,d\omega$$

Integrating equation (4.17) with respect to ω, and recalling that the white noise assumption implies that $\Phi_{\ddot{q}_m\ddot{q}_r}$ is relatively constant in the bandwidth, yields:

$$\frac{\bar{p}^2}{(\rho_o c_o^2)^2} \cong \frac{1}{V^2}\frac{\pi}{4}\sum_r \frac{F_r^2(x,y,z)}{(M_r^A)^2}\frac{1}{(\omega_r^A)^3\zeta_r^A} \cdot \left[\iint_{A_f} F_r(x,y,z_o)\Psi_m(x,y)\,dxdy\right]^2 \cdot \Phi_{\ddot{q}_m\ddot{q}_m}(\omega) \quad (4.18)$$

If the flexible area is small compared to an acoustic wavelength, $F_r(x,y,z_o)$ can be replaced by its value at the centroid, $F_r(x_o,y_o,z_o)$. The implication and justification for this assumption will be discussed later. The integral over $\Psi_m(x,y)$ is equivalent to the spatial average of $\Psi_m(x,y)$ times the area of the flexible wall (A_f). Equation (4.18) can then be rewritten:

$$\frac{\bar{p}^2}{(\rho_o c_o^2)^2} \cong \frac{\pi}{4}\left(\frac{A_f}{V}\right)^2 \sum_r \frac{F_r^2(x,y,z)}{(M_r^A)^2}\frac{F_r^2(x_o,y_o,z_o)}{(\omega_r^A)^3\zeta_r^A} \cdot \left\langle\Psi_m(x,y)\right\rangle_{A_f}^2 \cdot \Phi_{\ddot{q}_m\ddot{q}_m}(\omega_r^A) \quad (4.19)$$

Since, there are an infinite number of acoustic modes ($r\to\infty$) the summation over r can be approximated by:

$$\sum_r \frac{F_r^2(x,y,z)}{\langle F_r^2\rangle^2}\frac{F_r^2(x_o,y_o,z_o)}{(\omega_r^A)^3\zeta_r^A} \cdot \Phi_{\ddot{q}_m\ddot{q}_m}(\omega_r^A) \equiv \frac{\left[\langle F_c^2\rangle\langle F_c^2\rangle_o\right]\Delta N^A}{\langle F_c^2\rangle^2(\omega_c)^3\zeta_c} \cdot \Phi_{\ddot{q}_m\ddot{q}_m}(\omega_c) \quad (4.20)$$

This assumes that the generalized mass (M_r^A), damping (ζ_r^A), frequency (ω_r^A), and power spectra ($\Phi(\omega_r^A)$) are slowly varying with respect to the rapidly varying transfer function (H_r^A) and can therefore be replaced by their values at the center frequency. The summation over the product of the acoustic modal functions is then replaced by the product of their spatial averages times the number of acoustic modes in the band.

Using these approximations in equation (4.19), the result for the mean-square pressure when there are a large number of acoustic modes, but a finite number of structural modes, is represented by equation (4.21).

$$\frac{\overline{p}^2}{(\rho_o c_o^2)^2} = \frac{\pi}{4}\left(\frac{A_f}{V}\right)^2 \langle \Psi_m(x,y) \rangle_{A_f}^2 \quad \frac{\langle F_c^2 \rangle_o \, \Delta N^A}{\langle F_c^2 \rangle (\omega_c)^3 \zeta_c} \cdot \Phi_{\dot{q}_m \dot{q}_m}(\omega_c) \tag{4.21}$$

This is the result for the mean square pressure when one structural mode excites a large number of acoustic modes in the bandwidth. The total mean-square pressure in the band is the summation of the contributions from each structural mode in the band.

This expression can also be written as a function of the power spectra of the individual point forces rather than the power spectra of the wall acceleration in generalized coordinates. That result and its derivation are presented in the appendix.

Result for an Infinite Number of Structural Modes and an Infinite Number of Acoustic Modes

Equation (4.21) is the result for the mean-square pressure when there are an infinite number of acoustic modes excited by one structural mode. It is instructive to take the limit of this expression summed over all structural modes, m, as m goes to infinity. This will produce a result which is valid for a case where there are both a large number of acoustic and a large number of structural modes in the band and can be compared to the previously derived result [Ref. 4] where the limits were taken in the opposite order.

In the AMA structural mode limit, $\langle\Psi_m\rangle^2 \rightarrow \langle\Psi_c\rangle^2$, and $\langle\Psi_m^2\rangle \rightarrow \langle\Psi_c^2\rangle$ and

$\Phi_{\dot{q}_n \dot{q}_n} = \dfrac{\langle\overline{\dot{w}}^2\rangle}{\langle\Psi_c^2\rangle \Delta M \, \Delta\omega}$, which follows from (4.16). Using the above relations and summing (4.21) over m, yields:

$$\frac{\overline{p}^2}{(\rho_o c_o^2)^2} \cong \frac{\pi}{4}\left(\frac{A_f}{V}\right)^2 \frac{\Delta N^A}{\Delta\omega} \frac{1}{(\omega_c)^3 \zeta_c} \frac{\langle\Psi_c(x,y)\rangle^2}{\langle\Psi_c^2(x,y)\rangle} \frac{\langle\overline{\dot{w}}^2\rangle}{\langle Z_c^2\rangle_o} \tag{4.22}$$

where $\langle Z_c^2\rangle_o$ is the ratio of the spatial average of F_c^2 over the volume to F_c^2 at the centroid of A_f. This is the result for the mean-square pressure when it is first assumed that an infinite number of acoustic modes responds, and then that an infinite number of structural modes also responds.

Previously, Kubota, Dionne and Dowell [Ref.4] derived a similar result for an infinite number of both structural and acoustic modes. Their derivation first assumed that an infinite number of structural modes was responding and then took the limit as the number of acoustic modes approached infinity. From Ref.4, that result is:

$$\frac{\langle\overline{p}^2\rangle}{(\rho_o c_o^2)^2} \cong \frac{\pi}{4}\left(\frac{A_f}{V}\right)^2 \frac{\Delta N}{\Delta\omega^A} \frac{\langle\overline{\dot{w}^2}\rangle_{\Delta\omega}}{(\omega_c^A)^3 \zeta_c^A \langle Z_c^2\rangle} \tag{4.23}$$

The two results are seen to be very similar. From dimensional considerations this is hardly surprising. What is significant are the differences. A discussion of the differences between these two asymptotic results follows.

Discussion of Results

Equations (4.22) and (4.23) show that the result for an infinite number of acoustic modes and an infinite number of structural modes is not independent of the order in which the limits are taken. This is often true in asymptotic methods.

The $\Delta\omega$ in the first equation (4.22) refers to the bandwidth associated with the individual structural modes. This was implicitly true in (4.23) also, but in (4.23) a very large number of structural modes had been already assumed in the frequency interval of interest. Perhaps more significant and surprising is that in (4.22), compared to (4.23) there is an additional multiplicative factor,

$$\frac{\langle \Psi_c(x,y) \rangle^2}{\langle \Psi_c^2(x,y) \rangle}.$$

Moreover, this ratio asymptotically approaches zero as ω_c approaches infinity. This is true because, $<\Psi_c^2>$ equals 1/2 for high center frequencies or high mode number, while $<\Psi_c>^2$ becomes smaller and smaller for higher center frequencies. This implies that for large modal number $<\Psi_c>^2$ approaches zero. Therefore, it is only the lower order structural modes that significantly contribute to the acoustic response.

The above ratio appears as a consequence of assuming that the flexible wall area is small compared to an acoustic wavelength, such that, $F_r(x,y,z_o)$ on the flexible wall area can be approximated by F_r at the centroid (x_o,y_o,z_o). From (4.18), the integral over the flexible area is: $I_{r,m} \equiv \iint_{A_f} F_r(x,y,z_o)\Psi_m(x,y)\,dxdy$. This assumption, removes $F_r(x,y,z_o)$ from inside this integral leaving only Ψ_c. The entire integral is squared, hence the term $<\Psi_c(x,y)>^2$, (A_f^2 also appears).

Consider now two limiting cases for A_f. First, if the entire wall is flexible (i.e., A_f = the entire wall area, L_xL_y), then the integral, $I_{r,m}$ is made up of a summation of terms which look like:

$$\frac{\cos(r_x\pi \mp m_x\pi)\cos(r_y\pi - m_y\pi) - 1}{\frac{(r_x\pi \mp m_x\pi)}{L_x}\frac{(r_y\pi - m_y\pi)}{L_y}} + \frac{\cos(r_x\pi \pm m_x\pi)\cos(r_y\pi + m_y\pi) - 1}{\frac{(r_x\pi \pm m_x\pi)}{L_x}\frac{(r_y\pi + m_y\pi)}{L_y}}$$

Assuming r >> m, since there are an infinite number of acoustic modes, r, for each structural mode, m, the above expression is approximately:

$$4 \cdot \frac{\cos(r_x\pi)\cos(r_y\pi) - 1}{\frac{(r_x\pi)}{L_x}\frac{(r_y\pi)}{L_y}} .$$

Obviously, primarily the lower acoustical modes contribute. Therefore, the case where the entire wall area is flexible is not of interest here, since in this analysis a large number of acoustical modes are being studied. The case of the entire wall vibrating is effectively the case where the scale of the wall is large compared to an acoustic wavelength. For small r and small m, CMA should be used, of course.

Now consider the other limiting case where the length scale of A_f is much smaller than an acoustic wavelength. The acoustic modal function, $F_r(x,y,z_o)$ can be approximated by $F_r(x_o,y_o,z_o)$, yielding:

$I_{r,m} \cong F_r(x_o,y_o,z_o) \iint_{A_f} \Psi_m(x,y)\,dxdy$. For $\Psi_m = \sin(m_x\pi x/L_x)\sin(m_y\pi y/L_y)$, the integral over Ψ_m equals:

$$\frac{L_x}{(m_x\pi)}\frac{L_y}{(m_y\pi)}\cos\left(\frac{m_x\pi}{L_x}\right)\cos\left(\frac{m_y\pi}{L_y}\right),$$

for say, x ranging from $x_o - \varepsilon$ to $x_o + \varepsilon$, and y ranging from $y_o - \varepsilon$ to $y_o + \varepsilon$. Thus primarily, the lower structural modes will contribute in this case. The acoustic modes will contribute, however, for all r. Therefore, only this case need be considered for a large number of acoustical modes, but a finite number of structural modes, i.e. the case where the length scale of A_f is smaller than an acoustic wavelength.

The comparison of equations (4.22) and (4.23) shows clearly that the double limit, $\Delta M \to \infty$ and $\Delta N^A \to \infty$, is not unique, that is, the result depends on the order in which ΔM and ΔN^A approach infinity. In equation (22), $\Delta N^A \to \infty$ and then $\Delta M \to \infty$. On the

other hand, in equation (4.23), $\Delta M \to \infty$ and then $\Delta N^A \to \infty$. This suggests incidentally, that the phrase Asymptotic Modal Analysis is particularly appropriate. All of these results using AMA are asymptotic and do break down if the assumptions under which they are derived are violated. It is clear, of course, that the real value of equation (4.22) is to demonstrate that the acoustic response of higher frequencies decreases rapidly for a large but finite number of structural modes, that is less in number than the acoustic modes.

In practice this means that one must first estimate ΔM and ΔN^A. The larger of the two is then allowed to approach infinity first and then the second. This determines whether equation (4.22) or (4.23) is applicable. Presumably there is yet another limit where $\Delta M \cong \Delta N^A$ and both go to infinity. Properly speaking, this is probably a matter of length scales, i.e. the dimension of the plate, the dimension of the cavity and the wavelengths of each. The time or frequency scales are clearly also important.

Conclusion

An asymptotic modal analysis result for the mean-square pressure in a bandwidth has been derived for the case where there are a large number of acoustic modes responding for each structural mode. The limit is then taken as the number of structural modes approaches infinity. Upon comparison of this result to previous work, where the limits were taken in the opposite order, it is shown that the order in which the number of modes goes to infinity is important. The significant difference in the two results is a ratio made up of spatially averaged structural modal functions, which only appears in the newly derived result. This ratio approaches zero as the center frequency approaches infinity.

Since the two approaches yield different results, it is important to determine which modes in the coupled system are approaching infinity faster. This information will result in the proper choice of an asymptotic modal analysis result for the mean-square pressure.

Appendix

In this appendix an alternative AMA expression for mean-square pressure is derived. Here, the variable describing the input excitation is the power spectra of point forces applied to the vibrating wall, rather than the power spectra of the wall acceleration in generalized coordinates.

From equation (4.4) in the text and power-spectra relations:

$$\Phi_{Q_m^E Q_n^E}(\omega) = \iint_{A_f} \iint_{A_f} \Psi_m(x,y)\Psi_n(x^*,y^*)\Phi_{p^E}(\omega;x,y,x^*,y^*)dxdydx^*dy^*$$

We can relate the generalized coordinates (q's) to the generalized forces (Q's) by:

$$\Phi_{q_m q_n}(\omega) = H_m(\omega)H_n(-\omega)\Phi_{Q_m Q_n}(\omega)$$

where the transfer function H_m is given by:

$$H_m(\omega) = \frac{1}{M_m\left[-\omega^2 + 2i\zeta_m\omega_m\omega + \omega_m^2\right]} .$$

It follows that:

$$\Phi_{\ddot{q}_m \ddot{q}_n}(\omega) = \omega^2 H_m(\omega)\, \omega^2 H_n(-\omega)\Phi_{Q_m Q_n}(\omega)$$

Using the above relations in equation (4.16) in the main text:

$$\Phi_{\ddot{w}}(\omega;x,y,x^*,y^*) = \sum_m \sum_n \Psi_m(x,y)\Psi_n(x^*,y^*)\omega^2 H_m(\omega)\omega^2 H_n(-\omega) \cdot \iint_{A_f} \iint_{A_f} \Psi_m(x,y)\Psi_n(x^*,y^*) \cdot \Phi_{p^E}(\omega;x,y,x^*,y^*)\, dxdydx^*dy^* \qquad \text{(A1)}$$

Equation (A1) relates the external pressure on the wall to the wall acceleration.

The above expression can be simplified by ignoring off-diagonal coupling ("joint acceptance"). This means omitting all terms in the double sum except those for which m=n. This step is justified because $H_m(\omega)H_n(-\omega) << |H_m(\omega)|^2$ and $H_n(\omega)H_m(-\omega) << |H_n(\omega)|^2$. Additionally, $\Phi_p{}^e$ is slowly varying with respect to the rapidly varying transfer

functions ($H_m(\omega)$) and therefore can be treated as a constant independent of ω. This is a consequence of assuming that the forcing is white noise. Equation (A1) then becomes:

$$\Phi_{\dot{w}}(\omega;x,y,x^*,y^*) = \sum_m \Psi_m(x,y)\Psi_m(x^*,y^*)\omega^4\left|H_m(\omega)\right|^2 \cdot\iint_{A_f}\iint_{A_f} \Psi_m(x,y)\Psi_m(x^*,y^*)\cdot \Phi_{p^E}(\omega_m;x,y,x^*,y^*)\,dxdydx^*dy^* \qquad (A2)$$

The load, p^e, can be described by many point forces, F_i. This is helpful in obtaining and understanding the results. It does not lead to any lack of generality in that any continuous spatial distribution may be represented by many point loads (I is the number of point loads).

$$p(x,y,t) = \sum_{i=1}^{I} \delta(x-x_i)\delta(y-y_i)F_i(t)$$

The associated power spectrum is

$$\Phi_{p^E}(\omega;x,y,x^*,y^*) = \sum_i\sum_j \delta(x-x_i)\delta(y-y_i)\delta(x^*-x_j^*)\delta(y^*-y_j^*)\Phi_{F_{ij}}(\omega)$$

where $\Phi_{F_{ij}}$ is the cross-power spectrum of the point loads.

Therefore, equation (A2) becomes:

$$\Phi_{\dot{w}}(\omega;x,y,x^*,y^*) = \sum_m \Psi_m(x,y)\Psi_m(x^*,y^*)\omega^4\left|H_m(\omega)\right|^2 \sum_i\sum_j \Psi_m(x_i,y_i)\Psi_m(x_j^*,y_j^*)\,\Phi_{F_{ij}}(\omega_m)$$

Using this expression for $\Phi_{\dot{w}}$ in equation (4.15*) of the text, yields:

$$\Phi_f(\omega;x,y,x^*,y^*) = \frac{1}{V^2}\sum_r \left(\frac{F_r(x,y,z)}{M_r^A}\right)^2\left|H_r(\omega)\right|^2 \iint_{A_f}\iint_{A_f} F_r(x,y,z_o)F_r(x^*,y^*,z_o) \cdot\sum_m \Psi_m(x,y)\Psi_m(x^*,y^*)\omega^4\left|H_m(\omega)\right|^2 \sum_i\sum_j \Psi_m(x_i,y_i)\Psi_m(x_j^*,y_j^*)\,\Phi_{F_{ij}}(\omega_m)\,dxdydx^*dy^*$$

This relates the power spectra of the forcing to the power spectra of the pressure. In order to obtain the mean-square pressure, this expression must be integrated with respect to frequency, by definition:

$$\bar{f}^2 \equiv \frac{\bar{p}^2}{(\rho_o c_o^2)^2} \equiv R_f(\tau=0;x,y,z) = \int_0^{\infty} \Phi_f(\omega;x,y,z)\, d\omega$$

Therefore, the mean-square pressure expression is:

$$\frac{\bar{p}^2}{(\rho_o c_o^2)^2} = \left(\int_0^{\infty} |H_r(\omega)|^2 \omega^4 |H_m(\omega)|^2 d\omega \right) \frac{1}{V^2} \sum_r \left(\frac{F_r(x,y,z)}{M_r^A} \right)^2 \cdot \left(\iint_{A_f} F_r(x,y,z_o) \cdot \sum_m \Psi_m(x,y) \sum_i \sum_j \Psi_m(x_i,y_i) \Psi_m(x_j,y_j)\, \Phi_{F_{ij}}(\omega_m) dx dy \right)^2 \quad (A4)$$

Here, the * superscript has been dropped since the point pairs x_i,y_i and x_i^*,y_i^* obey $x_i = x_i^*$ and $y_i = y_i^*$, i.e. they range over the same points on the structure. Therefore, the * superscript is superfluous. Note also that the previous equation retains a fully modal character of the classical type. We have not yet passed from the domain of modal analysis to AMA.

Figure A1, shows the smoothness of the functions $|H_m(\omega)|^2$ and $\Phi_{F_{ij}}(\omega)$ relative to $|H_r(\omega)|^2$, for the case where there are a large number of acoustic modes for each structural mode. The figure shows the response at one structural mode whose resonance frequency is ω_m. Implicit in this drawing is the assumption that the acoustic damping is less than the structural damping. In this case, $|H_m(\omega)|^2$ and $\Phi_{F_{ij}}(\omega)$ can be treated as constants relative to the rapidly varying $|H_r(\omega)|^2$.

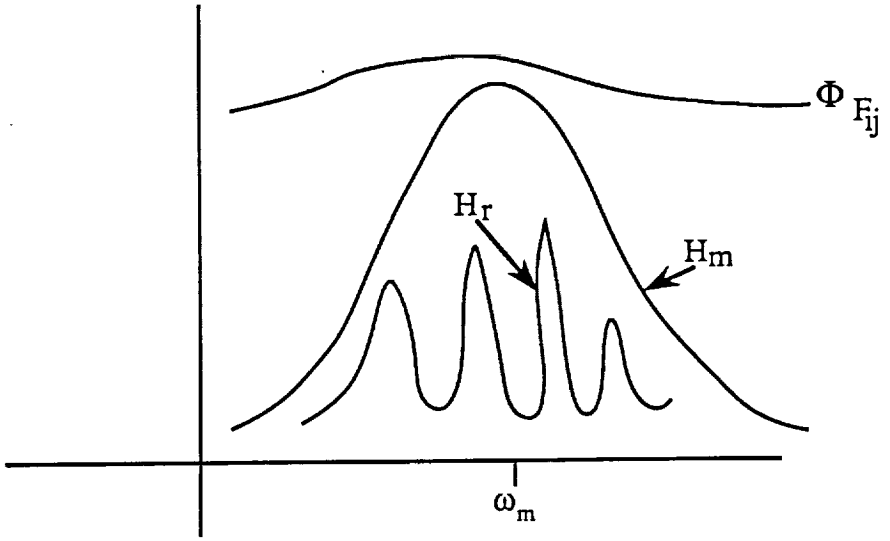

Figure A1. Qualitative sketch of transfer functions, $|H_m(\omega)|^2$, $|H_r(\omega)|^2$ and power spectra, $\Phi_{F_{ij}}(\omega)$.

The frequency integral then becomes:

$$\left| H_m(\omega_m) \right|^2 \Phi_{F_{ij}}(\omega_m) \int_0^\infty \left| H_r(\omega) \right|^2 \omega^4 \, d\omega$$

where

$$\left| H_m(\omega_m) \right|^2 = \left| \frac{1}{M_m\left(2i\zeta_m\omega_m^2\right)} \right|^2 = \frac{1}{4M_m^2\zeta_m^2\omega_m^4} \quad .$$

The frequency integral is equal to $\int_0^\infty |H_r(\omega)|^2\omega^4 d\omega \equiv \zeta_r(\omega_r^A)^4$ for small damping ratio ζ_r.

The higher order damping terms are not retained here. Substituting this into (A4) yields:

$$\frac{\overline{p}^2}{(\rho_o c_o^2)^2} = \sum_r \frac{1}{4} \frac{\zeta_r^A(\omega_r^A)^4}{M_m^2\zeta_m^2\omega_m^4} \Phi_{F_{ij}}(\omega_o) \frac{1}{V^2} \left(\frac{F_r(x,y,z)}{M_r^A}\right)^2 \cdot \left(\iint_{A_f} F_r(x,y,z_o) \; \Psi_m(x,y) \sum_i \sum_j \Psi_m(x_i,y_i)\Psi_m(x_j,y_j) \, dxdy \right)^2$$

This is the mean square pressure as a function of the external forcing F_{ij} for one structural mode. This expression is still of the CMA type, since there have been no restrictions on the summation over r.

Assuming the flexible area is small compared to the cavity dimensions, $F_r(x,y,z_o)$ can be approximated by its value at the centroid of the flexible area (x_o,y_o,z_o). In the AMA limit, the parameters, ζ_r^A, ω_r^A and M_r^A can be replaced by their values at the center frequency. The summation over r, as $r \rightarrow \infty$ can be approximated by:

$$\sum_r (F_r(x,y,z))^2 \approx \langle F_c(x,y,z)\rangle^2 \Delta N^A$$

Therefore, the expression for the mean-square pressure in terms of the power spectra of the external forcing is:

$$\frac{\bar{p}^2}{(\rho_o c_o^2)^2} = \frac{1}{4} \frac{\zeta_c^A (\omega_c^A)^4}{M_m^2 \zeta_m^2 \omega_m^4} \Phi_{F_{ij}}(\omega_c) \frac{\Delta N^A}{V^2} \left(\frac{1}{\langle Z_c(x,y,z)\rangle_o^2}\right) \cdot \left(\iint_{A_f} \Psi_m(x,y) \sum_i \sum_j \Psi_m(x_i,y_i)\Psi_m(x_j,y_j)\, dxdy \right)^2 \qquad \text{(A5)}$$

where $\langle Z_c^2\rangle_o$ is the ratio of $\langle F_c^2\rangle$ over the volume to $\langle F_c^2\rangle$ over A_f.

Equation (A5) represents the contribution from one structural mode. Implicit in this result is the assumption that infinitely many acoustic modes are present in the bandwidth of a single structural mode. The total mean-square pressure is found by summing over the finite number of structural modes (m) in the bandwidth of interest.